ACCSCIENCE PUBLISHING

Advances in

Radiotherapy & Nuclear Medicine

ISSN: 3060-8554 (Print)
ISSN: 2972-4392 (Online)
Volume 2 · Issue 4
December 2024

ACCSCIENCE PUBLISHING

Advances in Radiotherapy & Nuclear Medicine

Print ISSN: 3060-8554
Online ISSN: 2972-4392

Advances in Radiotherapy & Nuclear Medicine is a peer-reviewed and open-access journal that aims to publish and disseminate novel research in the breadth of radiation oncology, physics, and biology.

The journal aims to advance our understanding in the radiotherapy and provide a platform to oncologists and physicians to showcase their findings in original fundamental and clinical research as well as to present new ideas that highlight the changes in the radiation oncological clinical practice.

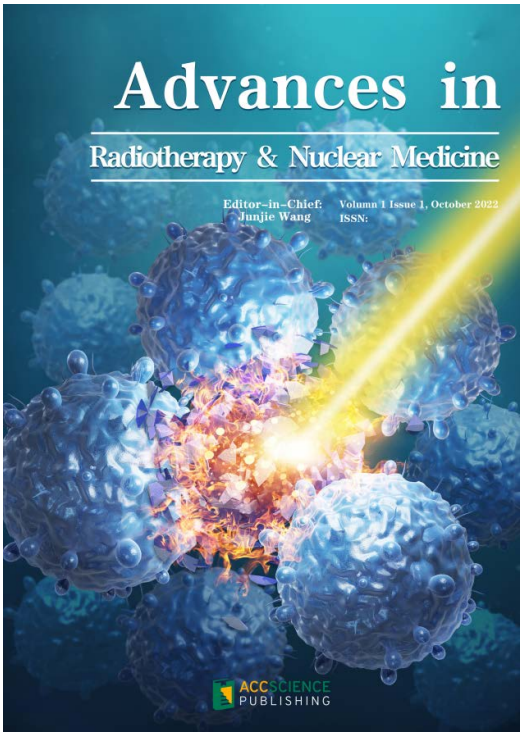

About the Publisher

AccScience Publishing is a publishing company based in Singapore. We publish a range of high-quality, open-access, peer-reviewed journals and books from a broad spectrum of disciplines.

Contact Us

Managing Editor
arnm.office@accscience.sg

AccScience Publishing
8 Burn Road, #15-03 Trivex, Singapore 369977.

Volume 2 • Issue 4 • December 2024
ISSN 3060-8554 (print) ISSN 2972-4392 (online)

Advances in Radiotherapy & Nuclear Medicine

ACCSCIENCE PUBLISHING

Access Science Without Barriers

ADVANCES IN RADIOTHERAPY & NUCLEAR MEDICINE

ISSN: 3060-8554 (print)
ISSN: 2972-4392 (online)

Editorial and Production Credits

Publisher: AccScience Publishing
Managing Editor: Freda Wang
Production Editor: Sharmila Velapasamy
Article Layout and Typeset: Sinjore Technologies (India)

For all advertising queries, contact arnm.office@accscience.sg.

Supplementary file

Supplementary files of articles can be obtained at https://accscience.com/journal/ARNM/2/4.

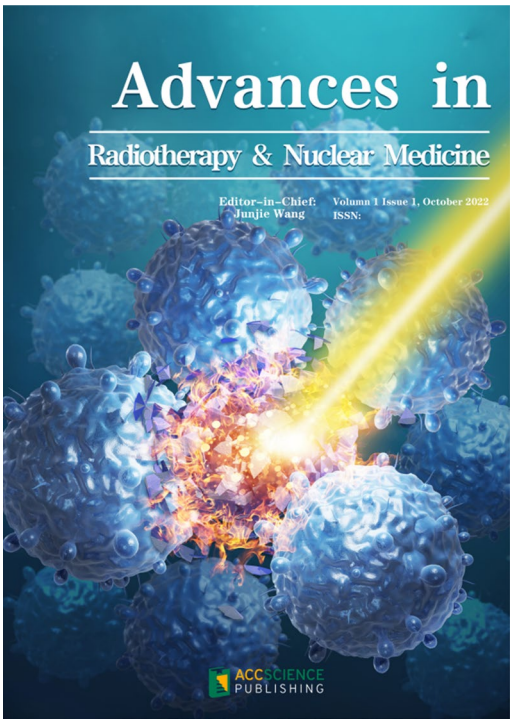

Advances in Radiotherapy & Nuclear Medicine

Editorial Board

Youth Editorial Board Members

*Editorial Board Members as of December 31, 2024

ACCSCIENCE PUBLISHING

Volume 2 | Issue 4 | December 2024 |

Advances in Radiotherapy & Nuclear Medicine

https://accscience.com/journal/ARNM

CONTENTS

ACCSCIENCE PUBLISHING

Advances in Radiotherapy & Nuclear Medicine

REVIEW ARTICLE

Applications of radionuclide-carrying liposomes for diagnosis and treatment of cancer

Rashmi Basu[1,2], Joyce G. Schwartz[3], and William T. Phillips[2]*

[1]Keystone School, San Antonio, Texas, United States of America

[2]Department of Radiology, Long School of Medicine, University of Texas Health-San Antonio, San Antonio, Texas, United States of America

[3]Department of Pathology, Methodist Hospital, San Antonio, Texas, United States of America

Abstract

Using nanocapsules to deliver diagnostic and therapeutic agents to targeted biological sites enhances the safety and effectiveness of healthcare by decreasing toxicity and increasing the accumulation of medicinal agents at targeted sites. Liposomes, nanocapsules made of naturally occurring lipids, boast many advantages for the delivery of therapeutic agents. This article reviews both the advantages and challenges associated with liposomal drug delivery for the treatment of cancerous tumors and infectious diseases. These minute spherical sacs of phospholipid molecules are flexible carriers that can be modified in various ways to optimize their use. Examples of this include alteration of the size of liposomes to selectively accumulate in tumor microenvironments and "PEGylation" of their surface to reduce uptake of liposomes by the mononuclear phagocytic system (MPS). While one of the main challenges of liposomal drug delivery is the heightened uptake of liposomes by the MPS, this unique property can be used to target diseased areas with a significant MPS presence. Furthermore, the liposomal structure can be manipulated to allow for the triggered release of internal contents with externally controlled factors. Liposomes carrying therapeutic radionuclides can be injected directly into solid tumors and dispersed throughout the tumor by convection-enhanced delivery. The flexibility and pliability of liposomes allow them to move through tight spaces within a tumor with much greater dispersion and penetration when compared to more rigid nanoparticles. Due to the benefits of radionuclide-carrying liposomes in disease diagnosis and delivery of chemotherapeutic agents, their utilization is expected to be expanded.

Keywords: Chelator; Drug delivery; Liposome; Macrophage; Mononuclear phagocyte system; Radionuclide

***Corresponding author:**
William T. Phillips
(phillips@uthscsa.edu)

Citation: Basu R, Schwartz JG, Phillips WT. Applications of radionuclide-carrying liposomes for diagnosis and treatment of cancer. *Adv Radiother Nucl Med*. 2024;2(4):4373.
doi: 10.36922/arnm.4373

Received: July 30, 2024

Accepted: September 12, 2024

Published Online: October 14, 2024

1. Introduction

Drug delivery is commonly used to increase the bioavailability of drugs, reduce contact between toxic drugs and healthy tissue, control the release of encapsulated contents, and possibly lessen the frequency of doses of treatment needed by patients. The concept of drug delivery can range from oral ingestion of encapsulated pill to intravenous administration of nanocapsules. The applications of drug delivery are extensive, ranging

from the promotion of wound healing to the delivery of cancer therapies. An example of how drug delivery improves medicine is the use of nanofibers to deliver treatment to wounds while reducing the chance of bacteria developing resistance to treatment. This method creates an environment around the damaged tissue that promotes cell healing.[1,2]

The use of nanocapsules for targeted drug delivery first became a field of focus for researchers back in the early 1950s.[3] Drug delivery using nanocapsules involves the encapsulation of a chosen drug or radionuclide in a specific material that can efficiently deliver the therapeutic agent to a targeted site. Encapsulated drugs can be delivered through a multitude of sites, including gastrointestinal, oral, rectal, parenteral, subcutaneous, intramuscular, intravenous, intra-arterial, transmucosal, transnasal, pulmonary, transdermal, and intraosseous anatomic routes.[4] To achieve the most benefit, the material used for encapsulation must be carefully considered, especially with nanocapsules that carry potentially toxic agents such as chemotherapeutic drugs or radionuclides.

The use of liposomes for drug delivery has significantly increased in the past few decades. Liposomes were first created in 1961 at the Babraham Institute of the University of Cambridge by Alex Bangham.[5] As of February 2023, 16 drugs using liposomes as drug-carrying capsules have been approved by the Food and Drug Administration (FDA) for clinical use.[6] These drugs include DaunoXome®, DepoCyt®, Doxil®, Lipodox®, Myocet®, Marqibo®, Vyxeos®, Onivyde®, Mepact®, Ambisome®, Arkayce®, Inflexal® V, Epaxel, DepoDur™, Exparel, and Visudyne®. Nine of these drugs are intended for cancer treatment.[7] Since 1992, more than 1000 articles mentioning liposomes have been published the National Library of Medicine each year, with over 3,500 articles published in 2023. Liposomes are capsules composed of a lipid bilayer of phospholipids with hydrophilic heads and hydrophobic tails, which allow for encapsulation of various compounds in different parts of the liposome.[8] Compounds that are soluble in water can be carried by the aqueous core of the liposome and compounds that dissolve in lipids can be carried by the lipid bilayer as shown in Figure 1.

2. Use of liposomes in radiology

Liposomes can be used to assist in medical imaging based on the detection of radionuclides. Using radionuclides for nuclear imaging is fundamental for identifying countless biological disorders including both cancerous and benign tumors, heart disease, and abnormalities in the brain related to neurodegenerative disorders. Positron emission tomography (PET) and single photon emission computed tomography (SPECT) are two imaging modalities used for the detection of radionuclides within the body. Both PET and SPECT are highly regarded for producing a precise location of radionuclides due to their emission of photons, which emit energy that easily penetrate tissue. Detection of radionuclides with these forms of imaging

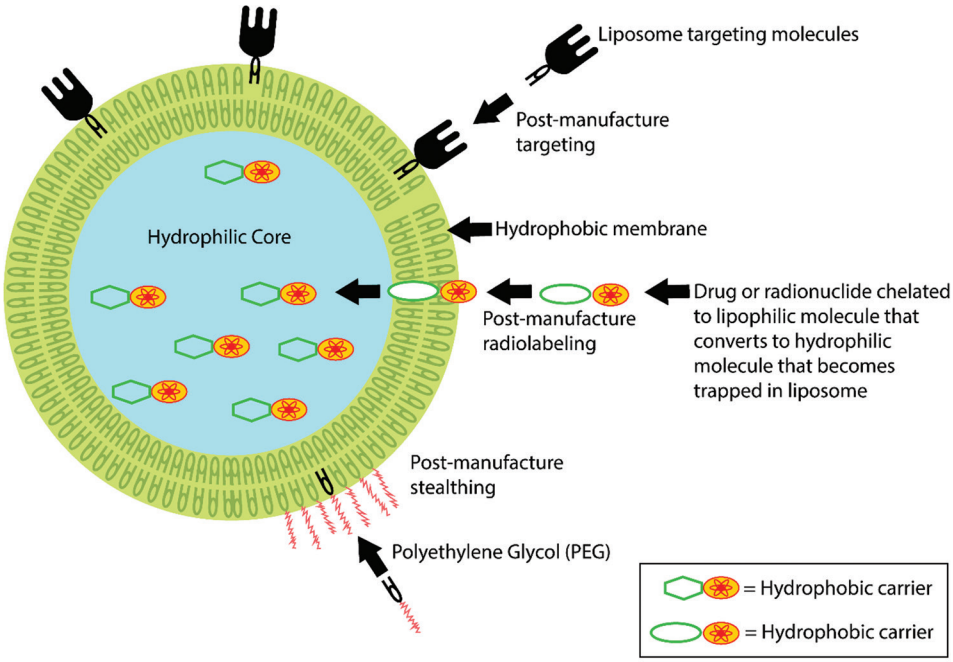

Figure 1. Illustration of an encapsulated liposome. Figure created by the authors.

can be combined with other imaging methods such as computerized tomography or magnetic resonance imaging to generate images of the body that provide precise anatomic localizations, highlighting regions where administered radionuclides are present. Encapsulated positron emitting or single photon emitting radionuclides within liposomes can be used to track their distribution in the body, to assess the efficacy of liposome-based drug delivery, and to monitor therapeutic radionuclides that emit beta particles for cancer therapy.[9]

Liposome-delivered chemotherapy is an effective adjuvant treatment to radiotherapy. A study by Hagtvet *et al.*[10] compared the therapeutic effects of radiotherapy on the volume of hypoxic tumors to the effects of radiotherapy along with doxorubicin carried within liposomes. The hypoxic tumors treated with both radiotherapy and liposomal doxorubicin showed a more significant decrease in tumor volume compared to tumors that received radiotherapy alone.[10] Liposomal doxorubicin has also been shown to have increased accumulation in cancerous tumors when combined with certain other modalities. For example, intravenously administered liposomal doxorubicin which was radiolabeled with technetium-99m (^{99m}Tc), had ~3-fold greater accumulation in solid tumors when combined with simultaneous radiofrequency ablation of the tumor as compared with the same radiolabeled liposomal doxorubicin that did not receive radiofrequency ablation (p <0.0001).[11]

3. Methods of creating liposomes

Liposomes can be adapted for many applications including modifications for drug delivery, diagnostic imaging, and specific targeting (Figure 1). They can be made by various methods that create products of differing qualities including size, stability, half-life, and permeability. These methods include thin-film hydration, spray drying, injection, reverse phase evaporation, microfluidic, and supercritical methods.

Thin film hydration involves dissolving lipids in a solvent solution within a flask, evaporating the solvent, and then adding a substance that will be encapsulated by the liposomes. When the flask is agitated, liposomes of varying sizes form with the majority having multiple lipid bilayers known as multilamellar liposome vesicles.

When spray-drying methods are used, phospholipids are dissolved in an organic mixture and mixed using a magnetic stir bar and stir plate. The compound that will be encapsulated by the liposomes is added to this mixture, and the resulting solution is sonicated into spheres. These spheres are spray-dried at high temperatures and then hydrated, yielding larger-sized liposomes (300 – 600 nm).

The injection method utilizes a mixture of phospholipids dissolved in ethanol. Once the solution is injected into a water or phosphate buffer, it begins forming liposomal membranes. After precipitation, these membranes proceed to continue forming and create lipid capsules.

Reverse-phase evaporation utilizes a mixture of phospholipids. An organic solvent is added to the flask of a rotary evaporator, and rotary evaporation is used to evaporate the solvent. The remaining lipids are then dissolved again in an organic solvent, leading to the creation of capsule-like structures. The substance that is to be encapsulated is added to this mixture, and the resulting solution is sonicated in a nitrogen environment.[12]

For the majority of biomedical applications, it is important to precisely control the size and homogeneity of the liposomes. Post-formation processing of liposomes is required to convert initially large multilamellar liposome vesicles into small unilamellar liposomes with greater homogeneity. This is generally performed by sonication, high-pressure homogenization, or extrusion through a set of filters of decreasing size. The most common size for intravenously administered liposomes is 90 – 130 nm.

Microfluidic and supercritical techniques are commonly used in liposome creation. Microfluidic techniques can be used in the injection method to control the mixing of the lipid and aqueous solutions. Supercritical methods include dissolving lipids in an organic solvent, pressurizing the mixture by introducing carbon dioxide and injecting the resulting mixture into an aqueous medium.

Potential problems associated with these techniques include a lack of ability to control the size of the liposomes, the necessity for expensive and specialized equipment, and difficulty in removing liposomes from solvent solutions.[12] The variety of techniques used in creating liposomes, however, gives scientists many options to optimize them for their intended use.

Shan *et al.*[13] recently described a new method of creating liposomes using a microfluidic mixing device to manufacture an aptamer-targeted liposome containing indocyanine green with a high encapsulation efficiency of 89.9% and a mean size of 129 ± 5.5 nm. The liposomes are targeted to tumors for fluorescent imaging and photothermal therapy.[13]

4. Advantages of liposomes for drug delivery

Using liposomes for drug delivery offers many advantages. One major advantage is that liposomes are composed of naturally occurring lipids in the human body, which have natural pathways of degradation after they have

delivered their therapeutic agent. Another advantage is that when liposomes are administered intravenously they can naturally accumulate in tumors due to the "leaky" microenvironment created by tumor angiogenesis.[9] The phenomenon of microenvironments showing heightened retention of macromolecular drugs, such as liposomes, is commonly described as, "the enhanced permeability and retention effect (EPR)."[14] This ability, paired with lessening contact between internal liposomal contents and non-targeted tissue, makes liposomal drug delivery a desirable technique in medicine. Liposomal drugs, such as Doxil®, have proven their usefulness. Doxil®, which is made of liposomes that encapsulate doxorubicin, increases drug concentrations in tumors and causes fewer adverse side effects compared to free doxorubicin.[15] It is these critical qualities of drug administration that make liposomes an ideal candidate for encapsulation and administration of radionuclides.

Passive targeting with liposomes for cancer therapy, with accumulation through EPR, is limited in some tumors. EPR occurs due to large gaps in the endothelial walls of tumor vessels. Gaps between vascular endothelial cells in normal tissue are approximately 5 – 10 nm. In tumor vessels, gaps in vascular endothelial tissue can range between 100 and 700 nm, or in some cases they appear even larger.[15] Liposomes themselves usually range from 50 nm to 500 nm in diameter, allowing them to selectively leak into the vascular interstitium in tumors but not into normal tissue. This phenomenon, however, does not occur with all types of tumors, so this type of passive targeting, while advantageous, cannot always be depended on because it can lead to a lack of true specificity for tumor tissue.[8] In some cases, it may be possible to circumvent the lack of an EPR effect through the use of active targeting. For instance, liposomes can be modified by attaching antibodies to their surface to improve drug targeting to specific cancerous sites.[15]

5. Loading radionuclides into liposomes for diagnostic and therapeutic applications

The optimal method for loading radionuclides into liposomes can also vary between different radionuclides. For instance, hydrophilic radiopharmaceuticals can be trapped within the core of the liposome while the lipid bilayer is being formed.[5]

Many methods of incorporating drugs and radionuclides into different types of liposomes have been explored. These methods include the attachment of radionuclides to the liposomal surface and active loading of radionuclides into the hydrophilic core of the liposome followed by the trapping of the radionuclides with an appropriate chelating agent. In the case of radiometals, ionophores can be used to load the radiometal into the liposome, which can then allow for the radiometal to bind to a chelator inside the liposome. In some cases, if a certain chemotherapy has the adequate potential for chelating a desired radiometal, the same approach can be taken using a chemotherapeutic agent as the chelating agent to bolster the therapeutic effect of the liposome.[16] A paper published by Goins *et al*. elucidates how the presence of glutathione in liposomes can be used to trap technetium and rhenium radionuclides in liposomes after using a lipophilic chelating agent to transport the radionuclide through the lipid bilayer where it interacts with the glutathione.[17] It should be noted that using chelating agents only within the liposome as opposed to the surface of the liposome is favorable. This is because the presence of chelating agents on the surface of the liposome can cause interactions with proteins in the bloodstream or body tissues after *in vivo* administration, which can impact the biodistribution of administered liposomes.[18] Li *et al*. also showed how liposomes encapsulating iodine-131 (^{131}I) showed higher levels of cytotoxicity toward cervical cancer cells compared to liposomes with ^{131}I attached to the surface.[19] In general, it is more beneficial to encapsulate radionuclides within the liposomes rather than attach them to the surface. The current U.S. FDA-approved liposomal products employ a variety of active and passive methods of loading with therapeutic material.[20]

Another commonly used method to encapsulate both chemotherapeutic and radiotherapeutic agents into liposomes is the pH gradient method. In the presence of a liposomal pH gradient, the concentration of ammonium is higher in the aqueous core than outside of the liposome, allowing for the trapping of radionuclides in the liposomes. Many anti-cancer chemotherapeutic liposomes have also used the pH gradient method to load drugs into liposomes.[17] The pH gradient loading method can also be used for entrapment of radionuclides. Bao *et al*.[21] first reported that rhenium and technetium radionuclides were transported through the liposome lipid bilayer and trapped within the interior of the liposome based on the pH gradient in the interior of the liposome.[21] In this method, the radionuclide chelator *N*,*N*-bis(2-mercaptoethyl)-*N*′,*N*′-diethylethylenediamine (BMEDA) can be used to transport ^{99m}Tc through the lipid bilayer of the liposome. The complex can then be entrapped in the liposomes with the aid of pH gradient as the aqueous and acidic core of the liposome results in the amino groups of this complex becoming protonated and thus entrapped.[21] In summary, a broad spectrum of techniques can be used to load radionuclides into liposomes, demonstrating the unique versatility that liposomes offer in their preparation and function.

6. Diagnostic applications of radionuclide-containing liposomes

Liposomes labeled with the most commonly used single photon agent, ^{99m}Tc, were shown by Goins *et al.* to be useful for detecting sites of cancer, sites of infection, and inflammation.[22,23] Investigators from the Netherlands have also shown the potential application of ^{99m}Tc liposomes in detecting sites of infection and inflammation.[24] Liposomes accumulate at sites of infection in the same manner they accumulate in tumors following intravenous administration, by the EPR mechanism. An example of this EPR-type accumulation in salivary gland infection is shown in Figure 2 where rats became infected with a sialodacryoadenitis virus, a type of coronavirus that infects rodents.

In Figure 2, a significant accumulation of liposomes can be seen in the left salivary gland (upper arrow) of the rat due to the enhanced permeability caused by the infection. The control rat shows no significant uptake in the salivary gland. The liposomes in the infected rat were most likely phagocytosed by neutrophils and macrophages at the site of the coronavirus infection. The hollow arrows, denoting the abdominal area, show the normal uptake of liposomes by the macrophages located within the spleen in both the control rat and in the rat infected with coronavirus. These images show the potential of liposomes for the delivery of anti-viral agents to sites of coronavirus infection.

Radiolabeled liposomes have also been shown to be useful for the diagnostic location of sentinel lymph nodes.[25] The sentinel lymph node is the first lymph node that cancer cells encounter when they metastasize from a cancerous site in the body. Localizing the sentinel lymph node and removing it for pathological examination is important.

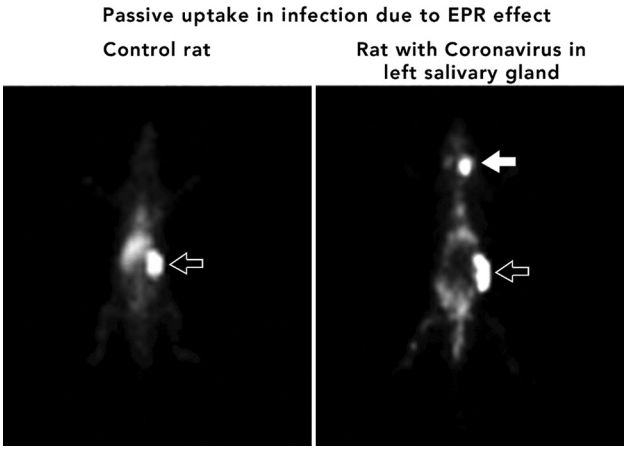

Figure 2. Scintigraphic imaging of the accumulation of ^{99m}Tc-radiolabeled liposomes in an area of infection. Significant uptake can be visualized in the infected salivary gland (white arrow) and normal uptake of liposome is visualized in the spleen in both control rat and the rat with coronavirus infection.
Abbreviation: EPR: Enhanced permeability and retention effect.

A novel method of trapping liposomes in sentinel lymph nodes was developed by Zavaleta *et al.*[26] In this method, ^{99m}Tc-radiolabeled liposomes were coated with biotin and simultaneously injected with avidin around a tumor. Their results showed both the biotin and avidin aggregating as they moved toward the sentinel lymph node and became entrapped. In this example, the ^{99m}Tc-liposomes also had encapsulated blue dye to guide the surgeon's radio-detection probe. The blue dye served as a visual guide, staining the lymph node for the surgeon. The multiple modifications of the diagnostic liposomes in this sentinel node application demonstrate the flexibility of the liposomal system for diagnostic imaging.[25,26]

In addition to labeling liposomes with single photon agents like ^{99m}Tc, liposomes can be radiolabeled with PET agents. PET has a higher resolution for imaging and it is inherently tomographic, enabling 3D localization. Liposomes have been radiolabeled with zirconium-89 (^{89}Zr) to detect uptake in atherosclerotic vessel walls.[27] This diagnostic PET imaging would aid in the development of liposome therapy for atherosclerotic disease as it would serve as an effective tool to screen for liposome targeting in individual subjects' plaques.

Liposomes also have great potential for carrying PET agents for diagnosis and localization of cancer. Liposomes radiolabeled with the radionuclide, ^{64}Cu, have been developed to image and treat tumors overexpressing epidermal growth factor receptor (EGRF).[28] The ^{64}Cu-labeled liposome is targeted to the tumor by an antibody inserted into the liposome by incubation with a micelle containing an anti-EGRF antibody. Because the ^{64}Cu-radionuclide carried by the liposomes emits both positrons for imaging and beta particles for radionuclide therapy, this ^{64}Cu-radiolabeled liposome is considered a theranostic agent. Such agents can be imaged to verify that the cancer has been successfully targeted, while simultaneously delivering therapeutic radiation to kill the tumor. Theranostic liposomal agents have great potential for improving the treatment of tumors that have, to date, been poorly responsive to therapy such as pancreatic cancer. A recent review has been published of theranostic liposomes and other nanoparticles for the treatment of pancreatic cancer.[28]

7. Intracavitary administration of liposomes

The biotin-avidin system has also been used for trapping liposomes within intracavitary locations such as the

peritoneum. Therapeutic liposomes are cleared from the peritoneal cavity at a slower rate compared to free chemotherapy drugs. Zavaleta *et al*.[26] developed a method of further increasing the retention of therapeutic liposomes with peritoneal administration. The liposomes developed by the group were coated in biotin, and avidin was injected into subjects after intraperitoneal administration of the biotin-coated liposomes. This was reported to cause aggregation of the liposomes with crosslinking of avidin with biotin-coated liposomes. This led to the retention of liposomes in the peritoneal cavity and in the lymph nodes that drain the peritoneal cavity. These lymph nodes are likely to contain metastatic cancer cells.[26]

8. Liposomes and the immune system

The human body typically perceives drug capsules as foreign material, which catalyzes an immune response. Consequently, liposomes have shown high rates of interaction with cells of the mononuclear phagocyte system (MPS). Due to this, many studies have shown that liposomes naturally accumulate in parts of the immune system, such as the liver and spleen.[29] This phenomenon is a common challenge with all types of liposomes carrying radionuclides, so strategies for avoiding clearance by the MPS and accumulation of liposomes in the liver and spleen should be explored to enhance the therapeutic performance of radionuclide-carrying liposomes. Kelly *et al*.[29] describe how the uptake of liposomes by the MPS can be affected by liposome size, charge, and the incorporation of ligands into the liposomal structure. Specifically, smaller liposomes have shown lower rates of clearance by the MPS because there is a decreased risk of opsonization by plasma proteins present in the blood. It has also been shown that liposomes with a high electrostatic charge are more likely to be cleared by the MPS system.[29]

Umeda *et al*.[30] recently described a method to decrease the accumulation of liposome-targeted diagnostic or radiotherapeutic nuclides in the MPS.[30] In their research, a therapeutic radionuclide was chelated to ethylenedicysteine, which cleared much more rapidly from normal liver and spleen compared to a conventional radiochelated molecule. Their method showed good retention in a targeted tumor. The rapid clearance from the MPS allowed for improved diagnostic imaging, and based on distribution studies should greatly decrease radiation exposure to the MPS of the liver and spleen while still delivering a high dose to the tumor.

The high accumulation of standard liposome formulations within the MPS can also be a potential advantage. La-Beck *et al*.[31] suggest how the uptake of liposomes by the MPS could be used to deliver imaging agents to sentinel lymph nodes after injection into interstitial or subcutaneous spaces around the tumor.[31] Sites of infection, cancer, inflammation, cardiovascular disease, cerebral ischemia, and stroke tend to have significantly higher levels of macrophages/mononuclear cells that are part of the MPS. Therefore, the clearance of liposomes by the MPS, while sometimes seen as a disadvantage, could also be used to target certain sites that have abnormally elevated levels of macrophages present. It has been shown that an increased number of macrophages within the tumor, tumor-associated macrophages, is associated with a decreased prognosis.[32] Radiolabeled liposomes are ideally suited for targeting tumors associated with macrophages since liposomes are highly phagocytosed by macrophages. This ideal fit of nanomedicine for targeting tumor-associated macrophages has been noted by other investigators.[33]

One way to limit the uptake of liposomes by the MPS is to alter their membrane. The liposome membrane can be masked with chemicals such as polyethylene glycol (PEG) to imitate the membranes of red blood cells, which reduces recognition by the MPS and increases the circulation time of liposomes.[34,35] A longer circulation time and greater levels of accumulation in tumors have been seen with PEG-liposomes. Unfortunately, the strategy of "PEGylation" does not appear to prevent a high uptake of liposomes by the liver and spleen compared to other parts of the body.[18] It is the "PEGylated" liposomes that are used in the previously mentioned FDA-approved drug, Doxil®.[36]

Beyond the MPS, liposomes can also be affected by high-density lipoprotein (HDL) and low-density lipoprotein (LDL) present in the blood. Interaction with these lipoproteins can warp liposomal structure and cause undesirable instability in the bloodstream. However, it has been shown that the addition of cholesterol to the structure of the liposomes offers greater levels of stability. It has been shown that the inclusion of cholesterol in liposomal structure inhibits liposomes from being turned into HDL or LDL. Furthermore, molecules can be attached to liposomal membranes when anchored by cholesterol.[37]

9. Liposomes that allow for triggered release

Liposomes can be modified to offer higher levels of control with timed release of internal contents. Ta and Porter[38] constructed thermosensitive liposomes that can remain stable until triggered by externally controlled heat to release their internal contents. Higher temperatures have also been shown to dilate gaps in tumor vasculature, so selective heating of cancerous regions can further increase the tendency of liposomes to leak out of blood vessels into

tumor microenvironments as opposed to extravasation into healthy areas.[38] Stolarz *et al.*[39] developed a type of liposome that offers control of release through X-ray irradiation. The experiment utilized the fact that chloral hydrate releases free protons after exposure to X-rays by incorporating it into the liposomal structure. The study showed that the treatment of tumors with liposomes paired with radiation showed more intense therapeutic effects compared to either the liposomes or radiation alone.

Prabhakar *et al.*[40] reported that the performance of liposomal drug delivery can be enhanced by directing ultrasonic waves toward a tumor during treatment with intravenously administered liposomes. Specifically, the ultrasound waves created holes known as "sonophoresis" in the membranes of cancerous cells, which increased cellular uptake of chemotherapy drugs that were carried by liposomes.[40]

These concepts are examples of ways liposomes can be used for the controlled release of chemotherapeutic drugs to create safer forms of diagnosis or treatment of cancerous tumors. While these same effects do not apply to the encapsulation of radionuclides, optimizing the performance of chemotherapy-carrying liposomes as an adjuvant treatment to radiotherapy can be considered a way to maximize the effects of treatment.

10. Convection-enhanced drug delivery with liposomes

Another method of liposome administration is through "convection-enhanced delivery (CED)" for the local treatment of tumors. Convection, in this particular application, refers to the pressure applied to a catheter from a syringe pump where the catheter has been inserted directly into the tumor. Constant pressure is applied to the injected fluid that is carrying liposomes. This method results in the convective spread of liposomes throughout the tumor. The technique has been shown to increase the volume of distribution of *liposomes* throughout the tumor and to create a more even distribution in the tumor region compared to CED distribution of radiolabeled *small molecules* as shown in Figure 3.

Figure 3 shows nuclear images of two solid animal tumors. Radiolabeled liposomes (120 nm in diameter), as shown in the left panel, were injected through CED, whereas small radiolabeled molecules (not liposomes; 3 nm in diameter), as shown in the right panel, were injected through CED. The radiolabeled *liposomes* were pushed by convective force through the tumor interstitial spaces, dispersing throughout the tumor. The *small molecules* were absorbed directly into the blood capillaries and remained focused in one area. The liposomes, due to their extreme pliability, were able to squeeze through and into the tight interstitial spaces, boring deep within the tumor. Liposomes appear to have particular advantages for this type of local convective delivery as compared to other types of solid nanoparticles due to their deformable and flexible membranes. A recent study has shown that CED-administered liposomes can move and spread throughout solid tumors much better than CED-administered rigid, solid nanoparticles.[41] Therefore, CED-administered liposomes can penetrate a significantly greater amount of tumor tissue following direct infusion into a tumor.

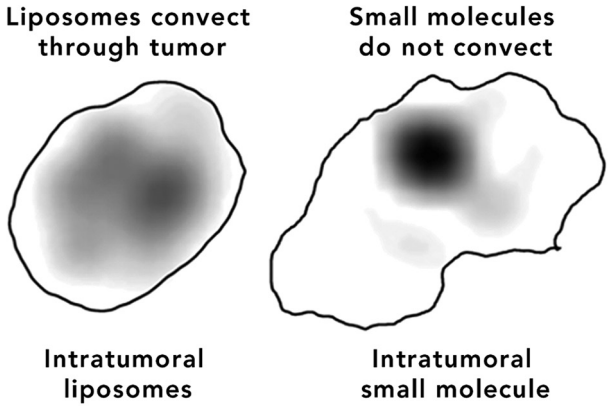

Figure 3. Animal tumors treated with radiolabeled liposomes versus small radiolabeled molecules both delivered by convection-enhanced delivery. Figure created by the authors.

CED provides an important advantage for delivering liposome-carried drugs and radionuclides into tumors. It also allows for increased delivery of liposomes to the central regions of tumors, which are less likely to come in contact with intravenously injected therapeutic nanocapsules in poorly vascularized tumors.[42,43] Recent articles have shown that patient-specific optimization of the CED treatment of recurrent glioblastoma with liposomes containing the theranostic radionuclide rhenium-186 (^{186}Re) greatly improves treatment.[44,45] ^{186}Re is inherently theranostic because it simultaneously emits an ideal energy photon for diagnostic nuclear imaging and an ideal energy beta particle with a 2 mm path length for cancer therapy.

CED takes advantage of the nanosize of the liposomes in the range of 100 nm and their lipid membrane deformability, which allows the liposomes to move through the tumor without being rapidly absorbed at the point of injection, as shown in Figure 3. ^{186}Re attached to a small molecule does not convect through a tumor and only covers a small portion of the tumor, whereas ^{186}Re-labeled liposomes can be pushed through the interstitial spaces of the tumors by convection resulting in much better coverage of the tumor.

11. Studies of therapeutic applications of radionuclide-containing liposomes

At present, ^{186}Re-labeled liposomes, known as ^{186}Re-obisbemeda, have completed Phase I clinical trials for recurrent glioblastoma through CED and are currently in Phase II trials.[46] In Phase I studies, much higher radiation doses were safely delivered to the glioblastoma (~300 Gy), versus standard external beam radiation therapy (~70 – 80 Gy). Phillips *et al.*[43] described how future studies using nuclear imaging to monitor the performance of CED will be crucial for developing safe CED-administered liposome radionuclide therapy.

^{186}Re-obisbemeda is also currently in a Phase I study for the treatment of leptomeningeal metastasis that commonly occurs in patients with breast cancer, prostate cancer, and brain cancer.[47] In this treatment, the ^{186}Re-obisbemeda is administered into an Ommaya reservoir, which connects to the central spinal fluid (CSF), allowing the ^{186}Re-obisbemeda to spread throughout the brain and spinal CSF to deliver high doses of radiation to the leptomeningeal metastasis.

Chang *et al.*[48] have shown the therapeutic potential of intravenously injected ^{188}Re-liposomes for the treatment of a variety of tumors including colorectal cancer, head and neck cancer, and ovarian cancer.[48] Li *et al.*[19] have also used peptide-targeted liposomes to treat cervical cancer with iodine-131-containing liposomes.[19]

12. Future steps and considerations

While liposomes have shown promising qualities as nanocapsules for increasing the efficiency of cancer chemotherapy and radionuclide-based radiotherapy, some challenges remain. The prominent uptake of liposomes by the MPS following intravenous delivery limits the delivery of treatment to the cancerous area. It can also cause damage to sites of uptake in the MPS, such as the bone marrow, in addition to the liver and spleen. The high MPS uptake of liposomes including those coated with PEG is one of the most significant obstacles posed by liposomal drug delivery, and it should be an area of focus for researchers to find ways to avoid clearance of liposomes by the MPS. The development of techniques such as PEGylation is a step in the right direction. Other approaches to avoid uptake by the MPS include delivery of radiotherapeutic liposomes to body cavities and subcutaneously for trapping in lymph nodes containing metastatic cancer cells.[26,49]

13. Conclusion

Liposomes are very versatile structures that can be modified in countless ways to suit the purpose they are intended to fulfill. They have many promising applications in radiology, nuclear medicine diagnostics, and radionuclide therapy. The ultimate goal for liposomal therapy is the mitigation of toxic side effects and increased accumulation of chosen substances to targeted sites in a selective manner. Different methods of radiolabeling can be used to attach various types of radionuclides to liposomes for both diagnostic and therapeutic purposes. The EPR effect with liposomes gives them an intrinsic advantage for passive targeting of tumor regions. Additional methods of active targeting can be taken to intensify selectivity. A significant obstacle for liposomal drug delivery is posed by uptake by the MPS system; however, if uptake in the liver, spleen, and bone marrow can be avoided, uptake of liposomes by macrophages within the tumor or in an infectious site can be an advantage. While treatment using liposomes comes with complications that should be carefully considered, they have already made a positive impact on patients' lives through FDA-approved liposomal drugs. The imaging of radiolabeled liposomes offers great potential to non-invasively track the delivery of drugs to targeted sites in the body. In addition, liposomes carrying therapeutic radionuclides have great potential for cancer therapy and are currently used in clinical trials for recurrent glioblastoma and leptomeningeal metastasis.

Acknowledgments

The authors thank Jonathan Sumner of UT Health San Antonio Creative Media Services for his help formatting the images in the article. The authors would also like to thank Dr. Jayanta K. Chaudhuri for technical support during the writing of this article.

Funding

None.

Conflict of interest

The authors declare they have no competing interests.

Author contributions

Conceptualization: Rashmi Basu
Visualization: Rashmi Basu
Writing – original draft: Rashmi Basu, William T. Phillips
Writing – review & editing: All authors

Ethics approval and consent to participate

Not applicable.

Consent for publication

Not applicable.

Availability of data

Not applicable.

References

1. Khan NU, Chengfeng X, Jiang MQ, *et al.* α-Lactalbumin based scaffolds for infected wound healing and tissue regeneration. *Int J Pharm*. 2024;663:124578.

   doi: 10.1016/j.ijpharm.2024.124578

2. Khan NU, Chengfeng X, Jiang MQ, *et al*. Obstructed vein delivery of ceftriaxone via poly(vinyl-pyrrolidone)-iodine-chitosan nanofibers for the management of diabetic foot infections and burn wounds. *Int J Biol Macromol*. 2024;277:134166.

   doi: 10.1016/j.ijbiomac.2024.134166

3. Park H, Otte A, Park K. Evolution of drug delivery systems: From 1950 to 2020 and beyond. *J Control Release*. 2022;342:53-65.

   doi: 10.1016/j.jconrel.2021.12.030

4. Coelho JF, Ferreira PC, Alves P, *et al*. Drug delivery systems: Advanced technologies potentially applicable in personalized treatments. *EPMA J*. 2010;1(1):164-209.

   doi: 10.1007/s13167-010-0001-x

5. Bozzuto G, Molinari A. Liposomes as nanomedical devices. *Int J Nanomedicine*. 2015;10:975-999.

   doi: 10.2147/ijn.S68861

6. Gu W, Andrews GP, Tian Y. Recent clinical successes in liposomal nanomedicines. *Int J Drug Discov Pharmacol*. 2023;2(1):52-59.

   doi: 10.53941/ijddp.0201009

7. He H, Yuan D, Wu Y, Cao Y. Pharmacokinetics and pharmacodynamics modeling and simulation systems to support the development and regulation of liposomal drugs. *Pharmaceutics*. 2019;11(3):110.

   doi: 10.3390/pharmaceutics11030110

8. Nsairat H, Khater D, Sayed U, Odeh F, Al Bawab A, Alshaer W. Liposomes: Structure, composition, types, and clinical applications. *Heliyon*. 2022;8(5):e09394.

   doi: 10.1016/j.heliyon.2022.e09394

9. Low HY, Yang CT, Xia B, He T, Lam WWC, Ng DCE. Radiolabeled liposomes for nuclear imaging probes. *Molecules*. 2023;28(9):3798.

   doi: 10.3390/molecules28093798

10. Hagtvet E, Røe K, Olsen DR. Liposomal doxorubicin improves radiotherapy response in hypoxic prostate cancer xenografts. *Radiat Oncol*. 2011;6:135.

    doi: 10.1186/1748-717x-6-135

11. Head HW, Dodd GD 3rd, Bao A, *et al.* Combination radiofrequency ablation and intravenous radiolabeled liposomal Doxorubicin: Imaging and quantification of increased drug delivery to tumors. *Radiology*. 2010;255(2):405-414.

    doi: 10.1148/radiol.10090714

12. Riccardi D, Baldino L, Reverchon E. Liposomes, transfersomes and niosomes: Production methods and their applications in the vaccinal field. *J Transl Med*. 2024;22(1):339.

    doi: 10.1186/s12967-024-05160-4

13. Shan H, Sun X, Liu X, *et al.* One-step formation of targeted liposomes in a versatile microfluidic mixing device. *Small*. 2022;19(7):e2205498.

    doi: 10.1002/smll.202205498

14. Fang J, Nakamura H, Maeda H. The EPR effect: Unique features of tumor blood vessels for drug delivery, factors involved, and limitations and augmentation of the effect. *Adv Drug Deliv Rev*. 2011;63(3):136-151.

    doi: 10.1016/j.addr.2010.04.009

15. Fulton MD, Najahi-Missaoui W. Liposomes in cancer therapy: How did we start and where are we now. *Int J Mol Sci*. 2023;24(7):6615.

    doi: 10.3390/ijms24076615

16. Man F, Gawne PJ, de Rosales RTM. Nuclear imaging of liposomal drug delivery systems: A critical review of radiolabelling methods and applications in nanomedicine. *Adv Drug Deliv Rev*. 2019;143:134-160.

    doi: 10.1016/j.addr.2019.05.012

17. Goins B, Bao A, Phillips WT. Techniques for loading technetium-99m and rhenium186/188 radionuclides into preformed liposomes for diagnostic imaging and radionuclide therapy. *Methods Mol Biol*. 2017;1522:155-178.

    doi: 10.1007/978-1-4939-6591-5_13

18. Poletto G, Evangelista L, Venturini F, *et al.* Nanoparticles and radioisotopes: A long story in a nutshell. *Pharmaceutics*. 2022;14(10):2024.

    doi: 10.3390/pharmaceutics14102024

19. Li W, Sun D, Li N, Shen Y, Hu Y, Tan J. Therapy of cervical cancer using ^{131}I-labeled nanoparticles. *J Int Med Res*. 2018;46(6):2359-2370.

    doi: 10.1177/0300060518761787

20. Liu P, Chen G, Zhang J. A review of liposomes as a drug delivery system: Current status of approved products, regulatory environments, and future perspectives. *Molecules*. 2022;27(4):1372.

    doi: 10.3390/molecules27041372

21. Bao A, Goins B, Klipper R, Negrete G, Phillips WT. 186Re-liposome labeling using 186Re-SNS/S complexes:

In vitro stability, imaging, and biodistribution in rats. *J Nucl Med*. 2003;44(12):1992-1999.

22. Goins B, Klipper R, Rudolph AS, Cliff RO, Blumhardt R, Phillips WT. Biodistribution and imaging studies of technetium-99m-labeled liposomes in rats with focal infection. *J Nucl Med*. 1993;34(12):2160-2168.

23. Goins B, Klipper R, Rudolph AS, Phillips WT. Use of technetium-99m-liposomes in tumor imaging. *J Nucl Med*. 1994;35(9):1491-1498.

24. Boerman OC, Rennen H, Oyen WJ, Corstens FH. Radiopharmaceuticals to image infection and inflammation. *Semin Nucl Med*. 2001;31(4):286-295.

doi: 10.1053/snuc.2001.26189

25. Phillips WT, Klipper R, Goins B. Use of (99m)Tc-labeled liposomes encapsulating blue dye for identification of the sentinel lymph node. *J Nucl Med*. 2001;42(3):446-451.

26. Zavaleta CL, Goins BA, Bao A, McManus LM, McMahan CA, Phillips WT. Imaging of 186Re-liposome therapy in ovarian cancer xenograft model of peritoneal carcinomatosis. *J Drug Target*. 2008;16(7):626-637.

doi: 10.1080/10611860802230372

27. Lobatto ME, Binderup T, Robson PM, *et al.* Multimodal positron emission tomography imaging to quantify uptake of ^{89}Zr-labeled liposomes in the atherosclerotic vessel wall. *Bioconjug Chem*. 2019;31(2):360-368.

doi: 10.1021/acs.bioconjchem.9b00256

28. Jeong HY, Kang SJ, Kim MW, *et al.* Development of PET radioisotope copper-64-labeled theranostic immunoliposomes for EGFR overexpressing cancer-targeted therapy and imaging. *Int J Mol Sci*. 2024;25(3):1813.

doi: 10.3390/ijms25031813

29. Kelly C, Jefferies C, Cryan SA. Targeted liposomal drug delivery to monocytes and macrophages. *J Drug Deliv*. 2011;2011:727241.

doi: 10.1155/2011/727241

30. Umeda IO, Koike Y, Ogata M, *et al*. New liposome-radionuclide-chelate combination for tumor targeting and rapid healthy tissue clearance. *J Control Release*. 2023;361:847-855.

doi: 10.1016/j.jconrel.2023.07.060

31. La-Beck NM, Liu X, Wood LM. Harnessing liposome interactions with the immune system for the next breakthrough in cancer drug delivery. *Front Pharmacol*. 2019;10:220.

doi: 10.3389/fphar.2019.00220

32. Li C, Xu X, Wei S, Jiang P, Xue L, Wang J. Tumor-associated macrophages: Potential therapeutic strategies and future prospects in cancer. *J Immunother Cancer*. 2021;9(1):e001341.

doi: 10.1136/jitc-2020-001341

33. Andón FT, Digifico E, Maeda A, *et al*. Targeting tumor associated macrophages: The new challenge for nanomedicine. *Semin Immunol*. 2017;34:103-113.

doi: 10.1016/j.smim.2017.09.004

34. Nosova AS, Koloskova OO, Nikonova AA, *et al.* Diversity of PEGylation methods of liposomes and their influence on RNA delivery. *Medchemcomm*. 2019;10(3):369-377.

doi: 10.1039/c8md00515j

35. Klibanov AL, Maruyama K, Torchilin VP, Huang L. Amphipathic polyethyleneglycols effectively prolong the circulation time of liposomes. *FEBS Lett*. 1990;268(1): 235-237.

doi: 10.1016/0014-5793(90)81016-h

36. Gabizon A, Shmeeda H, Barenholz Y. Pharmacokinetics of pegylated liposomal doxorubicin: Review of animal and human studies. *Clin Pharmacokinet*. 2003;42(5): 419-436.

doi: 10.2165/00003088-200342050-00002

37. Rommasi F, Esfandiari N. Liposomal nanomedicine: Applications for drug delivery in cancer therapy. *Nanoscale Res Lett*. 2021;16(1):95.

doi: 10.1186/s11671-021-03553-8

38. Ta T, Porter TM. Thermosensitive liposomes for localized delivery and triggered release of chemotherapy. *J Control Release*. 2013;169(1-2):112-125.

doi: 10.1016/j.jconrel.2013.03.036

39. Stolarz AJ, Chhetri BP, Borrelli MJ, *et al.* Liposome formulation for tumor-targeted drug delivery using radiation therapy. *Int J Mol Sci*. 2022;23(19):11662.

doi: 10.3390/ijms231911662

40. Prabhakar A, Banerjee R. Nanobubble liposome complexes for diagnostic imaging and ultrasound-triggered drug delivery in cancers: A theranostic approach. *ACS Omega*. 2019;4(13):15567-15580.

doi: 10.1021/acsomega.9b01924

41. Amirrashedi M, Jensen AI, Tang Q, *et al.* The influence of size on the intracranial distribution of biomedical nanoparticles administered by convection-enhanced delivery in minipigs. *ACS Nano.* 2024;18(27):17869-17881.

doi: 10.1021/acsnano.4c04159

42. Phillips WT, Goins B, Bao A, *et al.* Rhenium-186 liposomes as convection-enhanced nanoparticle brachytherapy for treatment of glioblastoma. *Neuro Oncol*. 2012;14(4): 416-425.

doi: 10.1093/neuonc/nos060

43. Phillips WT, Bao A, Brenner AJ, Goins BA. Image-guided interventional therapy for cancer with radiotherapeutic

nanoparticles. *Adv Drug Deliv Rev*. 2014;76:39-59.

doi: 10.1016/j.addr.2014.07.001

44. Christenson C, Wu C, Hormuth DA 2nd, Huang S, Bao A, Brenner A, Yankeelov TE. Predicting the spatio-temporal response of recurrent glioblastoma treated with rhenium-186 labelled nanoliposomes. *Brain Multiphys*. 2023;5:100084.

    doi: 10.1016/j.brain.2023.100084

45. Wu C, Hormuth DA 2nd, Christenson CD, *et al.* Image-guided patient-specific optimization of catheter placement for convection-enhanced nanoparticle delivery in recurrent glioblastoma. *Comput Biol Med*. 2024;179:108889.

    doi: 10.1016/j.compbiomed.2024.108889

46. Brenner A, Michalek J, Moore M, *et al.* Update report of the RESPECT-GBM phase I/IIA dose escalation trial of rhenium-186 nanoliposome (^{186}RNL) in recurrent glioma [RGBM] via Convection Enhanced Delivery (CED). *Neuro Oncol*. 2023;25:v86.

    doi: 10.1093/neuonc/noad179.0332

47. Brenner A, Youssef M, LaFrance N, *et al.* LOCL-04 safety and feasibility of rhenium-186 nanoliposome (^{186}rnl) in leptomeningeal metastases [lm] phase 1/2a dose escalation trial. *Neurooncol Adv*. 2022;4(Suppl 1):i12.

    doi: 10.1093/noajnl/vdac078.046

48. Chang CH, Chang MC, Chang YJ, Chen LC, Lee TW, Ting G. Translating research for the radiotheranostics of nanotargeted ^{188}re-liposome. *Int J Mol Sci*. 2021;22(8):3868.

    doi: 10.3390/ijms22083868

49. Phillips WT, Klipper R, Goins B. Novel method of greatly enhanced delivery of liposomes to lymph nodes. *J Pharmacol Exp Ther*. 2000;295(1):309-313.

ACCSCIENCE PUBLISHING

Advances in Radiotherapy & Nuclear Medicine

REVIEW ARTICLE

^{68}Ga-PSMA PET CT/MRI in the initial diagnosis and staging of prostate cancer: A review

Oluwatobi I. Akinmuleya[1,2], Philip F. Cohen[3], and Kalevi Kairemo[4,5]*

[1]Department of Medicine, Faculty of Medicine, Shenyang Medical College, Liaoning, Shenyang, China

[2]Department of Medicine, Greater Accra Regional Hospital, Ghana

[3]Department of Nuclear Medicine, Lions Gate Hospital, North Vancouver, Canada

[4]Department of Theranostics, Docrates Cancer Center, Helsinki, Finland

[5]Department of Nuclear Medicine, The University of Texas MD Anderson Cancer Center, Houston, Texas, United States of America

Abstract

Prostate-specific membrane antigen-positron emission tomography (PSMA-PET) imaging has demonstrated potential in addressing prostate cancer (PCa) diagnostic difficulties. According to current guidelines, gallium-68 (^{68}Ga)-PSMA-PET is used as an adjunct to traditional imaging modalities in patients with primary PCa. The purpose of this review, conducted using Preferred Reporting Items for Systematic Review and Meta-Analysis (PRISMA) guidelines, is to give an overview of studies that have examined the role of ^{68}Ga-PSMA in the initial diagnosis of PCa, its performance in TNM staging, its correlation with prostate-specific antigen (PSA) levels, targeted biopsies, and the International Society of Urological Pathology (ISUP) scores using computed tomography (CT) or magnetic resonance imaging (MRI). The findings demonstrate that, in addition to MRI alone, combining ^{68}Ga-PSMA-PET with MRI-targeted biopsy improves the initial identification of clinically significant prostate cancer (csPCa), particularly for ambiguous prostate imaging-reporting and data system (PI-RADS) three lesions. ^{68}Ga-PSMA-PET/CT is useful when MRI results for csPCa are uncertain, but consistent techniques are required. Regarding risk assessment and therapy planning, ^{68}Ga-PSMA-PET has a strong correlation with both PSA levels and ISUP scores. It accurately detects primary PCa lesions, making it suitable for high-risk patients. In ^{68}Ga-PSMA-PET, higher maximum standardized uptake value (SUV_{max}) readings are linked to more aggressive illness. For N and M staging, ^{68}Ga-PSMA-PET/CT is more sensitive and specific than conventional imaging; however, for T-staging, multiparametric MRI (mpMRI) provides better accuracy. ^{68}Ga-PSMA-PET/MRI shows improved accuracy for primary PCa detection compared to mpMRI alone. Challenges include the lack of standardized SUV_{max} cutoff values. ^{68}Ga-PSMA-PET is useful for the initial diagnosis and staging of PCa, complementing MRI, although further research is needed to standardize imaging techniques and interpretations.

Keywords: Prostate cancer; PSMA; Radionuclide; PET/CT; PET/MRI; Primary diagnosis; Clinically significant cancer

***Corresponding author:**
Kalevi Kairemo
(kalevi.kairemo@gmail.com)

Citation: Akinmuleya OI, Cohen PF, and Kairemo K. ^{68}Ga-PSMA PET CT/MRI in the initial diagnosis and staging of prostate cancer: A review. *Adv Radiother Nucl Med*. 2024;2(4):4590.
doi: 10.36922/arnm.4590

Received: August 20, 2024

Accepted: September 23, 2024

Published Online: December 16, 2024

1. Introduction

Prostate cancer (PCa) is the second most commonly diagnosed cancer among men globally,[1] necessitating effective early detection and accurate staging for optimal patient management. According to current guidelines, conventional imaging remains the primary method for imaging primary PCa.[2] However, recent advancements in imaging technology have introduced multiparametric magnetic resonance imaging (mpMRI) and prostate-specific membrane antigen positron emission tomography (PSMA-PET), have greatly improved the diagnosis of PCa.[3,4] While mpMRI is valuable, it has drawbacks, including moderate specificity, variable negative predictive values coupled with interpretation variability, which highlights the necessity for supplementary imaging modalities.[5-7]

Gallium-68 (^{68}Ga)-PSMA-PET has emerged as a promising tool for the initial diagnosis of PCa, particularly noted for its high sensitivity and specificity in detecting both primary and recurrent disease.[4] Recent studies demonstrate that ^{68}Ga-PSMA-PET surpasses conventional imaging techniques in staging primary PCa and offers additional diagnostic benefits.[8,9] This imaging modality is particularly effective in patients with intermediate-to high-risk PCa, offering improved accuracy in staging and potentially guiding more precise biopsies.[4] Unlike traditional methods, ^{68}Ga-PSMA-PET can identify PSMA-avid lesions, allowing for targeted biopsies that enhance tissue sampling accuracy and improve risk stratification.[10]

Comparative studies between ^{68}Ga-PSMA-PET and mpMRI have highlighted the relative strengths of each modality. ^{68}Ga-PSMA-PET shows promise not only in the initial diagnosis but also in correlating imaging findings with Gleason scores (GS) and providing detailed TNM staging. Its integration with mpMRI in PET/MRI studies leverages the anatomical features of MRI with the molecular imaging capabilities of ^{68}Ga-PSMA-PET, potentially offering a comprehensive approach to PCa diagnosis and staging.[11]

This review aims to investigate the role of ^{68}Ga-PSMA-PET in the initial diagnosis of PCa, its correlation with histopathology, and its performance in TNM staging. Furthermore, it will evaluate how ^{68}Ga-PSMA-PET compares to mpMRI, particularly in combined PET/MRI studies.

2. Materials and methods

2.1. Search strategy

A systematic review of the literature was conducted using PubMed to retrieve systematic reviews focusing on the role of ^{68}Ga-PSMA imaging in the initial diagnosis of PCa, its correlation with histopathology, and its performance in TNM staging, as well as its correlation with targeted biopsies in conjunction with simultaneous computed tomography (CT) or magnetic resonance imaging (MRI). The search was performed in accordance with the Preferred Reporting Items for Systematic Review and Meta-Analysis guidelines. The search terms included: ("Ga-68-PSMA-PET" OR "Gallium-68 PSMA PET" OR "^{68}Ga-PSMA-PET/CT" OR "prostate-specific membrane antigen PET") AND "systematic review."

2.2. Evidence synthesis

Using the systematic search strategy stated above, 110 articles were identified. On initial screening, 21 were not relevant to the research question, and three were editorial comments or consensus documents that were excluded from the study. From the remaining 86 articles, 67 were excluded for one or more of the following reasons: they lacked data relevant to the study outcomes, used alternative imaging agents other than ^{68}Ga-PSMA, or were not available for thorough review. Articles that contained information about ^{68}Ga-PSMA-PET were included in the study. Ultimately, 19 articles matched the inclusion criteria (Figure 1).

2.3. Data extraction

General details were retrieved for each study considered, such as generic data (authors and year of publication), patients' characteristics (number of patients), and diagnostic performance (type of imaging, sensitivity, and specificity).

3. Results

3.1. Initial diagnosis

The literature review by Satapathy *et al.*[12] noted that the ^{68}Ga-PSMA-PET has a high sensitivity (0.97) in the initial detection of PCa, but highlighted its moderate specificity (0.66) as a major drawback. Other studies in the literature review reported specificities ranging from 44.6% to 81.8%, with only one study reporting 100% specificity. A possible explanation for this variability could be the use of normal metabolic activity found in the prostate gland as the threshold for determining pet-positive lesions, as well as inter-observer variability in the way the imaging is performed and reported.[12,13]

A comprehensive review by Evangelista *et al.*[11] highlighted that integrated PET/MRI offers greater diagnostic value in locating PCa than either mpMRI or PET imaging alone. This conclusion was supported by several primary studies cited in the review.

The integration of ^{68}Ga-PSMA-PET with MRI-targeted biopsy has demonstrated enhanced initial diagnosis of

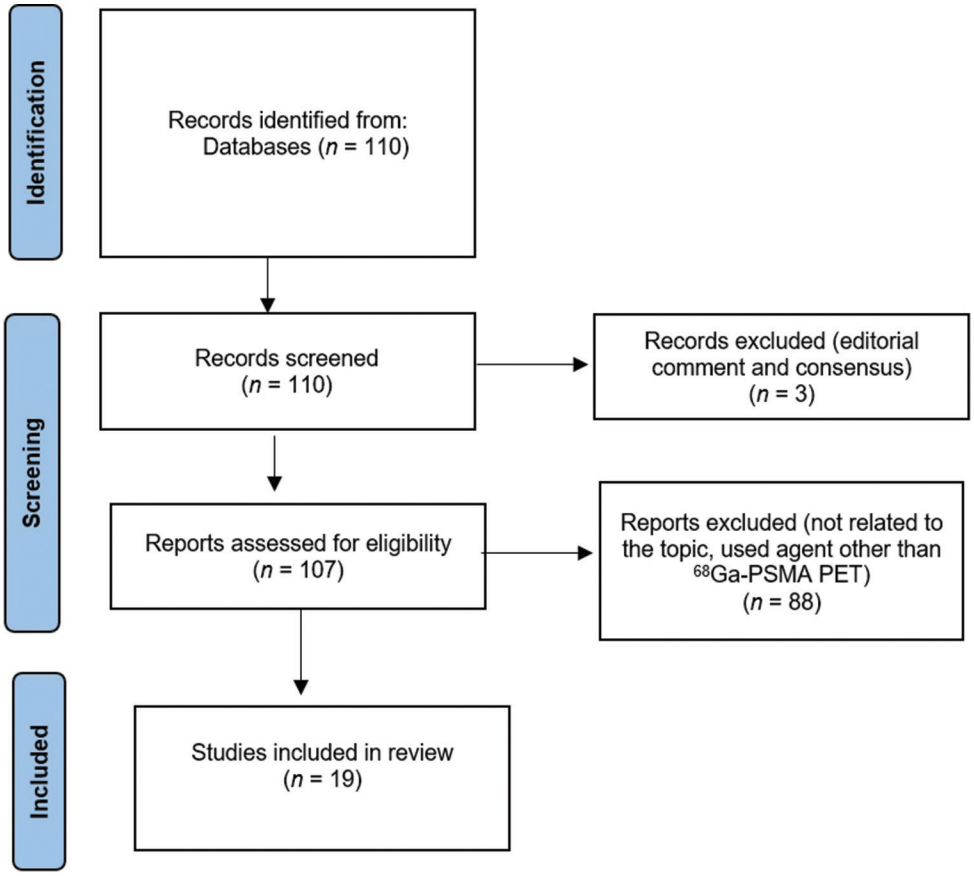

Figure 1. Schematic representation of PRISMA workflow for manuscript's selection
Abbreviations: PRISMA: Preferred reporting items for systematic reviews and meta-analyses; ^{68}Ga-PSMA-PET: Gallium-68-prostate-specific membrane antigen-positron emission tomography.

clinically significant prostate cancer (csPCa), particularly in ambiguous lesions such as prostate imaging-reporting and data system (PI-RADS) 3, offering added value beyond MRI alone.[10] In cases with equivocal MRI findings or suspicion of clinically significant disease, ^{68}Ga-PSMA-PET/CT has demonstrated promise as a non-invasive imaging modality for the initial diagnosis of PCa, complementing MRI.[14] Prospective trials have underscored the importance of ^{68}Ga-PSMA-PET in primary PCa diagnosis. However, a systematic review noted notable variability in imaging protocols and reporting methods, necessitating standardized reporting practices to enhance the broader applicability of trial results.[13]

^{68}Ga-PSMA-PET accuracy in detecting primary PCa lesions and its potential to aid in recurrence detection and staging make it a promising screening method, particularly when combined with other modalities like MRI.[15] ^{68}Ga-PSMA-PET demonstrates high diagnostic accuracy for primary prostatic lesions, with comparable sensitivity, specificity, and diagnostic odds ratios, supporting its incorporation into the initial workup of high-risk PCa patients.[16] Table 1 shows the summary of the main findings of the articles in this section.

3.2. Relation of PET findings with histopathology

PSMA, a type 2 transmembrane glycoprotein, is overexpressed in prostate tumors and correlates with elevated serum levels of prostate-specific antigen (PSA) and higher GS, indicating its potential as a biomarker for PCa severity and progression.[17,18] There is a significant association between the intensity of ^{68}Ga-PSMA uptake and GS in confirmed lesions suggesting that parameters such as maximum standardized uptake value (SUV_{max}) and SUV_{ratio} of the primary tumor could serve as predictors of csPCa.[14] Patients with higher levels of total PSA and GS tend to exhibit higher SUV_{max} values, indicating a potential association between tumor aggressiveness and SUV_{max}. Moreover, SUV_{max} values have been correlated with nodal involvement and primary tumor aggressiveness, providing valuable insights into disease prognosis and management strategies.[19]

Table 1. Summary of the main findings of articles about the role of ^{68}Ga-PSMA-PET in the initial diagnosis of prostate cancer

Author and year	Sample size	Sensitivity	Specificity	Conclusion
Kawada *et al.*[10]	497	0.89 (95% CI, 0.85 – 0.93)	0.56 (95% CI, 0.29 – 0.80)	^{68}Ga-PSMA-PET-TB shows promise but needs more validation in diagnosis.
Evangelista *et al.*[11]	2104	0.949 (95% CI, 0.875 – 0.986)	0.909 (95% CI, 0.437 – 0.789)	^{68}Ga-PSMA-PET shows promising accuracy in diagnosing primary prostate cancer.
Satapathy *et al.*[12]	389	0.97 (95% CI, 0.90 – 0.99)	0.66 (95% CI, 0.52 – 0.78)	^{68}Ga-PSMA-PET/CT is highly sensitive for initial diagnosis but with moderate specificity.
Caracciolo *et al.*[14]	1379	NR	NR	^{68}Ga PSMA-PET/CT is highly sensitive for initial prostate cancer diagnosis.

Abbreviations: ^{68}Ga-PSMA-PET-TB: Gallium-68-prostate-specific membrane antigen-positron emission tomography-targeted biopsy; CT: Computed tomography; CI: Confidence interval.

In a retrospective study by Pepe *et al.*[20], it was noted that an SUV_{max} >8 indicated the presence of csPCa with a false-positive rate of 4.8%. The use of ^{68}Ga-PSMA-PET demonstrates promising potential as a non-invasive diagnostic tool for PCa, showing strong correlation with GS and PSA levels for risk assessment and treatment planning.[21] The uptake of ^{68}Ga-PSMA on PET/CT is notably higher in individuals with PCa who have a GS of ≥8 or PSA levels of ≥10 ng/mL compared to those with GS ≤7 or PSA ≤10 ng/mL. This shows the potential of PET findings to reflect the aggressiveness and severity of PCa, as assessed by GS and PSA levels.[15] A review by Jiao *et al.*[19] has also shown that SUV_{max} values are significantly higher in patients with GS >7 or PSA >10 ng/mL compared to those with GS ≤7 or PSA ≤10 ng/mL. Table 2 shows the summary of the main findings of the articles in this section.

3.3. Performance in TNM staging

PSMA-PET imaging, particularly ^{68}Ga-PSMA-PET/CT, has emerged as a superior method for N and M staging in high-risk PCa patients, showing increased sensitivity and accuracy in detecting lymph nodes and distant metastases. In addition, ^{68}Ga-PSMA-PET demonstrates remarkable sensitivity in the early detection of PCa, surpassing conventional imaging techniques. The integration of ^{68}Ga-PSMA-PET/CT with clinical nomograms enhances the prediction of lymph node metastasis (LNM), potentially reducing unnecessary surgeries and improving nodal staging accuracy.[22-24] Moreover, ^{68}Ga-PSMA-PET exhibits moderate sensitivity and outstanding specificity in detecting seminal vesicle invasion (SVI) and extraprostatic extension (EPE) in newly diagnosed PCa patients undergoing radical prostatectomy. Studies comparing PET/MRI to PET/CT suggest that PET/MRI offers superior sensitivity in detecting SVI, potentially attributed to its multiparametric approach, while variability in imaging protocols underscores the need for standardized assessment criteria to enhance the accuracy of ^{68}Ga-PSMA-PET in local staging.[23,25] However, the analysis revealed comparable diagnostic accuracy for EPE detection between ^{68}Ga-PSMA-PET/MRI and ^{68}Ga-PSMA-PET/CT, with overlapping performance ranges.[23] While ^{68}Ga-PSMA-PET/CT capable in detecting smaller lesions, it is less accurate than mpMRI in T-staging, particularly in identifying EPE and SVI. SUV_{max} cutoff values ranging from 3.0 to 4.0 aid in differentiating PCa lesions, with ^{68}Ga-PSMA-PET showing greater correspondence with histopathology in detecting gross tumor volume compared to mpMRI.[26] For T staging, ^{68}Ga-PSMA-PET/MRI offers superior accuracy in identifying T3 PCa, particularly discerning EPE and SVI.[19]

Table 2. Summary of the main finding of the articles on the relation of ^{68}Ga-PSMA-PET to histopathology

Author and year	Parameter	Finding
Caracciolo *et al.*[14]	^{68}Ga PSMA-PET/CT	There is a high correlation between ^{68}Ga-PSMA-PET/CT and histopathology for clinically significant prostate cancer identification.
Sood *et al.*[15]	SUV_{max} in High-Risk Patients	Higher in patients with GS ≥8 or PSA level ≥10 ng/mL compared to those with GS
Zhao *et al.*[17], Wu *et al.*[18]	^{68}Ga-PSMA Expression	Overexpression in prostate tumors, associated with higher PSA levels and GS
Jiao *et al.*[19]	^{68}Ga-PSMA-PET	Higher SUV_{max} values in patients with GS > 7 or PSA > 10 ng/ml, correlation with nodal involvement and primary tumor aggressiveness
Hu *et al.*[21]	Gleason score	There is a close correlation between PSA levels and GS

Abbreviations: ^{68}Ga-PSMA-PET/CT: Gallium-68-prostate-specific membrane antigen-positron emission tomography/computed tomography; GS: Gleason scores; PSA: Prostate-specific antigen; SUV_{max}: Maximum standardized uptake value.

For the identification of LNM, analyses of diagnostic accuracy and detection rate indicate potentially better performance with ^{68}Ga-PSMA-PET/MRI compared to

^{68}Ga-PSMA-PET/CT.[11,23] A comprehensive review of 18 diagnostic test accuracy trials evaluating ^{68}Ga-PSMA-PET for primary lymph node staging in PCa reported superior sensitivity (59%) and specificity (93%) compared to conventional CT and MRI. Despite variations in diagnostic accuracy attributed to factors such as research design and technical aspects, these findings underscore the potential of ^{68}Ga-PSMA-PET as a valuable imaging tool for primary staging.[27] ^{68}Ga-PSMA-PET imaging, especially ^{68}Ga-PSMA-PET/CT, exhibits heightened sensitivity and specificity in detecting LNM compared to conventional methods, highlighting its potential utility in primary staging.[19,28]

^{68}Ga-PSMA-PET imaging outperforms conventional imaging in N and M staging for high-risk PCa patients, offering superior sensitivity and accuracy in detecting lymph nodes and distant metastases.[26] ^{68}Ga-PSMA-PET imaging demonstrates superior sensitivity and specificity compared to conventional imaging techniques such as bone scans, detecting additional metastases, including those missed by bone scans, with an additional 17.6% involvement of bone regions. In intermediate to high-risk PCa patients, ^{68}Ga-PSMA-PET reveals LNM in extrapelvic sites (M1a) in up to 36.0% of cases, highlighting its efficacy in identifying distant metastases, particularly in high-risk populations.[26] In a review by Jiao *et al.*[19], it was noted that ^{68}Ga-PSMA-PET/CT also demonstrates the same result stated above when compared to conventional imaging in detecting metastases with sensitivity of 96.2% and specificity of 99.1%. In addition, ^{68}Ga-PSMA-PET/CT can detect more undetected metastases, especially extrapelvic lesions, highlighting its utility in the M staging of PCa.[19]

3.4. Comparison with MRI and ^{68}Ga-PSMA-PET/MRI

MRI, a commonly used imaging modality in PCa staging, is limited by its reliance on morphological information and lymph node size criteria, resulting in low sensitivity in detecting LNM, thus necessitating more accurate alternatives.[18] Arising as a comprehensive imaging solution, ^{68}Ga-PSMA-PET/MRI combines precise visualization of local tumors through MRI with the sensitive detection of LNM and distant metastases through ^{68}Ga-PSMA-PET, although at a higher cost and requiring more intricate image analysis compared to PET/CT.[23] ^{68}Ga-PSMA-PET/MRI shows superior detection and accuracy in diagnosing recurrent PCa compared to ^{68}Ga-PSMA-PET/CT, offering clearer findings and improved localization of primary PCa compared to mpMRI and standalone PET.

^{68}Ga-PSMA-PET/MRI demonstrates higher accuracy than mpMRI alone in detecting primary PCa, offering improved sensitivity and specificity. In addition, combining ^{68}Ga-PSMA-PET/MRI enhances lesion detection rates, particularly in cases classified as PI-RADS 3, while established SUV_{max} cutoff values aid in discriminating csPCa, thereby reducing the need for unnecessary biopsies.[26] ^{68}Ga-PSMA-PET/MRI demonstrates superior accuracy in detecting primary PCa compared to mpMRI alone, with a pooled sensitivity of 94.9%. However, the lack of standardized SUV_{max} cutoff values for PSMA-PET analysis presents a challenge in clinical practice, highlighting the need for further research to optimize biopsy guidance and PCa detection strategies.[19]

In a review by Dhar *et al.*[29], Area Under the Receiver Operating Characteristic Curve values indicated very good diagnostic accuracy for mpMRI, ^{68}Ga-PSMA-PET, and their combination (0.852, 0.889, and 0.796, respectively). However, the limited studies using both modalities resulted in wider confidence intervals. ^{68}Ga-PSMA-PET/CT independently predicts treatment response for salvage radiation, while ^{68}Ga-PSMA-PET/MRI shows notable accuracy in staging primary PCa and is potentially superior to mpMRI in a review by Zhao *et al.*[17] Combining ^{68}Ga-PSMA-PET/CT with MRI enhances sensitivity for detecting csPCa, necessitating further large-scale prospective studies for validation, while ^{68}Ga-PSMA-PET/MRI demonstrates higher accuracy in detecting primary PCa compared to mpMRI alone, with established SUV_{max} cutoff values supporting biopsy-free diagnosis.[14]

4. Discussion

So far, the majority of clinical evidence for ^{68}Ga-PSMA-PET has supported its use in staging PCa. Only in recent years has considerable attention been given to the potential benefits of PSMA-PET in diagnosing suspected PCa. Ga-68-PSMA-11, marketed under the trade names Locametz® and Illuccix®, has been used globally in a large number of patients, showing its profound clinical impact. This PET method has replaced some conventional imaging techniques, such as bone scintigraphy. The shift toward PET imaging has led to significant changes in clinical management, as evidenced in numerous analyses, including our own, highlighting its transformative role in diagnostic imaging.

The use of ^{68}Ga-PSMA-PET in the initial detection of PCa has shown promising results, with variability in specificity highlights challenges in achieving consistent diagnostic accuracy. Despite these limitations, ^{68}Ga-PSMA-PET's ability to correlate with GS and PSA levels supports its utility in risk evaluation and management planning. The integration of PET/MRI offers a comprehensive approach by combining the anatomical detail of MRI with the functional imaging capabilities of PET, thus improving the accuracy of initial diagnoses and reducing the need

for invasive biopsies. In Figure 2, it demonstrates high diagnostic accuracy in identifying primary lesions, lymph node involvement, and distant metastases, aiding in TNM staging and treatment planning.

^{68}Ga-PSMA-PET, particularly when combined with CT or MRI, has shown high diagnostic accuracy in TNM staging of PCa, with notable sensitivity in detecting primary lesions and superior performance in identifying lymph nodes and distant metastases. As shown in Figure 3,

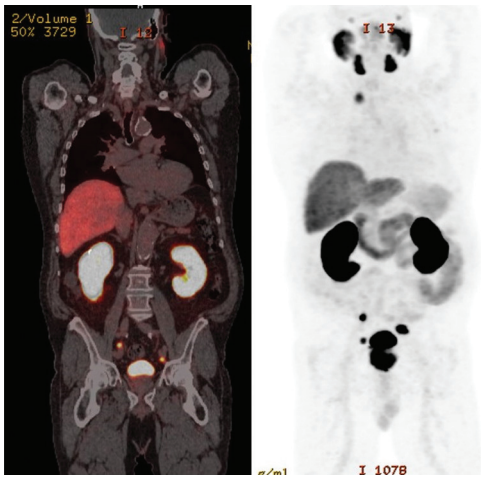

Figure 2. Comparison of ^{68}Ga-PSMA PET/CT (left) and ^{68}Ga-PSMA-PET (right) scans for staging prostate cancer. The images demonstrate high diagnostic accuracy in identifying primary lesions, lymph node involvement, and distant metastases, aiding in TNM staging and treatment planning.
Abbreviations: ^{68}Ga-PSMA-PET: Gallium-68-prostate-specific membrane antigen-positron emission tomography; CT: Computed tomography.

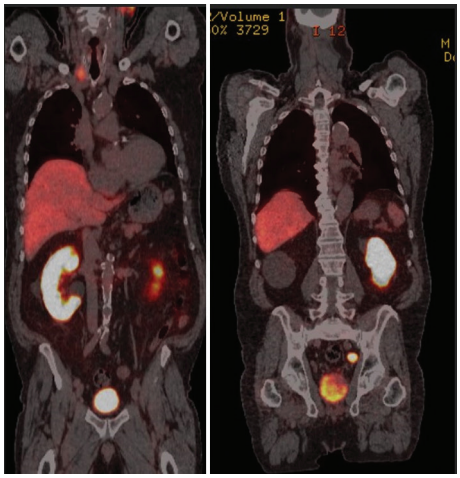

Figure 3. ^{68}Ga-PSMA-PET/CT scans show primary prostate cancer with intense PSMA uptake in the iliac lymph nodes and other regions. The left image highlights multiple sites of uptake, while the right image focuses on the primary lesion and associated metastases.
Abbreviations: ^{68}Ga-PSMA-PET/CT: Gallium-68-prostate-specific membrane antigen-positron emission tomography/computed tomography.

the image exhibits high PSMA uptake, demonstrating its effectiveness in detecting primary lesions, lymph node involvement, and distant metastases.

^{68}Ga-PSMA-PET/CT not only aids in staging but also helps predict nodal involvement and tumor aggressiveness, thereby informing treatment strategies and potentially reducing unnecessary surgical interventions. There is a significant association between PSMA uptake and GS, indicating that ^{68}Ga-PSMA PET can serve as a predictive tool for tumor aggressiveness and disease prognosis. Higher SUV_{max} values correlate with elevated GS and PSA levels, suggesting that ^{68}Ga-PSMA-PET findings can reflect the severity of PCa and aid in stratifying patients based on their risk profiles.

5. Conclusion

The incorporation of ^{68}Ga-PSMA-PET, particularly when integrated with MRI, holds significant promise for the initial diagnosis and management of PCa. Its ability to correlate with key clinical parameters and improve diagnostic accuracy underscores its potential as a valuable tool in clinical practice. However, addressing current limitations through standardization and further research is essential to fully realize the benefits of PSMA-PET in PCa care.

Acknowledgments

None.

Funding

None.

Conflict of interest

Kalevi Kairemo is the Editorial Board Member of this journal, but was not in any way involved in the editorial and peer-review process conducted for this paper, directly or indirectly. Separately, other authors declared that they have no known competing financial interests or personal relationships that could have influenced the work reported in this paper.

Author contributions

Conceptualization: Philip F. Cohen, Kalevi Kairemo
Writing – original draft: I.O. Akinmuleya
Writing – review & editing: All authors

Ethics approval and consent to participate

Not applicable.

Consent for publication

Images submitted for publication were approved by the Institutional Review Board Ethics Committee (IRB) at the INITIO PET Clinic.

Availability of data

Not applicable.

References

1. Wang L, Lu B, He M, *et al*. Prostate cancer incidence and mortality: Global status and temporal trends in 89 countries from 2000 to 2019. *Front Public Health*. 2022;10:811044.

   doi: 10.3389/fpubh.2022.811044

2. Mohler JL, Antonarakis ES, Armstrong AJ, *et al*. Prostate cancer, version 2.2019, NCCN clinical practice guidelines in oncology. *J Natl Compr Canc Netw*. 2019;17(5):479-505.

   doi: 10.6004/jnccn.2019.0023

3. Ghai S, Haider MA. Multiparametric-MRI in the diagnosis of prostate cancer. *Indian J Urol*. 2015;31(3):194-201.

   doi: 10.4103/0970-1591.159606

4. Bouchelouche K, Choyke PL. Advances in prostate-specific membrane antigen PET of prostate cancer. *Curr Opin Oncol*. 2018;30(3):189-196.

   doi: 10.1097/CCO.0000000000000439

5. Zhen L, Liu X, Yegang C, *et al.* Accuracy of multiparametric magnetic resonance imaging for diagnosing prostate cancer: A systematic review and meta-analysis. *BMC Cancer*. 2019;19(1):1244.

   doi: 10.1186/s12885-019-6434-2

6. Rosenkrantz AB, Ginocchio LA, Cornfeld D, *et al*. Interobserver reproducibility of the PI-RADS version 2 lexicon: A multicenter study of six experienced prostate radiologists. *Radiology*. 2016;280(3):793-804.

   doi: 10.1148/radiol.2016152542

7. Richenberg J, Løgager V, Panebianco V, *et al*. The primacy of multiparametric MRI in men with suspected prostate cancer. *Eur Radiol.* 2019;29(12):6940-6952.

   doi: 10.1007/s00330-019-06166-z

8. Hofman MS, Lawrentschuk N, Francis RJ, *et al*. Prostate-specific membrane antigen PET-CT in patients with high-risk prostate cancer before curative-intent surgery or radiotherapy (proPSMA): A prospective, randomised, multicentre study. *Lancet*. 2020;395(10231):1208-1216.

   doi: 10.1016/S0140-6736(20)30314-7

9. Emmett L, Buteau J, Papa N, *et al.* The additive diagnostic value of prostate-specific membrane antigen positron emission tomography computed tomography to multiparametric magnetic resonance imaging triage in the diagnosis of prostate cancer (PRIMARY): A prospective multicentre study. *Eur Urol*. 2021;80(6):682-689.

   doi: 10.1016/j.eururo.2021.08.002

10. Kawada T, Yanagisawa T, Rajwa P, *et al*. Diagnostic performance of prostate-specific membrane antigen positron emission tomography-targeted biopsy for detection of clinically significant prostate cancer: A systematic review and meta-analysis. *Eur Urol Oncol.* 2022;5(4):390-400.

    doi: 10.1016/j.euo.2022.04.006

11. Evangelista L, Zattoni F, Cassarino G, *et al.* PET/MRI in prostate cancer: A systematic review and meta-analysis. *Eur J Nucl Med Mol Imaging*. 2021;48(3):859-873.

    doi: 10.1007/s00259-020-05025-0

12. Satapathy S, Singh H, Kumar R, *et al.* Diagnostic accuracy of 68Ga-PSMA PET/CT for initial detection in patients with suspected prostate cancer: A systematic review and meta-analysis. *AJR Am J Roentgenol*. 2021;216(3):599-607.

    doi: 10.2214/AJR.20.23912

13. Ptasznik G, Moon D, Buteau J, *et al*. A systematic review of the variability in performing and reporting intraprostatic prostate-specific membrane antigen positron emission tomography in primary staging studies. *Eur Urol Open Sci*. 2023;50:91-105.

    doi: 10.1016/j.euros.2023.01.010

14. Caracciolo M, Castello A, Urso L, *et al*. The role of [68Ga] PSMA PET/CT for clinical suspicion of prostate cancer in patients with or without previous negative biopsy: A systematic review. *Cancers* (*Basel*). 2022;14(20):5036.

    doi: 10.3390/cancers14205036

15. Sood A, Kishan AU, Evans CP, *et al*. The impact of positron emission tomography imaging and tumor molecular profiling on risk stratification, treatment choice, and oncological outcomes of patients with primary or relapsed prostate cancer: An international collaborative review of the existing literature. *Eur Urol Oncol*. 2024;7(1):27-43.

    doi: 10.1016/j.euo.2023.06.002

16. Yadav D, Hwang H, Qiao W, *et al*. 18F-fluciclovine versus PSMA PET imaging in primary tumor detection during initial staging of high-risk prostate cancer: A systematic review and meta-analysis. *Radiol Imaging Cancer*. 2022;4(2):e210091.

    doi: 10.1148/rycan.210091

17. Zhao Y, Simpson BS, Morka N, *et al*. Comparison of multiparametric magnetic resonance imaging with prostate-specific membrane antigen positron-emission tomography imaging in primary prostate cancer diagnosis: A systematic review and meta-analysis. *Cancers* (*Basel*). 2022;14(14):3497.

    doi: 10.3390/cancers14143497

18. Wu H, Xu T, Wang X, *et al*. Diagnostic performance of 68Gallium labelled prostate-specific membrane antigen positron emission tomography/computed tomography and magnetic resonance imaging for staging the prostate cancer with intermediate or high risk before radical prostatectomy: A systematic review and meta-analysis. *World J Mens Health*. 2020;38(2):208-219.

doi: 10.5534/wjmh.180124

19. Jiao J, Zhang J, Li Z, *et al*. Prostate specific membrane antigen positron emission tomography in primary prostate cancer diagnosis: First-line imaging is afoot. *Cancer Lett*. 2022;548:215883.

    doi: 10.1016/j.canlet.2022.215883

20. Pepe P, Pepe L, Tamburo M, *et al*. 68Ga-PSMA PET/CT and prostate cancer diagnosis: which SUVmax value? *In Vivo*. 2023;37(3):1318-1322.

    doi: 10.21873/invivo.13211

21. Hu X, Wu Y, Yang P, *et al*. Performance of 68Ga-labeled prostate-specific membrane antigen ligand positron emission tomography/computed tomography in the diagnosis of primary prostate cancer: A systematic review and meta-analysis. *Int Braz J Urol*. 2022;48(6):891-902.

    doi: 10.1590/S1677-5538.IBJU.2020.0986

22. Morigi JJ, Anderson J, DE Nunzio C, *et al*. Prostate specific membrane antigen positron emission tomography/computed tomography and staging high risk prostate cancer: A non-systematic review of high clinical impact literature. *Minerva Urol Nephrol*. 2021;73(1):32-41.

    doi: 10.23736/S2724-6051.20.03739-X

23. Ling SW, De Jong AC, Schoots IG, *et al*. Comparison of 68Ga-labeled prostate-specific membrane antigen ligand positron emission tomography/magnetic resonance imaging and positron emission tomography/computed tomography for primary staging of prostate cancer: A systematic review and meta-analysis. *Eur Urol Open Sci*. 2021;33:61-71.

    doi: 10.1016/j.euros.2021.09.006

24. Abrams-Pompe RS, Fanti S, Schoots IG, *et al*. The role of magnetic resonance imaging and positron emission tomography/computed tomography in the primary staging of newly diagnosed prostate cancer: A systematic review of the literature. *Eur Urol Oncol*. 2021;4(3):370-395.

    doi: 10.1016/j.euo.2020.11.002

25. Woo S, Ghafoor S, Becker AS, *et al*. Prostate-specific membrane antigen positron emission tomography (PSMA-PET) for local staging of prostate cancer: A systematic review and meta-analysis. *Eur J Hybrid Imaging*. 2020;4(1):16.

    doi: 10.1186/s41824-020-00085-9

26. Hernes E, Revheim ME, Hole KH, *et al*. Prostate-specific membrane antigen PET for assessment of primary and recurrent prostate cancer with histopathology as reference standard: A systematic review and meta-analysis. *PET Clin*. 2021;16(2):147-165.

    doi: 10.1016/j.cpet.2021.03.001

27. Petersen LJ, Zacho HD. PSMA PET for primary lymph node staging of intermediate and high-risk prostate cancer: An expedited systematic review. *Cancer Imaging*. 2020;20(1):10.

    doi: 10.1186/s40644-020-0290-9

28. Tu X, Zhang C, Liu Z, *et al*. The role of 68Ga-PSMA positron emission tomography/computerized tomography for preoperative lymph node staging in intermediate/high risk patients with prostate cancer: A diagnostic meta-analysis. *Front Oncol*. 2020;10:1365.

    doi: 10.3389/fonc.2020.01365

29. Dhar A, Cendejas-Gomez JJ, Castro Mendez L, *et al*. Using multiparametric magnetic resonance imaging and prostate specific membrane antigen positron emission tomography to detect and delineate the gross tumour volume of intraprostatic lesions-a systematic review and meta-analysis. *Radiother Oncol*. 2024;192:110070.

    doi: 10.1016/j.radonc.2023.110070

ACCSCIENCE PUBLISHING

Advances in Radiotherapy & Nuclear Medicine

REVIEW ARTICLE

Expert consensus on the utilization of three-dimensional-printed templates for interstitial brachytherapy with iodine-125 seeds in the treatment of recurrent head and neck cancer

Qiman Han[1†], Bin Qiu[1†], Yi Chen[1], Zhe Ji[1], Yuliang Jiang[1], Suqing Tian[1], Kaixian Zhang[2], Ruoyu Wang[3], Zhe Wang[3], and Junjie Wang[1*]

[1]Department of Radiation Oncology, Peking University Third Hospital, Beijing, China

[2]Department of Oncology, Tengzhou Central People's Hospital, Zaozhuang, Shandong, China

[3]Department of Medical Oncology, Affiliated Zhongshan Hospital of Dalian University, Dalian, Liaoning, China

Abstract

Head and neck cancer (HNC) encompasses a range of malignancies that originate from the upper aerodigestive tract. Despite employing a multimodal treatment approach, the recurrence rate for HNC remains high with limited treatment options. One effective treatment method for HNC is interstitial brachytherapy with radioactive seeds, which delivers high localized doses of radiation while minimizing damage to surrounding healthy tissues. The integration of three-dimensional-printed templates (3D-PT) with computed tomography (CT)-guided techniques enhances the precision and control of radioactive seed implantation. This approach enhances treatment accuracy and efficacy, making it a valuable option in the management of HNC and other malignancies. Several factors, such as the specific target site, puncture trajectory, and radiation dosage distribution, can influence the efficacy and safety of seed implantation. At present, there is a lack of comprehensive reports detailing the clinical and technical processes and standards related to 3D-PT-assisted CT-guided particle implantation therapy for recurrent HNC. This consensus aims to address this gap by focusing on the application of 3D-PTs for interstitial brachytherapy using iodine-125 seeds in the treatment of recurrent HNC.

Keywords: 3D-printing template; Iodine-125 seeds; Radioactive seed implantation; Brachytherapy; Recurrent head and neck cancer

[†]These authors contributed equally to this work.

***Corresponding author:**
Junjie Wang
(junjiewang@pku.edu.cn)

Citation: Han Q, Qiu B, Chen Y, *et al.* Expert consensus on the utilization of three-dimensional-printed templates for interstitial brachytherapy with iodine-125 seeds in the treatment of recurrent head and neck cancer. *Adv Radiother Nucl Med.* 2024;2(4):4212.
doi: 10.36922/arnm.4212

Received: July 11, 2024

Accepted: September 25, 2024

Published Online: January 2, 2025

1. Introduction

Head and neck cancer (HNC) refers to a diverse group of malignancies that originate from the anatomical sites of the upper aerodigestive tract.[1] HNC typically encompasses neck neoplasms, otolaryngology malignancies, and oral-maxillofacial tumors, including nasopharyngeal carcinoma, oropharyngeal carcinoma, hypopharyngeal carcinoma, oral cancer, paranasal sinus cancer, laryngeal cancer, thyroid cancer, salivary gland cancer, and primary unknown metastatic neck cancer. Notably, squamous cell carcinoma of the head and neck accounts for approximately 90% of these cases.[1] Other histological types,

such as adenocarcinoma, adenosquamous carcinoma, and sarcoma, are less common. In the 2022 classification of head and neck tumors by the World Health Organization, additional categories such as mesenchymal tumors, melanomas, hematolymphoid tumors, neuroendocrine tumors, and hereditary tumor syndromes were listed separately.[2]

Globally, the annual incidence of HNC surpasses 550,000 cases, resulting in approximately 300,000 fatalities.[3] HNC accounts for 30% of all malignant tumors, with surgical intervention being the primary therapeutic approach. The 5-year overall survival (OS) of patients diagnosed with stage I–II disease is typically between 70% and 90%.[1,4] Concurrent chemoradiotherapy with a cisplatin-based regimen has long been established as the standard in the definitive management of locally advanced or inoperable HNC.[4] Systematic reviews have consistently demonstrated local-regional control (LRC) rates ranging from 58% to 61%, with 2-year OS rates between 67% and 74% and progression-free survival rates from 62% to 69%.[5] Despite the multimodal treatment approach for HNC, locoregional recurrence or development of distant metastases was reported in 50 – 60% of patients with Stage III or IV disease. Unfortunately, most of these relapses are ineligible for surgery or re-radiotherapy, leaving systemic therapy and optimal supportive care as primary options. Historical data from the 20th century indicated that the median OS of patients with metastatic HNC following comprehensive therapy was only 6 months.[6] This poor prognosis has led to extensive research over the past two decades into various treatment modalities, including brachytherapy, chemotherapy, targeted therapy, immunotherapy, and more.[6-8]

Brachytherapy using radioactive seeds is recognized as a standard treatment for early-stage prostate cancer.[9] This technique involves the insertion of iodine-125 (^{125}I) seeds (measuring 4.5×0.8 mm and enclosed in a nickel-titanium alloy shell) into the prostate gland with a transrectal ultrasound-guided template to effectively target and eradicate the tumor. One of the key benefits of his approach is its ability to deliver high local doses of radiation while minimizing damage to the surrounding healthy tissues. The procedure is minimally invasive and typically performed in a single session. In addition to its application in prostate cancer, some researchers have used this technology for the treatment of malignant tumors across various fields.[10-19]

In 2002, Professor Wang Junjie introduced computed tomography (CT)-guided techniques for radioactive seed implantation (RSI) in managing recurrent HNC, yielding exceptional outcomes in local tumor control. However, the complex anatomical structures of the head and neck region and the presence of numerous critical organs, pose significant challenges in accurately implementing pre-operative planning requirements. These complexities can lead to suboptimal post-operative dose verification, due to difficulties in fully achieving the planned radiation doses. To address this challenge, In 2002, Professor Zhang Jianguo pioneered the development of three-dimensional-printed templates (3D-PTs), significantly enhancing precision during RSI while facilitating effective pre-operative planning.[20]

In 2015, Professor Wang Junjie designed 3D-PTs with coordinates, fixed needle paths, and digital features. The 3D-PTs are categorized into two types: the 3D printing non-co-planar template (3D-PNCT) and the 3D printing co-planar template (3D-PCT).[20] Tumor information is transferred into the computer treatment planning system after digital processing using imaging-guided technology. Physicians and physicists collaborate to delineate target areas, define prescription doses for the tumor and critical organs, design needle paths, and print personalized templates using 3D printers. These templates assist in guiding RSI and achieving highly conformal irradiation of tumor targets. The 3D-PNCT is recommended for non-co-planar seed needle insertion in complicated tumor locations. This technology allows for the design of needle paths from different angles, directions, and depths to accommodate irregular tumor shapes, complex anatomical locations, and the presence of numerous critical organs, ensuring that post-operative dose verification aligns with the pre-operative planning requirements. Conversely, 3D-PCT is recommended for RSI, where needle paths can be aligned parallel to the tumor. These templates are standardized to make operations more convenient.

Using 3D-PT technology with CT-guided techniques ensures that seed implantation in brachytherapy is a precisely planned, controllable, and assessable procedure. This approach enhances the accuracy and efficacy of low-dose-rate brachytherapy, making it a minimally invasive surgical technique with improved treatment outcomes (Figures 1 and 2). Several critical factors, such as the target site, puncture trajectory, and dose distribution, can influence the efficacy and safety of seed implantation. Advances in medical imaging have led to the development of sophisticated devices that enable precise localization of target sites.[21] While these technological advancements assist operators in making accurate needle punctures, inexperienced practitioners may still struggle to ensure the correct spatial distribution of the needles. Previous studies have demonstrated the efficacy and safety of 3D-PT-assisted ^{125}I RSI for treating HNC.[22-25] However,

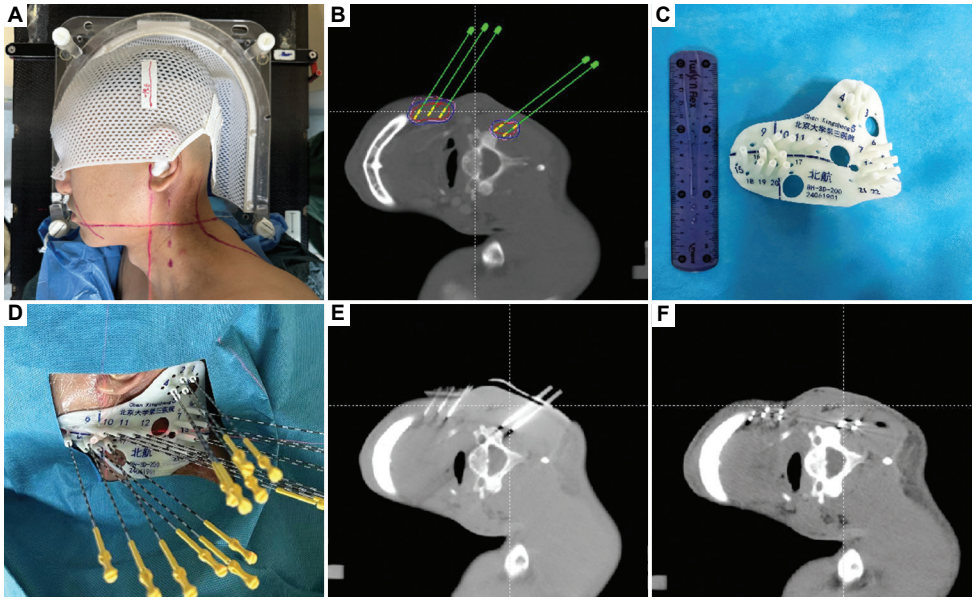

Figure 1. The three-dimensional-printing non-co-planar template utilized in computed tomography-guided iodine-125 radioactive seed implantation. (A) Pre-operative assessment. (B) Print personalized 3D-printing non-co-planar template through 3D printing. (C) Pre-operative planning design. (D) Insert needles. (E) Verify needle positions. (F) Perform ^{125}I seed implantation.

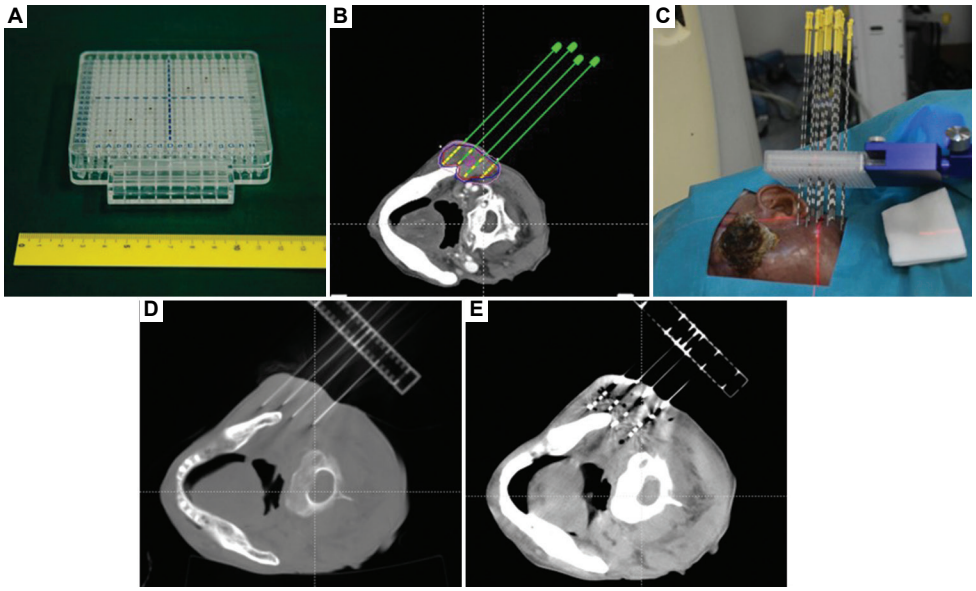

Figure 2. The three-dimensional-printing co-planar template utilized in computed tomography-guided iodine-125 radioactive seed implantation. (A) Print personalized 3D-printing co-planar template through 3D printing. (B) Pre-operative planning design. (C) Insert needles. (D) Verify needle positions. (E) Perform ^{125}I seed implantation.

deviations during the RSI process can affect the efficacy and safety of particle implantation, presenting a significant challenge in achieving consistency between pre-operative and post-operative plans. At present, there is no comprehensive report on the clinical process or technical standards for 3D-PT-assisted CT-guided RSI in the treatment of recurrent HNC. Hence, this consensus primarily focuses on the application of 3D-PT for interstitial brachytherapy using ^{125}I seeds for the treatment of recurrent HNC.

2. Scope and methodology

2.1. Scope of the consensus

The term "brachytherapy" originates from Greek and encompasses five modalities: intracavitary irradiation,

intraluminal irradiation, interstitial irradiation, intraoperative irradiation, and mold irradiation. Among these modalities, high dose rate after loading brachytherapy and low dose rate interstitial seed implantation brachytherapy are the most commonly employed techniques. High dose rate after loading brachytherapy is primarily utilized for treating cervical cancer, endometrial cancer, breast cancer, skin cancer, and prostate cancer. This technique is characterized by significant fractionation and short treatment courses. Interstitial seed implantation brachytherapy is mainly employed for recurrent HNC, lung cancer, pancreatic cancer, prostate cancer, soft-tissue tumors, and various pelvic recurrent metastatic cancer types.[26] It is characterized by its single-session completion using minimally invasive techniques.

2.2. The consensus formation process

The consensus formation process involved active participation from various medical associations and centers, including the China Society for Radiation Oncology, the Expert Committee on Radiation Oncology, the Chinese Medical Doctor Association, the Brachytherapy and Intelligent Radiotherapy Division of the Chinese Nuclear Society, and the Beijing Radiation Therapy Quality Control and Improvement Center. Experts from diverse departments, such as radiation therapy, surgery, interventional radiology, internal medicine, ultrasound, and nuclear medicine, were convened to form a committee. Under the guidance of a chairman, these experts collaborated to draft an initial version of the consensus document, which was subsequently circulated among committee members for feedback. Extensive discussions and deliberations within the committee ultimately led to a finalized consensus. The scope of this consensus was specifically concentrated on the utilization of 3D-PTs to guide seed implantation brachytherapy for recurrent HNC.

2.3. Purpose and target audience of the consensus

The purpose of the consensus was to clarify the responsibilities of doctors, physicists, therapists, and nurses involved in brachytherapy using radioactive seeds. This consensus aims to provide a clear understanding of the indications, technical standards, and operational procedures associated with seed implantation, ultimately benefiting cancer patients.

2.4. Literature search

The consensus incorporated studies published up to December 2023, encompassing both printed and online sources. The search was conducted using the Medline database with MeSH terms, such as "Brachytherapy" and "Head and Neck Cancer" or "3D-printing Template." The consensus statement does not include discussions on other treatment modalities such as external beam radiotherapy, chemotherapy, or immunotherapy.

3. Findings

3.1. Basic concepts of interstitial RSI

Interstitial RSI is a form of permanent brachytherapy that adheres to the principles of radiation therapy. This principle includes delineating the target area, defining organs at risk (OARs), setting the prescribed dose, and establishing dose constraints for OARs.[27,28]

3.1.1. Definition of target area and OARs

According to the International Commission on Radiation Units and Measurements Report 83,[27] the target area and OARs are defined as follows:

i. Gross tumor volume (GTV): This represents the visible lesion with a specific shape identified through imaging modalities and clinical examinations.
ii. Clinical target volume (CTV): This encompasses the GTV, subclinical foci, and areas potentially affected by the tumor.
iii. Planning target volume (PTV): This includes the CTV with appropriate expansion to account for patient organ motion, daily positioning variability, target area location during treatment, and changes in the target volume. However, PTV is primarily applicable in external beam radiation and is rarely considered in interstitial RSI.
iv. OAR: This refers to adjacent normal tissues or organs covered by the irradiated area.

3.1.2. Prescription dose and evaluation parameters for the target area

3.1.2.1. Prescription dose

The prescription dose refers to the radiation dose that can locally control the tumor based on evidence-based medicine or clinical practice. However, there is a notable absence of prospective studies focused on dose escalation in interstitial RSI for HNC. According to the American Brachytherapy Society, the recommended prescription dose for prostate cancer treated with ^{125}I seed implantation ranges from 140 to 160 Gy. Post-operative evaluations should confirm that the dose received by 90% of the target volume (D90) meets or exceeds 100% of the prescribed dose. In addition, external beam radiation is typically prescribed at a dose of 115 Gy.[9] Referring to previous studies on prostate cancer and HNC treated with radioactive seeds, recommended doses are summarized as follows: for patients previously treated with radiation therapy: 90 – 120 Gy; for those who

have not been previously treated with radiation therapy: 120 – 160 Gy, with an activity range of 0.3 – 0.6 mCi.[29]

3.1.2.2. Evaluation of dosimetric parameters

Dosimetric descriptive parameters include parameters for the target area and OARs, such as D90, the dose received by 100% of the target area (D100), the volume of the target area covered by the 100% prescription dose line (V100), the volume of the target area covered by the 150% prescription dose line (V150), and the volume of the target area covered by the 200% prescription dose line (V200). In addition, treatment plan quality is often evaluated using the conformity index (CI), homogeneity index (HI), and external index (EI).

Conformity index is calculated as follows:

$$CI = (VT_{ref}/V_{ref}) \times (VT/V_{ref}) \quad (I)$$

where VT_{ref} is the GTV receiving the prescription dose, VT is the GTV receiving the prescription dose, and V_{ref} is the total volume covered by the prescription dose.

HI is calculated as follows:

$$HI = ((VT_{ref} - VT1.5_{ref})/VT_{ref}) \times 100\% \quad (II)$$

where $VT1.5_{ref}$ is the GTV receiving 150% of the prescription dose.

EI evaluates the percentage of the prescribed dose that falls outside the target area, and is calculated as follows:

$$EI = (V_{ref} - VT_{ref})/V_{ref} \times 100\% \quad (III)$$

3.1.2.3. Limits on OARs

In interstitial RSI with ^{125}I seeds, the impact of radiation doses on normal tissue and their associated side effects remains unclear, highlighting the necessity for further research. At present, it is recommended to refer to the parameters of high dose rate after loading brachytherapy.

3.1.2.4. Physical characteristics of ^{125}I seeds

The commonly used clinical radioactive seeds are ^{125}I with a half-life of 60 days and emit photons with an energy of 27 keV. In recent years, seed chains have gradually replaced individual seeds internationally due to their ease of placement within tissues.

3.2. Indications and contraindications for RSI for recurrent HNC

3.2.1. Indications

i. Recurrence of malignant tumors post-surgery or post-radiotherapy, with a diameter of ≤5 cm. Local recurrence post-surgery or post-radiotherapy, or recurrent neck lymph node metastases post-radiotherapy, with a diameter of ≤5 cm.
ii. Pathological diagnosis was required.
iii. The necessity of availability of an appropriate puncture pathway.
iv. Karnofsky performance scale (KPS) score >70 points.
v. The necessity of tolerability of the RSI procedure.
vi. Expected survival time should exceed 3 months.

3.2.2. Contraindications

i. Severe bleeding with platelet count ≤50×10^9/L and severe coagulation disorders (prothrombin time >18 s, prothrombin activity <40%). Anticoagulant and antiplatelet drugs should be discontinued at least 1 week before seed implantation.
ii. Tumor rupture is contraindicated.
iii. Severe diabetes is also considered as a contraindication.
iv. Lack of an appropriate puncture pathway renders the therapy unfeasible if it cannot achieve the planned target area dose according to the prescription dose design requirements.

3.2.3. Relative contraindications

i. Extensive metastasis with an anticipated survival time of ≤3 months.
ii. Severe complications, immunocompromised state, and renal insufficiency.
iii. Allergy to iodine contrast agents is considered a relative contraindication.

3.3. Technical workflow of RSI

The 3D-PT-assisted CT-guided RSI is primarily employed for treating recurrent or metastatic head and neck tumors. It can also be used as salvage treatment in cases where tumors have not fully regressed following external beam radiation. Adherence to standardized technical procedures and principles is essential for the successful execution of RSI. The standardized process for 3D-PT-assisted CT-guided RSI for HNC includes eight steps: pre-operative assessment, CT simulation for localization, pre-treatment planning design, 3D-PT production, repositioning of 3D-PT, insertion of needles, seed implantation, post-treatment evaluation of dosimetric parameters, and follow-up (Figure 3, Table 1).

3.4. Classification of RSI for recurrent HNC

Given the heterogeneity of head and neck tumors and the intricate anatomical structures, it is imperative to functionally categorize recurrent sites to meet the technical prerequisites for RSI.

Adhering to a five-region classification scheme is essential, which includes the following regions: the skull base region, maxillary sinus region, parapharyngeal space region, the floor of mouth region, and neck lymph node

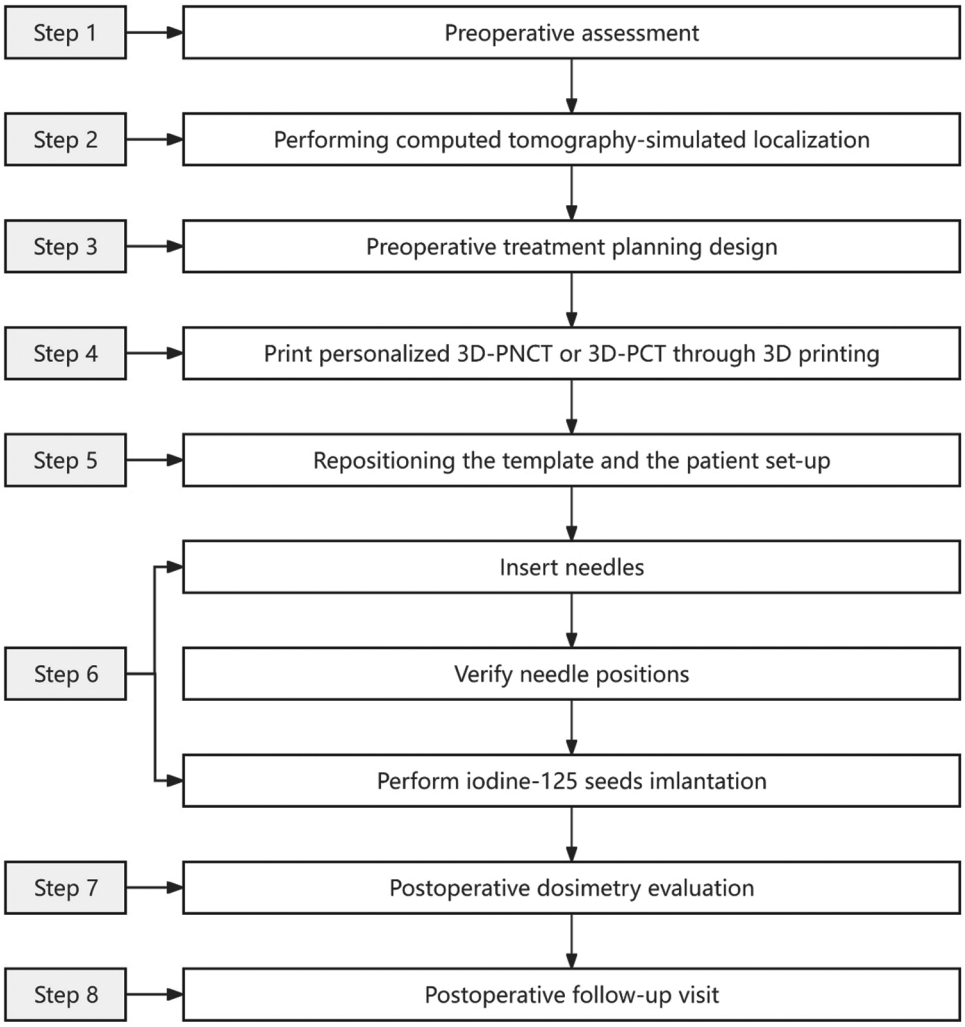

Figure 3. The flowchart of three-dimensional-printed template-assisted computed tomography-guided iodine-125 radioactive seed implantation for head and neck cancer.
Abbreviations: 3D-PCT: 3D-printing co-planar template; 3D-PNCT: 3D-printing non-co-planar template; CT: Computed tomography.

region. Detailed information regarding patient positioning, anesthesia methods, and template types for RSI in each region can be found in Table 2.

4. Discussion

Radiation dose at the tumor site can be increased by placing the radiation source near or within the tumor. This technique can also cause a rapid decline in dosage in the surrounding area. Brachytherapy has been recognized as an effective treatment modality by the Head and Neck Working Group of the European Brachytherapy Group and the ABS.[30,31] The use of ^{125}I RSI offers significant advantages in the treatment of recurrent or metastatic malignant tumors.[32,33] To ensure the accuracy and safety of ^{125}I RSI, meticulous pre-operative planning is essential. Radiation oncologists carefully design and optimize entry points and needle trajectories to minimize potential damage to surrounding critical structures while achieving optimal dose distribution in the target area.[34]

Precise positioning and distribution of seed needles are critical due to the intricate anatomical structures in the head and neck. Relying solely on image guidance may result in inaccuracies in the placement of the puncture needle or seeds, potentially harming surrounding tissues or organs. However, the use of 3D-PT significantly reduces the challenges associated with puncturing during RSI. These templates can effectively compensate for the lack of experience among novice operators and enhance the consistency of the procedures. The implementation of 3D-PT also ensures accurate dose determination. Compared to traditional puncture techniques, template

Table 1. Protocol of three-dimensional-printed template-assisted computed tomography-guided iodine-125 radioactive seed implantation for recurrent head and neck cancer

Steps	Executors
1. Pre-operative assessment i. Collect medical history, conduct a physical examination, and confirm diagnosis. ii. Complete pre-operative hematological and biochemical tests to evaluate general physical conditions. iii. Perform imaging examinations to assess local and systemic tumor conditions.	Physician
2. Pre-operative CT-simulated localization i. Discussion for indications and assess surgical risks ii. Prepare for localization. If necessary, provide patient positioning training in supine, prone, and lateral positions. iii. Pre-operative preparation: Skin disinfection following the established protocol. iv. Positioning device preparation: Utilize mesh masks and body vacuum cushions for combined fixation techniques. v. Location simulated by CT imaging: • Position fixation: Choose a position suitable for surgical procedures, considering patient comfort and tolerance. • Enhanced CT scans: Use laser positioning coordinates to mark surface entry, exit, and left and correct laser line positions. • Mark tumor boundaries on the skin: Determine the upper and lower tumor boundaries and the left and right tumor boundaries, marking the corresponding areas on the skin. • Marking needle points: Select the tumor center as the fixed needle channel design point or choose bony structures as reference points for easy CT scanning and identification. Establish an X-Y axis coordinate system centered on the tumor.	Physician, physicist, therapist, nurse
3. Pre-operative planning design i. Transmit CT scan images and related imaging information to the treatment planning system for localization, image fusion, and 3D image reconstruction. ii. Outline target areas and organs at risk. iii. Design needle paths and establish prescription doses and limits for OARs. iv. Physicians collaborate with physicists in the planning process, obtaining senior physician approval.	Physician, physicist
4. 3D-PT-assisted CT-guided 125I RSI i. Pre-operative preparation: The patient is repositioned on the CT simulator, the position is fixed, and the surgical field is locally disinfected and draped. ii. Anesthesia method: Deep vein compound anesthesia, local infiltration anesthesia, lingual nerve anesthesia, etc., are adopted as needed. Children require undergoing general anesthesia. iii. Repositioning the template: Align the laser lines on the body surface with the X and Y axes of the 3D-PT coordinate system. iv. Insert fixed needles: Insert three fixed needles into the body, penetrating 2 to 3 cm. Confirm their relationship with anatomical structures, such as bone structure, using a CT scan to match them with pre-operative planning design. Adjust for deviations, aiming for an error of≤2 mm, ideally≤1 mm. v. Insert seed needles: Insert seed needles to specified depths according to the pre-operative planning design. vi. Verify needle positions: Rescan with CT to verify that needle tips align with the pre-operative plan. Make minor adjustments if there are any discrepancies to ensure alignment with the pre-operative design. vii. Perform seed implantation: Carry out seed implantation according to pre-operative planning design requirements. viii. Assess dose distribution: Immediately rescan with CT after seed implantation to confirm that seeds are distributed in the target area. Supplement seeds if there are positional deviations or movements.	Physician, physicist, therapist, nurse
5. Post-operative evaluation of dosimetry parameters i. Post-operative CT scan: Transmit post-operative CT scan images to the planning system. ii. Delineate target areas and OARs: Transfer pre-operative target areas directly onto post-operative CT scan images, perform 3D image reconstruction, and conduct post-operative evaluation of dosimetric parameters. iii. Evaluation of dosimetric parameters includes D90 for target area coverage, CI, HI, and EI, as well as doses received by 0.1, 1, and 2 cc of OARs.	Physician, physicist
6. Follow-up visit	Physician, nurse

Abbreviations: 3D-PT: Three-dimensional-printed template; CI: Conformity index; CT: Computed tomography; D90: Dose received by 90% of the target volume: EI: External index; HI: Homogeneity index; OAR: Organs at risk; RSI: Radioactive seed implantation.

guidance offers distinct advantages, including improved efficiency in pre-operative preparation and repair. The fixed template facilitates precise alignment of its crosshair with the patient's body surface, enabling even inexperienced operators to minimize discrepancies between pre-operative plans and post-operative outcomes to within millimeters. Given that variations in seed distribution directly impact the radiation dose, the use of 3D templates is crucial for ensuring both accuracy and safety during the procedure,[35,36] Rembowska *et al.*[37] reported that the spatial

Table 2. Characteristics of radioactive seed implantation in each area for recurrent head and neck cancer

Site	Cranial base	Maxillary sinus region	Parapharyngeal space region	The floor of the mouth region	Neck lymph node region
Patient positioning	Lateral decubitus position	Lateral decubitus position	Lateral decubitus position	Supine position	Lateral decubitus position
Anesthesia method	Deep vein compound anesthesia	Deep vein compound anesthesia/ local infiltration anesthesia	Local anesthesia technique	Lingual nerve block combined with local infiltration anesthesia technique	Local anesthesia technique
Template type	3D-PNCT	3D-PNCT	3D-PNCT	3D-PNCT	3D-PNCT/3D-PCT

Abbreviations: 3D-PCT: Three-dimensional-printing co-planar template; 3D-PNCT: Three-dimensional-printing non-co-planar template.

distribution of needles is essential for dose accuracy. In contrast, traditional puncture techniques can be influenced by the technical skills and experience of the operators. In addition, Qiu *et al.*[25] conducted a retrospective analysis on the accuracy of 3D-PT-assisted ^{125}I RSI for recurrent or metastatic HNCs. The findings indicated that the average depth of the needle insertion during the procedure was 6.23 ± 0.24 cm compared to 6.21 ± 0.24 cm preoperatively, with an average angle of 83.14 ± 3.64 degrees versus 83.09 ± 3.66 degrees when comparing pre-operative and intraoperative measurements. Furthermore, Huang *et al.*[38] conducted a study comparing the distance and angle deviations of the needle tip during pre-operative and intraoperative implantation of ^{125}I radioactive seeds guided by individualized 3D-PTs. The patients were divided into four groups based on the puncture site: the parotid and masseter region group, the maxillary and paranasal region group, the submandibular region, and the upper neck region group. The researchers found that the distance deviation in the submandibular posterior region group was significantly smaller than those in other regions, particularly in the parotid and maxillary areas.

The precision of 3D-PT-assisted CT-guided ^{125}I RSI has been demonstrated in multiple studies, with post-operative dose measurements fully aligning with the pre-operative plans as outlined in the requirements.[39-42] Hongtao *et al.*[42] applied ^{125}I seeds in treating malignant tumors using individualized 3D-PTs, finding that the dose parameters for particle implantation guided by these templates were nearly identical before and after planning. Liang *et al.*[40] reported that the use of 3D templates significantly reduced patient radiation exposure and alleviated the anxiety and pressure experienced by both operators and patients, with an average CT scan frequency of only 5.7 times. In addition, Sun *et al.*[41] conducted a comparison of dosimetric data for pre-operative planning and post-operative verification of ^{125}I particle implantation assisted by a 3D-PT under CT guidance for mobile tumors in the thoracic cavity. The results indicated that the post-operative dosimetric parameters showed minimal changes compared to the pre-operative values, with no statistically significant differences ($P > 0.05$), suggesting that this method offers good accuracy. Specifically, the differences in post-operative parameters were as follows: post-operative lesion volume (5.57%), D90 (0.34%), V100 (0.33%), V150 (−1.20%), V200 (21%), minimum peripheral dose (2.8%), CI (−14.2%), EI (4.71%), and HI (-10.4%). Ji *et al.*[35] conducted a comparison of the dose distribution between the post-operative and pre-operative plans for radioactive particle implantation assisted by 3D-PT, demonstrating that using a 3D-printed guiding template significantly improved the accuracy of radioactive particle implantation. Importantly, there were no statistically significant differences in dosimetric parameters (D90, minimum peripheral dose, V150, and V200) between the post-operative and pre-operative plans. Furthermore, Qiu *et al.*[25] assessed the precision of personalized 3D-PT-assisted ^{125}I RSI for recurrent or metastatic HNC. The study revealed that the post-operative dosimetric parameters were effectively aligned with the planned dosimetry, showing no significant deviations. Similarly, Liang *et al.*[40] conducted a dosimetric study investigating the use of 3D-PT-assisted ^{125}I radioactive particle implantation in patients with cervical lymph node metastases. The results showed no statistically significant differences between the pre-operative and post-operative measurements of D90, V90, V100, and V150.

The clinical studies of RSI for HNC were typically retrospective, focusing on recurrent HNC cases (Tables 3 and 4).[22,24,25,38,40,43-46] Compared to CT-guided RSI, the 3D-PT-assisted ^{125}I RSI for HNC has been shown to reduce the dosimetric differences between pre- and post-planning and lowered the difficulty of puncture.[40] Moreover, incorporating individual template guidance can reduce the time required for implantation and minimize damage to normal tissues.[38]

Jiang *et al.*[47] conducted a retrospective study involving 14 cases of CT-guided ^{125}I RSI for the treatment of recurrent HNCs. The median follow-up period was 13 months, with a median local control duration of 18 months (95%

Table 3. Clinical outcomes of iodine-125 radioactive seed implantation for head and neck cancer with computed tomography guidance

Author	Year	Design	Simple size	Median local control	Local control rate	Median survival	Survival rate	Complications
Li *et al.*[43]	2016	Retrospective	34	17.7 m	1-y 65.3%, 2-y 28.6%, 3-y 9.5%	12.5 m	1-y 55.2%, 2-y 20.3%, 3-y 10.9%	Five (15%) patients experienced Grade III toxic events, and nine (26%) patients experienced Grade II toxic events.
Ji *et al.*[22]	2018	Retrospective	101	10 m	1-y 40.6%, 3-y 26.6%, 5-y 26.6%	15	1-y 54.3%, 3-y 15.5%, 5-y 15.5%	26 (25.7%) cases of skin or mucosa ulceration, 14 (13.9%) cases of pain, and two (2%) cases of dry mouth.
Jiang *et al.*[44]	2021	Multicenter retrospective	113	15 m	1-y 57.4%, 2-y 41.8%, 3-y 29.3%, 5-y 15.2%	20 m	1-y 63.6%, 2-y 44.6%, 3-y 29.9%, 5-y 21.7%	18 (15.9%) cases of Grade I/II, eight (7.0%) cases of Grade III radiation dermatitis, 14 (12.4%) cases of Grade I/II, and three (2.7%) cases of Grade III mucosal reactions.
Zhang *et al.*[45]	2024	Retrospective	132	16 m	1-y 47%, 2-y 22%	15 m	1-y 42%, 2-y 27%	Grade I skin toxicity occurred in seven (5.3%) cases, Grade IV skin toxicity in one (0.8%) case, Grade I mucosal ulcer in four (3.0%) cases, and Grade I dry mouth in four (3.0%) cases.

Abbreviations: m: Months; y: Year.

Table 4. Clinical outcomes of iodine-125 radioactive seed implantation for head and neck cancer with three-dimensional printed template assistance

Author	Year	Design	Sample size	Median local control	Local control rate	Median survival	Survival rate	Complications
Huang *et al.*[14]	2016	Retrospective	25	-	-	-	-	No abnormal hemorrhages or anatomical complications related to inaccurately placed implants were observed.
Liang *et al.*[40]	2018	Retrospective	15	-	-	-	-	No intraoperative complications and post-operative complications were observed in 3 days.
Jiang *et al.*[24]	2018	Retrospective	42	-	-	-	-	Three cases had a grade I skin reaction. Blood toxicity did not occur, nor did spinal cord injury.
Qiu *et al.*[25]	2021	Retrospective	41	7 m	3-m 63.2%	12 m	-	The two major complications were mucosal and skin ulcers. Minor radiodermatitis (n=2) and skin pigmentation (n=1) improved without additional treatment.
Li *et al.*[46]	2023	Retrospective	33	10 m	1-y 47.8%, 2-y 36.4%	8 m	1-y 41.3%, 2-y 32.2%	Pain was found in three (9.1%) patients, followed by Grade I to II acute skin reactions in three (9.1%) patients, Grade II to III late skin reactions in two (6.1%) patients, Grade I to II early mucosal reactions in four (12.1%) patients, and mandibular osteonecrosis in one (3.0%) patient.

Note: "-" refers to not reported.
Abbreviations: m: Months, y: Year.

confidence interval [CI]: 6.1 – 29.9 months). The local control rates at 1, 2, 3, and 5 years were reported as 52%, 39%, 39%, and 39%, respectively, while the survival rates were 65%, 39%, 39%, and 39%, respectively, with a median survival time of 20 months (95% CI: 8.7 – 31.3 months). In a follow-up long-term study, Jiang *et al.*[44] investigated the efficacy and safety of CT-guided ^{125}I radioactive particle implantation as a salvage treatment following external beam radiotherapy or surgery in 113 patients with recurrent HNC. The median follow-up time for this study was 20 months, during which 87 patients passed away. The local control rates at 1, 2, 3, and 5 years were found to be 57.4%, 41.8%, 29.3%, and 15.2%, respectively. The median time to progression was 15 months (95% CI: 6.1 – 23.9 months), and the median OS was 20 months (95% CI: 12.4 – 27.6 months). The OS rates at 1, 2, 3, and 5 years were 63.6%, 44.6%, 29.9%, and 21.7%, respectively. Univariate and multivariate analyses showed that both the KPS score and post-operative D90 were significantly correlated with patient OS. Complications primarily consisted of Grade I/II skin and mucosal reactions: 18 cases (15.9%) experienced Grade I/II reactions, while eight cases (7.0%) developed Grade III radiation dermatitis. In addition, 14 cases (12.4%) exhibited Grade I/II mucosal reactions, with only three cases (2.7%) reporting Grade III mucosal reactions. No complications of Grade IV or higher severity were observed.

In a separate retrospective study, Li *et al.*[47]examined 33 cases of recurrent HNCs that had undergone two or more courses of radiotherapy. The LRC at 1 and 2 years were found to be 47.8% and 36.4%, respectively, with a median LRC duration of 10 months. In addition, the OS rates at 1 and 2 years were observed to be 41.3% and 32.2%, respectively, with a median OS duration of 8 months.

The half-value layer of ^{125}I seeds is approximately 0.025 mm Pb, and their half-life is around 60 days. After this period, the energy decreases by half, and within 6 months, it reduces to only 10% of its initial level. Beyond 1 year, the radiation can be considered negligible. To ensure safety, it is recommended to avoid contact with children and pregnant women for 2 months following seed implantation. For prolonged exposure (several hours or more), it is advised to maintain a distance of 1.5 – 2 cm or recommended that patients wear lead necklaces, vests, and aprons made of lead for 2 months. Jiang *et al.*[24] performed 3D-PNCT-assisted RSI in 42 patients with locally recurrent malignant tumors of the head and neck, with a prescribed dose ranging from 110 to 160 Gy. The median follow-up time was 8.5 months. No cases experienced acute reactions of grade ≥3, while three cases exhibited grade I skin reactions.

5. Conclusion

The efficacy and safety of CT-guided ^{125}I RSI for managing recurrent HNC have been well established. The use of 3D-PTs to aid in the placement of ^{125}I seeds effectively constrains the positioning and orientation of the needles during interstitial treatment. This practice ensures precise, controllable, and assessable needle insertion by practitioners, thereby enhancing overall treatment effectiveness and safety. This consensus document focuses on the workflow of 3D-PT for interstitial brachytherapy using ^{125}I seed implantation to treat recurrent HNC. It aims to promote the standardization of 3D-PT-assisted CT-guided ^{125}I RSI brachytherapy in treating recurrent HNC. This paper systematically summarizes the technical processes and standards for ^{125}I RSI assisted by 3D-PTs for treating recurrent HNC. Its objective is to provide a comprehensive understanding of the indications and technical specifications for RSI while ensuring adherence to standardized clinical practices among physicians, medical physicists, therapists, and nurses.

Acknowledgments

None.

Funding

None.

Conflict of interest

Junjie Wang is the Editor-in-Chief, while Kaixian Zhang, Ruoyu Wang and Zhe Wang are the Editorial Board Members of this journal and Guest Editors for this special issue, but were not in any way involved in the editorial and peer-review process conducted for this paper, directly or indirectly. Separately, other authors declared that they have no known competing financial interests or personal relationships that could have influenced the work reported in this paper.

Author contributions

Conceptualization: Zhe Ji, Yuliang Jiang, Suqing Tian, Kaixian Zhang, Ruoyu Wang, Zhe Wang, Junjie Wang
Writing – original draft: Qiman Han, Bin Qiu, Zhe Ji
Writing – review & editing: Bin Qiu, Yi Chen, Junjie Wang

Ethics approval and consent to participate

Not applicable.

Consent for publication

Not applicable.

Availability of data

Data for this study can be obtained from the cited original articles.

References

1. Mody MD, Rocco JW, Yom SS, Haddad RI, Saba NF. Head and neck cancer. *Lancet*. 2021;398(10318):2289-2299.

   doi: 10.1016/S0140-6736(21)01550-6

2. Vered M, Wright JM. Update from the 5th Edition of the World Health Organization classification of head and neck tumors: Odontogenic and maxillofacial bone tumours. *Head Neck Pathol*. 2022;16(1):63-75.

   doi: 10.1007/s12105-021-01404-7

3. Tallari RV, Singh OP, Yogi V, Yadav S. Five versus ten fractions per week radiotherapy in locally advanced head and neck cancer. *J Cancer Res Ther*. 2017;13(2):224-229.

   doi: 10.4103/0973-1482.199785

4. Oculoplastic and Orbital Disease Group of Chinese Ophthalmological Society of Chinese Medical Association, Thyroid Group of Chinese Society of Endocrinology of Chinese Medical Association. *Zhonghua Yan Ke Za Zhi*. 2022;58(9):646-668.

   doi: 10.3760/cma.j.cn112142-20220421-00201

5. Mohamed A, Twardy B, Zordok MA, *et al*. Concurrent chemoradiotherapy with weekly versus triweekly cisplatin in locally advanced squamous cell carcinoma of the head and neck: Comparative analysis. *Head Neck*. 2019;41(5): 1490-1498.

   doi: 10.1002/hed.25379.

6. Johnson DE, Burtness B, Leemans CR, Lui VWY, Bauman JE, Grandis JR. Head and neck squamous cell carcinoma. *Nat Rev Dis Primers*. 2020;6:92.

   doi: 10.1038/s41572-020-00224-3

7. Ruffin AT, Li H, Vujanovic L, Zandberg DP, Ferris RL, Bruno TC. Improving head and neck cancer therapies by immunomodulation of the tumour microenvironment. *Nat Rev Cancer*. 2023;23(3):173-188.

   doi: 10.1038/s41568-022-00531-9

8. Cramer JD, Burtness B, Le QT, Ferris RL. The changing therapeutic landscape of head and neck cancer. *Nat Rev Clin Oncol*. 2019;16(11):669-683.

   doi: 10.1038/s41571-019-0227-z

9. Davis BJ, Horwitz EM, Lee WR, *et al*. American Brachytherapy Society consensus guidelines for transrectal ultrasound-guided permanent prostate brachytherapy. *Brachytherapy*. 2012;11(1):6-19.

   doi: 10.1016/j.brachy.2011.07.005

10. Chen Y, Jiang Y, Ji Z, *et al*. Dosimetry, efficacy, and safety of three-dimensional printing noncoplanar template-assisted and CT-guided-^{125}I seed implantation for recurrent retroperitoneal lymphatic metastasis after external beam radiotherapy. *Brachytherapy*. 2020;19(3):380-388.

    doi: 10.1016/j.brachy.2020.02.009

11. Wang J, Chai S, Wang R, *et al*. Expert consensus on computed tomography-assisted three-dimensional-printed coplanar template guidance for interstitial permanent radioactive ^{125}I seed implantation therapy. *J Cancer Res Ther*. 2019;15(7):1430-1434.

    doi: 10.4103/jcrt.JCRT_434_19

12. Jiang YL, Ji Z, Tian SQ, *et al*. CT-guidance interstitial Iodine-125 seed brachytherapy as a salvage therapy for recurrent head and neck carcinoma. *Zhonghua Yi Xue Za Zhi*. 2018;98:3686-3691.

    doi: 10.3760/cma.j.issn.0376-2491.2018.45.011

13. Luo YJ, Liu ZL, Ye PC, *et al*. Safety and efficacy of intraoperative iodine-125 seed implantation brachytherapy for rectal cancer patients: A retrospective clinical research. *J Gastroenterol Hepatol*. 2016;31(6):1076-1084.

    doi: 10.1111/jgh.13261

14. Huang M, Lin Q, Wang H, *et al*. Survival benefit of chemoembolization plus Iodine125 seed implantation in unresectable hepatitis B-related hepatocellular carcinoma with PVTT: A retrospective matched cohort study. *Eur Radiol*. 2016;26(10):3428-3436.

    doi: 10.1007/s00330-015-4198-x

15. Yang M, Fang Z, Yan Z, *et al*. Transarterial chemoembolisation (TACE) combined with endovascular implantation of an iodine-125 seed strand for the treatment of hepatocellular carcinoma with portal vein tumour thrombosis versus TACE alone: A two-arm, randomised clinical trial [published correction appears in *J Cancer Res Clin Oncol*. 2014 Apr;140(4):687-688]. *J Cancer Res Clin Oncol*. 2014;140(2):211-219.

    doi: 10.1007/s00432-013-1568-0

16. Sun H, Zhang M, Liu R, Liu Y, Hou Y, Wu C. Endovascular implantation of ^{125}I seed combined with transcatheter arterial chemoembolization for unresectable hepatocellular carcinoma. *Future Oncol*. 2018;14(12):1165-1176.

    doi: 10.2217/fon-2017-0354

17. Mo Z, Zhang T, Zhang Y, *et al*. Feasibility and clinical value of CT-guided ^{125}I brachytherapy for metastatic soft tissue sarcoma after first-line chemotherapy failure. *Eur Radiol*. 2018;28(3):1194-1203.

    doi: 10.1007/s00330-017-5036-0

18. Qu A, Jiang P, Sun H, *et al*. Efficacy and dosimetry analysis of image-guided radioactive ^{125}I seed implantation as salvage treatment for pelvic recurrent cervical cancer after external beam radiotherapy. *J Gynecol Oncol*. 2019;30(1):e9.

doi: 10.3802/jgo.2019.30.e9

19. Tong L, Liu P, Huo B, Guo Z, Ni H. CT-guided ^{125}I interstitial brachytherapy for pelvic recurrent cervical carcinoma after radiotherapy. *Onco Targets Ther*. 2017;10:4081-4088.

doi: 10.2147/OTT.S139571

20. Xue H, Qiu B, Wang H, *et al*. Stereotactic ablative brachytherapy: Recent advances in optimization of radiobiological cancer therapy. *Cancers* (*Basel*). 2021;13(14):3493.

doi: 10.3390/cancers13143493

21. Suppiah S, Chang WL, Hassan HA, *et al*. Systematic review on the accuracy of positron emission tomography/computed tomography and positron emission tomography/magnetic resonance imaging in the management of ovarian cancer: Is functional information really needed? *World J Nucl Med*. 2017;16(3):176-185.

doi: 10.4103/wjnm.WJNM_31_17

22. Ji Z, Jiang Y, Tian S, *et al*. The effectiveness and prognostic factors of CT-guided radioactive I-125 seed implantation for the treatment of recurrent head and neck cancer after external beam radiation therapy. *Int J Radiat Oncol Biol Phys*. 2019;103(3):638-645.

doi: 10.1016/j.ijrobp.2018.10.034

23. Chen Y, Jiang Y, Ji Z, *et al*. Efficacy and safety of CT-guided ^{125}I seed implantation as a salvage treatment for locally recurrent head and neck soft tissue sarcoma after surgery and external beam radiotherapy: A 12-year study at a single institution. *Brachytherapy*. 2020;19(1):81-89.

doi: 10.1016/j.brachy.2019.09.006

24. Jiang Y, Ji Z, Guo F, *et al*. Side effects of CT-guided implantation of ^{125}I seeds for recurrent malignant tumors of the head and neck assisted by 3D printing non Co-planar template. *Radiat Oncol*. 2018;13(1):18.

doi: 10.1186/s13014-018-0959-4

25. Qiu B, Jiang Y, Ji Z, *et al*. The accuracy of individualized 3D-printing template-assisted I 125 radioactive seed implantation for recurrent/metastatic head and neck cancer. *Front Oncol*. 2021;11:664996.

doi: 10.3389/fonc.2021.664996

26. Chargari C, Deutsch E, Blanchard P, *et al*. Brachytherapy: An overview for clinicians. *CA Cancer J Clin*. 2019;69(5): 386-401.

doi: 10.3322/caac.21578

27. Hodapp N. Der ICRU-Report 83: Verordnung, Dokumentation und Kommunikation der fluenzmodulierten Photonenstrahlentherapie (IMRT) The ICRU Report 83: Prescribing, recording and reporting photon-beam intensity-modulated radiation therapy (IMRT). *Strahlenther Onkol*. 2012;188(1):97-99.

doi: 10.1007/s00066-011-0015-x

28. Mahé MA, Barillot I, Chauvet B. Recommandations en radiothérapie externe et curiethérapie (Recorad): 2(e) édition Guidelines for external radiotherapy and brachytherapy: 2nd edition. *Cancer Radiother*. 2016;20 Suppl: S4-S7.

doi: 10.1016/j.canrad.2016.07.014

29. Marsico M, Gabbani T, Lunardi S, Galli A, Biagini MR, Annese V. Percutaneous ultrasound-guided fiducial marker placement for liver cancer robotic stereotactic radio-surgery treatment: A comparative analysis of three types of markers and needles. *Arab J Gastroenterol*. 2017;18(2):83-86.

doi: 10.1016/j.ajg.2017.05.007

30. Kovács G, Martinez-Monge R, Budrukkar A, *et al*. GEC-ESTRO ACROP recommendations for head & neck brachytherapy in squamous cell carcinomas: 1st update-Improvement by cross sectional imaging based treatment planning and stepping source technology. *Radiother Oncol*. 2017;122(2):248-254.

doi: 10.1016/j.radonc.2016.10.008

31. Takácsi-Nagy Z, Martínez-Mongue R, Mazeron JJ, Anker CJ, Harrison LB. American Brachytherapy Society Task Group Report: Combined external beam irradiation and interstitial brachytherapy for base of tongue tumors and other head and neck sites in the era of new technologies. *Brachytherapy*. 2017;16(1):44-58.

doi: 10.1016/j.brachy.2016.07.005

32. Jiang P, Liu C, Wang J, Yang R, Jiang Y, Tian S. Computed tomography (CT)-guided interstitial permanent implantation of (125) I seeds for refractory chest wall metastasis or recurrence. *Technol Cancer Res Treat*. 2015;14(1):11-18.

doi: 10.7785/tcrt.2012.500402

33. Lin L, Wang J, Jiang Y, *et al*. Interstitial ^{125}I seed implantation for cervical lymph node recurrence after multimodal treatment of thoracic esophageal squamous cell carcinoma. *Technol Cancer Res Treat*. 2015;14(2):201-207.

doi: 10.7785/tcrt.2012.500409

34. Pappas IP, Ryan P, Cossmann P, Kowal J, Borgeson B, Caversaccio M. Improved targeting device and computer navigation for accurate placement of brachytherapy needles. *Med Phys*. 2005;32(6):1796-1801.

doi: 10.1118/1.1901363

35. Ji Z, Jiang Y, Guo F, *et al*. Dosimetry verification of radioactive seed implantation for malignant tumors assisted by 3D printing individual templates and CT guidance. *Appl Radiat Isot*. 2017;124:68-74.

doi: 10.1016/j.apradiso.2016.12.009

36. Ji Z, Sun H, Jiang Y, *et al*. Comparative study for CT-guided ^{125}I seed implantation assisted by 3D printing coplanar and

non-coplanar template in peripheral lung cancer. *J Contemp Brachytherapy*. 2019;11(2):169-173.

doi: 10.5114/jcb.2019.84503

37. Rembowska AME, Cook M, Hoskin PJ, Mahdevan A. The stepping source dosimetry system as an extension of the manchester system. *Radiother Oncol*. 1996;39(39):25-25.

doi: 10.1016/0167-8140(96)87899-6

38. Huang MW, Zhang JG, Zheng L, Liu SM, Yu GY. Accuracy evaluation of a 3D-printed individual template for needle guidance in head and neck brachytherapy. *J Radiat Res*. 2016;57(6):662-667.

doi: 10.1093/jrr/rrw033

39. Zhang HT, Di XM, Yu HM, *et al*. Dose comparison between pre and post operation of ^{125}I seeds implantation guided by 3D print template. *Zhonghua Yi Xue Za Zhi*. 2016;96(9):712-715.

doi: 10.3760/cma.j.issn.0376-2491.2016.09.010

40. Liang Y, Wang Z, Zhang H, *et al*. Three-dimensional-printed individual template-guided ^{125}I seed implantation for the cervical lymph node metastasis: A dosimetric and security study. *J Cancer Res Ther*. 2018;14(1):30-35.

doi: 10.4103/jcrt.JCRT_619_17

41. Sun HT, Jiang YL, Ji Z, *et al*. 3D printing non-coplanar template-assisted 125-iodine seed implantation for thorax movement tumor: Individual template design method. *Zhonghua Yi Xue Za Zhi*. 2019;99(47):3699-3702.

doi: 10.3760/cma.j.issn.0376-2491.2019.47.005

42. Hongtao Z, Xuemin D, Huimin Y, *et al*. Dosimetry study of three-dimensional print template-guided precision ^{125}I seed implantation. *J Cancer Res Ther*. 2016;12(Supplement):C159-C165.

doi: 10.4103/0973-1482.200607

43. Li L, Yang J, Li X, *et al*. (125)I seed permanent implantation as a palliative treatment for stage III and IV hypopharyngeal carcinoma. *Clin Exp Otorhinolaryngol*. 2016;9(3):185-191.

doi: 10.21053/ceo.2015.00213

44. Jiang Y, Zhen P, Dai J, *et al*. Long-term safety and efficacy of CT-guided I 125 radioactive seed implantation as a salvage therapy for recurrent head and neck squamous carcinoma: A multicenter retrospective study. *Front Oncol*. 2021;11:645077.

doi: 10.3389/fonc.2021.645077

45. Zhang Y, Liang Y, Liu Z, Zhang H, Gao Z, Wang J. Efficacy of radioactive ^{125}I seed implantation in treating inoperable or refused operation head and neck cancers. *J Cancer Res Ther*. 2024;20(2):642-650.

doi: 10.4103/jcrt.jcrt_1891_23

46. Li Y, Jiang Y, Wang J. Safety and efficacy of CT-guided radioactive iodine-125 seed implantation as a salvage treatment for recurrent head and neck cancer after two or more courses of radiotherapy. *Radiat Oncol*. 2023;18(1):73.

doi: 10.1186/s13014-023-02254-z

47. Jiang YL, Meng N, Wang JJ, *et al*. CT-guided iodine-125 seed permanent implantation for recurrent head and neck cancers. *Radiat Oncol*. 2010;5:68.

doi: 10.1186/1748-717X-5-68

ACCSCIENCE PUBLISHING

Advances in Radiotherapy & Nuclear Medicine

ORIGINAL RESEARCH ARTICLE

Evaluating the impact of brachytherapy duration on therapeutic outcomes in patients with cervical cancer

Haonan Han[1†], Hailing Hou[2†], Lin Qiu[3], Chingyun Cheng[4], Keying Xu[4], Minglei Kang[5], Tingting Chen[2], Yanling Yang[2], Xiangpan Li[6*], and Liming Xu[2*]

[1]Hubei Key Laboratory of Tumor Microenvironment and Immunotherapy, College of Basic Medical Sciences, China Three Gorges University, Yichang, Hubei, China

[2]Department of Radiation Oncology, Key Laboratory of Cancer Prevention and Therapy, National Clinical Research Center for Cancer, Tianjin's Clinical Research Center for Cancer, Tianjin Medical University Cancer Institute and Hospital, Tianjin, China

[3]Tianjin Union Medical Center, Tianjin Medical University, Tianjin, China

[4]Department of Radiation Oncology, Rutgers Cancer Institute of New Jersey, New Brunswick, New Jersey, United States of America

[5]New York Proton Center, New York, United States of America

[6]Department of Radiation Oncology, Renmin Hospital of Wuhan University/Hubei General Hospital, Wuhan, China

[†]*These authors contributed equally to this work.*

***Corresponding authors:**
Xiangpan Li
(rm001227@whu.edu.cn);
Liming Xu
(xuliming@tjmuch.com)

Citation: Han H, Hou H, Qiu L, *et al.* Evaluating the impact of brachytherapy duration on therapeutic outcomes in patients with cervical cancer. *Adv Radiother Nucl Med.* 2024;2(4):4310. doi: 10.36922/arnm.4310

Received: July 23, 2024

Accepted: September 3, 2024

Published Online: October 21, 2024

Abstract

The total duration of radiotherapy for patients with cervical cancer should be limited to 56 days to optimize treatment outcomes. This study aimed to statistically evaluate the effects of extended radiotherapy duration on survival and complications in 649 patients with cervical cancer treated with brachytherapy at our institution from 2014 to 2019. All patients had undergone intensity-modulated external beam radiation therapy, with 525 receiving two-dimensional (2D) brachytherapy and 124 receiving three-dimensional (3D) brachytherapy. Using the inverse probability of treatment weighting (IPTW) and propensity score matching (PSM), clinical data regarding treatment duration, survival outcomes, and complications were analyzed. PSM revealed that overall survival (OS) did not significantly differ between patients receiving prolonged treatment (>56 days) and those receiving treatment for a standard duration (<56 days) ($P > 0.05$). However, among patients who had received 2D brachytherapy, prolonged treatment correlated with increased recurrence and metastasis risks ($P < 0.001$); this trend was not evident in patients receiving 3D brachytherapy ($P = 0.287$). Higher FIGO stages were associated with worse OS and higher progression risks, which persisted post-IPTW adjustment. Extended radiotherapy duration was linked to a higher incidence of rectal and bladder reactions, particularly in the 2D group. Consequently, strictly controlling radiotherapy duration for patients receiving 2D brachytherapy is essential to reduce recurrence and metastasis risks. Close monitoring of rectal and bladder reactions is also recommended.

Keywords: Cervical cancer; Radiotherapy; Brachytherapy; Treatment duration

1. Introduction

Cervical cancer is the third most common gynecologic malignancy in developed countries and the second most common cancer among women in developing nations. Clinical management of cervical cancer primarily involves surgery and radiation therapy, and the concurrent use of chemoradiotherapy is the mainstay in patients in the advanced stage. Several studies have demonstrated that brachytherapy plays a pivotal curative role in locally advanced cervical cancer, contributing to an improved prognosis.[1,2] However, the conventional approach of combining external beam radiation therapy (EBRT) with intracavitary brachytherapy (BT) remains a critical therapeutic strategy for cervical cancer. According to the American Society for Radiation Oncology's Clinical Practice Guideline titled "Radiation Therapy for Cervical Cancer: Executive Summary of an ASTRO Clinical Practice Guideline,"[3] brachytherapy is an indispensable component in the management of cervical cancer. Based on the cervical cancer radiation dose and multifaceted biological factors,[4] the recommended course of cervical cancer radiation therapy, which encompasses the first phase of EBRT and the second phase of BT, should be completed within 8 weeks. According to the American Brachytherapy Society's consensus guidelines for locally advanced cervical cancer,[5] the recommended tumor point (point A) dose ranges from 80 to 90 Gy equivalent dose in 2-Gy fractions, which can be adjusted based on the tumor size during brachytherapy.

A retrospective study conducted by Song *et al.* in 2013[6] demonstrated that patients with cervical cancer who were administered concurrent chemoradiotherapy for local pelvic control for >56 days experienced adverse effects on pelvic local control. This may have led to an increase in pelvic control failure cases, a decrease in disease-specific survival rates, and a reduction in overall survival (OS). Fyles *et al.*[7] demonstrated that the treatment duration significantly impacts pelvic local control. Their study employed mathematical models based on the linear-quadratic theory and analytical methods such as logistic regression and Cox regression. They found that by providing brachytherapy for >30 days as the definitive treatment for cervical cancer, the control rate in the pelvic area decreased by approximately 1% daily. Furthermore, cancer stage and age were identified as high-risk factors of reduced pelvic control. Perez *et al.*[8] also confirmed that prolonging the treatment duration in patients with stage IB, IIA, IIB, and III cervical cancer significantly affects pelvic tumor control and disease-specific survival rates. The prolongation of treatment results in a daily decrease of approximately 0.85% in pelvic tumor control. Petereit *et al.*[9] used a cutoff of 55 days and revealed significant differences in the 5-year survival and pelvic control rates between patients who were treated for <55 days and those who were treated for ≥55 days (5-year OS, 65% vs. 54%, $P = 0.03$; pelvic control rate, 87% vs. 72%, $P = 0.006$). Based on these findings, the current international radiation therapy guidelines recommend the completion of radiotherapy for cervical cancer within 8 weeks (56 days).

Based on the findings of the aforementioned studies, we used a threshold of 56 days in our study. We aimed to evaluate the differences in survival, treatment techniques, and other variables between patients treated for ≤ 56 days and those treated for > 56 days. The objective of this study was to identify any correlations and significant distinctions in these groups. Through data analysis, we aimed to determine whether the duration of radiation treatment impacts the survival outcomes of patients with cervical cancer. The findings of this study can help better tailor the scheduling of surgical and radiation oncologists, enhance patient compliance, and provide guidance for clinical practice.

2. Materials and methods

2.1. General information

We retrospectively collected the medical records of 649 patients with cervical cancer who were treated with concurrent intensity-modulated radiation therapy (IMRT) and intracavitary brachytherapy at our institution from 2014 to 2019. The clinical data of all the patients were extracted from the outpatient or inpatient records. All patients had undergone standard physical examinations, abdominal–pelvic computed tomography (CT) scans, enhanced magnetic resonance imaging of the pelvic, or positron emission tomography–CT scans. The tumor samples were subjected to histopathological evaluation, and the findings were consistent with the pathological diagnostic criteria for cervical cancer.

The patients were categorized into two groups on the basis of the total duration of radiation therapy. The observation group (OG; duration >56 days) included 464 cases (71.5%), and the control group (CG; duration ≤56 days) included 185 cases (28.5%). The patient age ranged from 29 to 88 years, with 370 patients (57.0%) aged ≤55 years old and 279 patients (43.0%) aged >55 years. All patients were concurrently administered IMRT and intracavitary brachytherapy. Brachytherapy was administered as two-dimensional (2D) radiation therapy in 525 patients and three-dimensional (3D) brachytherapy in 124 patients.

Based on the disease staging, 18, 93, 373, 24, 104, 18, and 19 patients had stage IB, IIA, IIB, IIIA, IIIB, IIIC, and

IVA of the disease, respectively. The inclusion criteria were patients clinically diagnosed with cervical cancer, including squamous cell carcinoma, adenocarcinoma, adenosquamous carcinoma, or small cell carcinoma, with clinical staging ranging from IB to IVA. Furthermore, data were stratified according to planned external radiation dose, FIGO staging, radiation therapy technique, and whether concurrent chemotherapy was administered. The results were summarized and tabulated (Table 1).

2.2. Propensity score matching (PSM)

The data of the 649 patients with cervical cancer were classified and analyzed. Based on whether the treatment duration exceeded 56 days or not, the patients were divided into the OG (>56 days) or CG (≤56 days). PSM was performed using factors such as age group, FIGO stage, and pathology, with a matching tolerance of 0.02. Matching was conducted separately for the overall dataset, patients who received 2D brachytherapy, and patients who received 3D brachytherapy. From the overall dataset of 649 patients, PSM yielded 162 pairs (total, 324 patients' data). From the subset of 525 patients who received 2D brachytherapy, PSM yielded 88 pairs (total, 176 patients' data). From the subset of 124 patients who received 3D brachytherapy, PSM yielded 25 pairs (total, 50 patients' data). The differences and characteristic data before and after PSM are shown in Table 2.

Table 1. Baseline clinical characteristics of the 649 patients with cervical cancer

Characteristics	n	Proportion (%)
Age		
≤55 years	370	57.0
55 years	279	43.0
Brachytherapy pattern		
3D	124	19.1
2D	525	80.9
Treatment time		
≤56 days	185	28.5
56 days	464	71.5
Pathological type		
Squamous carcinoma	596	91.8
Adenocarcinoma	45	6.9
Adenosquamous carcinoma	5	0.8
Others	3	0.5
FIGO stage		
IB	18	2.8
IIA	93	14.3
IIB	373	57.5
IIIA	24	3.7
IIIB	104	16.0
IIIC	18	2.8
IVA	19	2.9
Concurrent chemotherapy		
Yes	476	73.3
No	173	26.7
Total	649	

Abbreviations: D: Dimensional; FIGO: International Federation of Gynecology and Obstetrics staging.

2.3. Inverse probability of treatment weighting (IPTW)

Further statistical analysis was performed using the IPTW method. The confounding factors encompassed age group, FIGO stage, pathology, chemotherapy, and brachytherapy. The weights were calculated through IPTW and the baseline differences before and after weighting were obtained (Table 3). After applying the IPTW method, the statistical differences between the OG and CG disappeared and the standardized mean difference values decreased (Figure 1A).

2.4. Efficacy evaluation and follow-up assessment

Acute adverse events (AEs) were graded according to the Common Terminology Criteria for AEs (version 5.0). Late AEs were graded according to the standards set by the Radiation Therapy Oncology Group. Tumor response was assessed according to the Response Evaluation Criteria in Solid Tumors (version 1.1). Baseline assessments were repeated every two cycles, and post-treatment assessments were conducted every 6 – 8 weeks until disease progression was observed. OS was defined as the interval between the initiation of treatment and the occurrence of an event or the past follow-up. Local or overall progression was defined as the status of cervical cancer from the date of pathological diagnosis until the confirmation of local or overall disease progression through radiological or other examinations (magnetic resonance imaging or enhanced CT).

2.5. Statistical methods

Data were analyzed using SPSS (version 25.0, IBM Corp, US) and R (version 4.3.2, R Foundation for Statistical Computing, Austria). Count and continuous data are presented as number (percentage) and mean ± standard deviation, respectively. PSM or IPTW was employed to match the two groups of patients. Chi-square tests and Kaplan–Meier (KM) survival analysis were conducted to compare the data. A significance level of $P < 0.05$ was considered statistically significant.

Table 2. Baseline characteristics of the patients after PSM of the overall cohort, those who were administered 2D brachytherapy, and those who were administered 3D brachytherapy

Characteristics	Before-PSM		*P*-value	Overall PSM		*P*-value	2D PSM		*P*-value	3D PSM		*P*-value
	OG	CG		OG	CG		OG	CG		OG	CG	
Ages												
≤55 years	273	97	0.137	84	84	1.000	50	56	0.355	11	10	0.774
>55 years	191	88		78	78		38	32		14	15	
Brachytherapy												
3D	27	97	0.000	25	74	0.000			-	25	25	-
2D	437	88		137	88		88	88				
Pathological type												
Squamous carcinoma	420	176	0.058	159	156	0.401	85	84	0.902	25	25	1.000
Adenocarcinoma	39	6		1	4		2	3		0	0	
Adenosquamous carcinoma	5	3		2	2		1	1		0	0	
FIGO stage												
IB	14	3	0.000	0	3	0.646	0	3	0.090	0	0	1.000
IIA	71	22		12	13		12	12		1	1	
IIB	259	114		111	114		60	61		16	16	
IIIA	20	4		6	4		0	3		0	0	
IIIB	82	22		29	22		7	8		6	6	
IIIC	2	16		2	2		0	1		2	2	
IVA	15	4		2	4					0	0	
Concurrent chemotherapy												
Yes	328	148	0.015	129	125	0.589	60	65	0.406	22	20	0.0440
No	136	37		33	37		28	23		3	5	
Total	464	185		162	162		88	88		25	25	

Abbreviations: PSM: Propensity score matching; 2D: Two-dimensional; 3D: Three-dimensional; OG: Observation group; CG: Control group; FIGO: International Federation of Gynecology and Obstetrics staging.

3. Results

3.1. Survival analysis

The median follow-up duration was 24.6 (range, 0.59 – 49.28) months. A total of seven patients were lost to follow-up. The median dose of escalated radiotherapy was 50.4 (range, 45.00 – 52.20) Gy. In the OG, the OS rate was 81.7%, and 85 patients died. In the CG, the OS rate was 88.1%, and 22 patients died. The OS rate was slightly lower in the OG than in the CG ($P = 0.046$). However, the survival analysis distribution homogeneity test did not reveal any statistically significant differences between the two groups ($P = 0.7154$) (Figure 1B). Survival analysis of the 324 PSM-selected patients confirmed that there was no significant statistical difference between the OG and CG ($P = 0.3142$) (Figure 1C). This was also observed in the KM analysis after IPTW weighting ($P = 0.3079$) (Figure 1D).

Among 2D brachytherapy patients, the survival risk was significantly different between those whose treatment duration exceeded 56 days and those whose treatment duration was within 56 days (hazard ratio = 2.65, 95% confidence interval: 1.16–6.07, $P = 0.0167$) (Figure 1E). After PSM of the patients who underwent 2D brachytherapy, the survival analysis of the 176 patients demonstrated that although there was a trend of difference, the risk between the OG and CG was not statistically significant ($P = 0.080$) (Figure 1F). After IPTW weighting, KM survival analysis revealed no significant difference ($P = 0.4123$) (Figure 1G). However, the HR was high. Survival analysis of the 54 PMS-selected patients (27 pairs) who underwent 3D brachytherapy did not reveal any significant difference in the survival risk between the OG and CG ($P = 0.4137$) (Figure 1H). This finding was further validated in the KM survival analysis after IPTW (HR = 1.63, 95% CI: 0.57–4.63, $P = 0.3486$) (Figure 1I).

3.2. Risk of recurrence and metastasis

Among the 649 included patients, 70 patients (15.1%) in the OG and 8 patients (4.3%) in the CG developed

Table 3. Baseline characteristics of the patients after the IPTW application

Group	Subgroup	Unmatched				IPTW			
		OG	CG	*P*-value	Test SMD	OG	CG	*P*-value	Test SMD
Case count (*n*)		185	464			184.0	467.5		
Age (*n*, %)	>56 years	88 (47.6)	191 (41.2)	0.162	0.129	77.5 (42.1)	197.0 (42.1)	0.995	0.001
FIGO stage (*n*, %)	≤55 years	97 (52.4)	273 (58.8)			106.6 (57.9)	270.5 (57.9)		
Brachytherapy (%)	2D	88 (47.6)	437 (94.2)	<0.001	1.195	148.7 (80.8)	375.2 (80.3)	0.892	0.014
	3D	97 (52.4)	27 (5.8)			35.3 (19.2)	92.3 (19.7)		
Chemotherapy (%)	No	37 (20.0)	136 (29.3)	0.020	0.217	51.5 (28.0)	121.7 (26.0)	0.704	0.044
	Yes	148 (80.0)	328 (70.7)			132.6 (72.0)	345.8 (74.0)		
FIGO stage (%)	IB	3 (1.6)	15 (3.2)	<0.001	0.476	4.6 (2.5)	12.8 (2.7)	0.999	0.059
	IIA	22 (11.9)	71 (15.3)			23.9 (13.0)	63.2 (13.5)		
	IIB	114 (61.6)	259 (55.8)			109.2 (59.4)	275.0 (58.8)		
	IIIA	4 (2.2)	20 (4.3)			5.8 (3.1)	16.6 (3.6)		
	IIIB	22 (11.9)	82 (17.7)			29.0 (15.8)	73.7 (15.8)		
	IIIC	16 (8.6)	2 (0.4)			5.1 (2.8)	13.9 (3.0)		
	IVA	4 (2.2)	15 (3.2)			6.4 (3.5)	12.2 (2.6)		
Pathology (%)	Adenocarcinoma	6 (3.2)	39 (8.4)	0.058	0.226	12.7 (6.9)	31.2 (6.7)	0.989	0.011
	Others	3 (1.6)	5 (1.1)			1.8 (1.0)	4.5 (1.0)		
	Squamous cell carcinoma	176 (95.1)	420 (90.5)			169.4 (92.1)	431.8 (92.4)		

Abbreviations: IPTW: Inverse probability of treatment weighting; OG: Observation group; CG: Control group; SMD: Standardized mean difference; 2D: Two-dimensional; 3D: Three-dimensional; FIGO: International Federation of Gynecology and Obstetrics staging.

recurrence. Furthermore, 124 patients (26.7%) in the OG and 26 patients (14.1%) in the CG developed metastasis. These differences between the groups were statistically significant ($P < 0.001$). However, KM survival analysis demonstrated that there was no significant difference in the disease-free survival (DFS) between the two groups ($P = 0.9482$) (Figure 2A).

After PSM, the analysis of the 324 patients revealed that 22 patients (13.6%) in the OG and 8 patients (4.9%) in the CG developed recurrence. Furthermore, 45 patients (27.8%) in the OG and 25 patients (15.4%) in the CG developed metastasis. These differences between the groups remained statistically significant ($P < 0.001$). However, KM survival analysis after PSM still did not reveal any significant difference in DFS between the two groups (Figure 2B). Nonetheless, DFS analysis after IPTW demonstrated that the patients in the OG had a higher risk of progression within the first 34 months than the patients in the CG. Furthermore, the risk of progression after 34 months was lower in the OG than in the CG (HR = 1.04, 95% CI: 0.67–1.63, $P = 0.0142$) (Figure 2C).

Among the 50 PSM-selected patients who received 3D brachytherapy, 3 patients (12.0%) in the OG and 5 patients (18.5%) in the CG developed recurrence. Furthermore, 2 patients (8.0%) developed metastasis in only the OG. These differences between the groups were not statistically significant ($P = 0.788$). The KM survival analysis yielded similar results ($P = 0.2495$) (Figure 2D). IPTW analysis could not be performed due to the limited number of outcome events.

Among the 176 PSM-selected patients who received 2D brachytherapy, 11 patients (12.5%) developed recurrence in only the OG. Furthermore, 26 patients (29.5%) in the OG and 18 patients (20.5%) in the CG developed metastasis. Thus, the risk of recurrence and metastasis was statistically significantly higher in the OG than in the CG ($P < 0.001$). However, KM survival analysis demonstrated no significant difference ($P = 0.6449$) (Figure 2E). After IPTW weighting, the DFS risk between the two groups was similar to that in the overall sample and exhibited a statistically significant difference (HR = 1.03, 95% CI: 0.63–1.69, $P = 0.0244$) (Figure 2F).

3.3. FIGO stage analysis

Survival or progression analysis was conducted for all patients based on FIGO staging. KM survival analysis revealed that patients with stage III – IV cancer had a

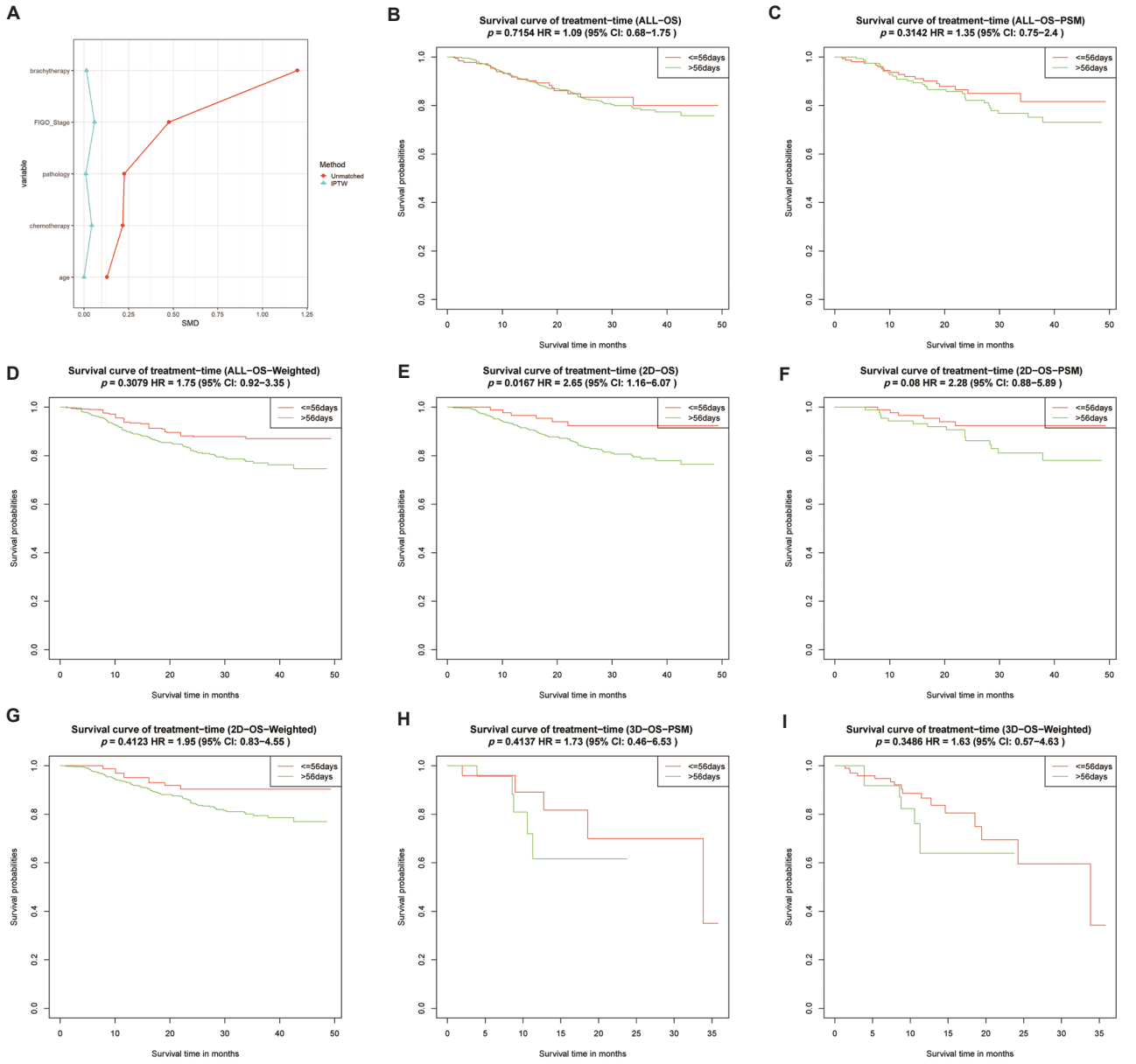

Figure 1. (A-I) Comparison before and after weighting the IPTW reference factors, along with survival analysis using overall survival as the outcome

higher risk of survival than patients with stage I – II cancer ($P < 0.001$) (Figure 3A). However, this difference lost statistical significance after IPTW adjustment ($P = 0.1068$) (Figure 3B). Among the patients who received 3D brachytherapy, there was no significant difference between the groups either in the overall analysis ($P = 0.2719$) (Figure 3C) or after IPTW adjustment ($P = 0.1731$) (Figure 3D). However, among the patients who received 2D brachytherapy, the results were similar to those of the overall patient cohort before IPTW adjustment; patients with stage III – IV cancer exhibited a higher risk of survival than patients with stage I – II cancer ($P < 0.001$) (Figure 3E). However, this difference lost statistical significance after IPTW adjustment ($P = 0.2179$) (Figure 3F).

KM survival analysis for all patients revealed that patients with stage III – IV cancer had a higher risk of disease progression than those with stage I – II cancer ($P < 0.001$) (Figure 3G). This result remained statistically significant after IPTW weighting ($P = 0.0012$) (Figure 3H). Among the patients who received 3D brachytherapy, there was no difference in the overall analysis ($P = 0.2346$) (Figure 3I) and IPTW analysis could not be performed due to the limited number of outcome events. Among the patients who received 2D brachytherapy, the results were

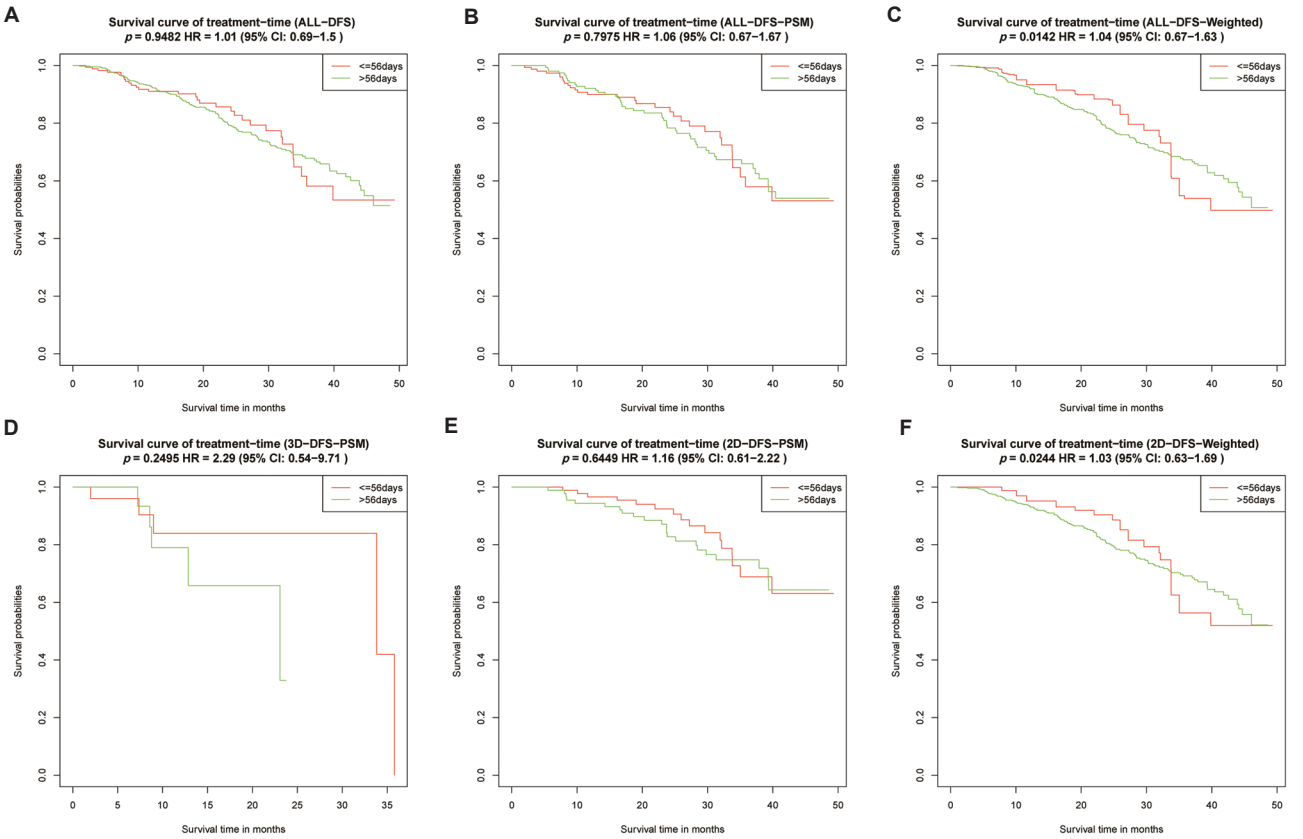

Figure 2. (A-F) The survival analysis with disease-free survival as the outcome

similar to those of the overall patient population before IPTW adjustment; patients with stage III – IV cancer exhibited a higher risk of survival ($P < 0.001$) (Figure 3J). This result remained statistically significant after IPTW adjustment ($P = 0.0023$) (Figure 3K).

3.4. Rectal and bladder responses

Among the 649 cases, there were no significant differences in early bladder response ($P = 0.125$) and late rectal response ($P = 0.137$) between the OG and CG. However, there was a significantly higher risk of early rectal response ($P = 0.001$) and late bladder response ($P < 0.001$) in the OG than in the CG. After PSM adjustment, no significant differences were found between the OG and CG in terms of early bladder response ($P = 0.792$), rectal response ($P = 0.262$), and late bladder response ($P = 0.175$). However, the OG had a significantly higher risk of late rectal response ($P = 0.050$) than the CG.

Among the PSM-selected patients who received 2D brachytherapy, there were no significant differences in the early bladder response ($P = 0.325$), early rectal response ($P = 0.664$), late bladder response ($P = 0.762$), or late rectal response ($P = 0.470$) between the OG and CG.

Among the PSM-selected patients who received 3D brachytherapy, there were no significant differences in the early bladder response ($P = 0.352$), early rectal response ($P = 0.312$), late bladder response ($P = 0.700$), or late rectal response ($P = 0.347$) between the OG and CG.

4. Discussion

Conventionally, it has been believed that radiation oncologists should aim to complete radiotherapy for patients with cervical cancer within 56 days to achieve optimal treatment outcomes while minimizing the risk of additional complications. This study aimed to further evaluate the impact of radiotherapy duration on patient prognosis and the development of adverse effects.

Survival analysis revealed that in the overall sample and in patients who received 3D brachytherapy, a treatment duration of >56 days did not affect the OS. However, in patients who received 2D brachytherapy, prolonged treatment may lead to reduced survival. The finding is consistent with the results of previous studies.[6,9]

Patients with higher FIGO stages (III – IV) exhibited a significantly higher survival or progression risk than

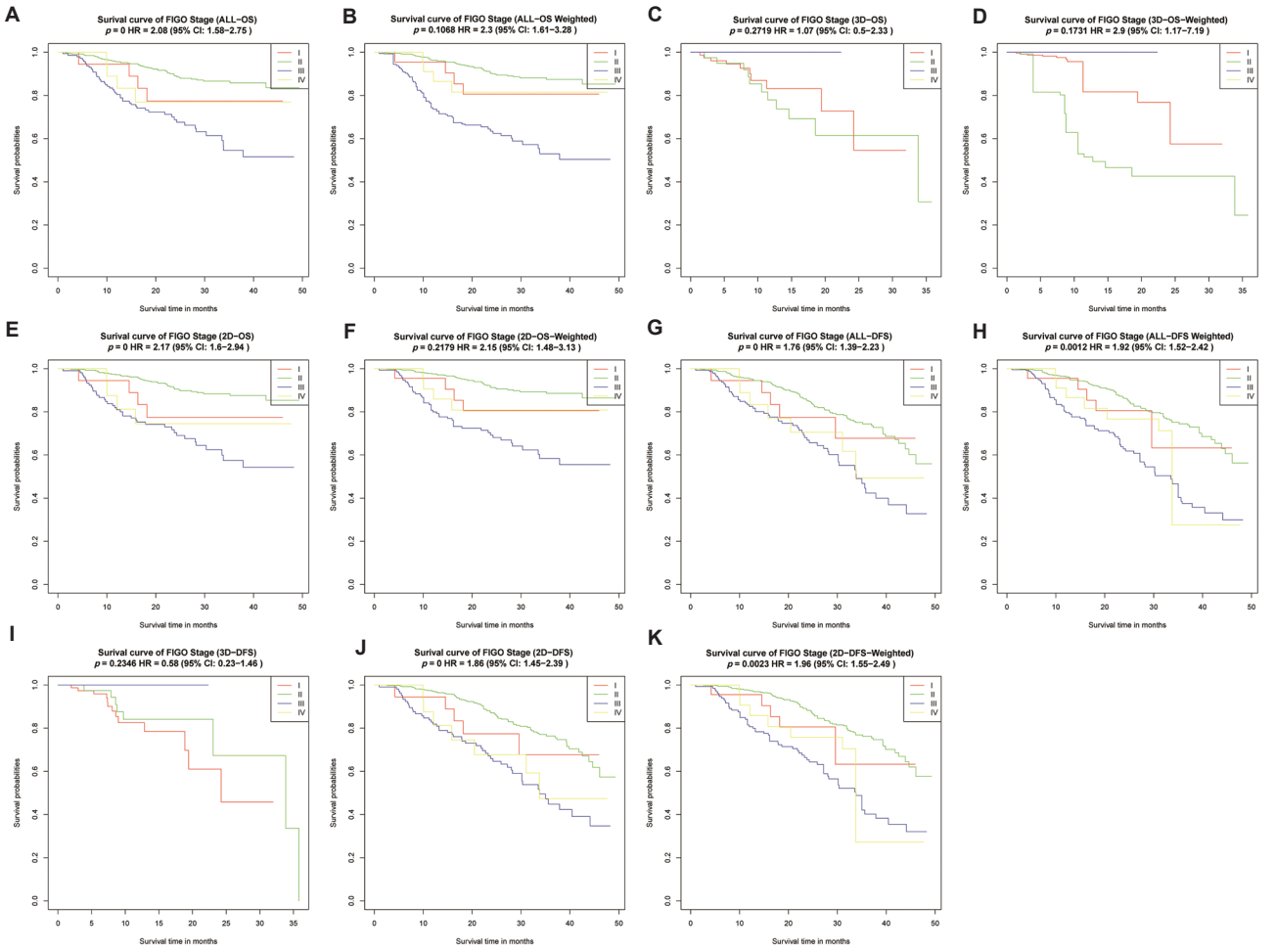

Figure 3. (A-K) K-M analysis of FIGO stage

patients with lower FIGO stages. This was overserved in the overall cohort as well as among the patients who received 2D brachytherapy. However, in patients who received 3D brachytherapy, there was no significant difference in survival or metastasis risk across the different FIGO stages. Thus, our findings indicate that prolonged treatment with 3D brachytherapy does not affect OS or disease progression. Furthermore, OS and progression risk may be lower in patients with higher FIGO stages (III – IV) who receive 3D brachytherapy.

We hypothesize that the technical limitations of 2D brachytherapy contribute to the increased risk of recurrence and metastasis with prolonged treatment duration. In contrast, the more precise dose distribution and positioning characteristics of 3D brachytherapy do not pose an increased risk of recurrence or metastasis with prolonged treatment (>56 days). Thus, 3D brachytherapy may enhance compliance and alleviate treatment duration constraints in patients with cervical cancer. The significantly higher risk of recurrence or metastasis in patients in the OG who were treated with 2D brachytherapy than those in the CG who were treated with 2D brachytherapy highlights the need for strict control of treatment duration to mitigate the risks of recurrence and metastasis. Alternatively, switching to 3D brachytherapy in appropriate circumstances may improve pelvic control rates.

In terms of grading the responses of surrounding normal tissues, when employing either brachytherapy technique, prolonged treatment did not increase the risk of early or late rectal or bladder responses in patients with cervical cancer. However, in terms of overall patients with cervical cancer undergoing brachytherapy, prolonged treatment significantly increased the risk of early rectal and late bladder responses. Thus, more vigilant monitoring of early and late rectal and bladder responses is warranted when administering brachytherapy to patients with cervical cancer. This is because prolonged treatment may contribute to an

increased incidence of these symptoms, irrespective of the brachytherapy technique chosen.

Since the 1990s, studies have compared the combined use of brachytherapy and EBRT with EBRT alone for treating cervical cancer. The findings have demonstrated a significant improvement in survival rates and enhanced local control with the combined use of brachytherapy and EBRT compared with EBRT alone.[10] Subsequent studies have further validated these findings.[11] Despite the advancements in radiation therapy techniques, innovations in EBRT cannot fully replace the pivotal role of brachytherapy in treating cervical cancer.[12-14] With the rapid advancement and widespread adoption of 3D image-guided brachytherapy (3D-IGABT) in recent years,[15] the limitations of traditional 2D brachytherapy have become increasingly apparent. Studies have demonstrated that 3D-IGABT allows for more precise distribution of doses to the clinical target volume and organs at risk,[16] offering significant advantages over the dose distribution achieved with 2D brachytherapy. Similar studies[17] have demonstrated that the overall long-term toxicity associated with 3D-IGABT is lower than that associated with 2D brachytherapy during the treatment of locally advanced cervical cancer. The total number of cases of late treatment-related toxic reactions and the severity of these reactions are significantly lower with 3D brachytherapy than with 2D brachytherapy. Thus, 3D brachytherapy can markedly improve treatment efficacy while reducing toxicity levels.[18-20]

Previous studies have demonstrated that the radiotherapy duration for patients with cervical cancer should be limited to 56 days. In the 1990s, Fyles *et al.*[7] demonstrated that a treatment duration of >30 days decreased the daily control rate by approximately 1%. Similarly, Girinsky *et al.*[21] demonstrated that radiotherapy administration for >52 days in cervical cancer decreased both the local control and OS rates by approximately 1% per day. Lanciano *et al.*[22] demonstrated a significant decrease in survival rates ($P = 0.0001$) and pelvic control rates ($P = 0.0001$) with increasing treatment durations that were categorized as <6 weeks, 6 – 8 weeks, 8 – 10 weeks, and >10 weeks. Treatment prolongation was significantly associated with grade III AEs and intrapelvic recurrence.

Based on the aforementioned findings, Chatani *et al.*[23] proposed that prolongation of treatment adversely impacts local control and survival in patients with cervical cancer. The multivariate analysis in their study revealed that the total treatment duration is the most significant factor affecting local control rates ($P = 0.0005$). Furthermore, significant differences in the 5-year cumulative recurrence rates were observed among different treatment time groups (35 – 42 days, 9%; 43 – 49 days, 9%; and 50 – 62 days, 42%; $P = 0.001$). Vitzthum *et al.*[24] also emphasized the importance of rational treatment scheduling, patient education, and organized radiochemotherapy to maintain the treatment duration within 56 days and mitigate the risk of reduced local control rates that are associated with treatment prolongation.

Subsequent studies have explored strategies to reduce the total radiotherapy duration and shorten the waiting times for radiotherapy. Vijayakumar *et al.*[25] proposed that patient compliance and education can effectively reduce the total radiotherapy time. Their study analyzed two groups, those treated within 60 days (32.1%) and those treated for >60 days (67.9%). The median radiotherapy duration was 68 (51 – 106) days. The authors argued that reducing radiotherapy duration may impact the local/regional control, DFS, and OS. Furthermore, it can reduce patients' financial and time burden in regions with limited healthcare resources. In economically disadvantaged areas, reducing the radiotherapy duration can improve compliance, enhance treatment efficiency in healthcare facilities, reduce wait times for radiotherapy, and decrease the probability of disease progression or death during the waiting period. Dereje *et al.*[26] proposed that prolonged waiting times may lead to patient deaths during the waiting period. Patients who are administered radiotherapy within 60 days of the initial diagnosis are three times less likely to exhibit tumor progression than those who have to wait for >4 months before starting treatment. Nascimento *et al.*[27] also demonstrated that waiting for radiotherapy for >64 days increases the 5-year OS risk.

With the rapid advancements in radiotherapeutic technology and the widespread availability of radiotherapy equipment, previously studied issues such as dose delivery, adverse effects, and local control of radiotherapy should be reconsidered. Recent studies have primarily focused on aspects such as dose distribution[28] and precision[29] in the comparison of 3D brachytherapy with 2D brachytherapy. Till date, no study has evaluated whether treatment prolongation affects the treatment outcomes of patients with cervical cancer who are being treated with different brachytherapy modalities (3D vs. 2D). This study's findings indicate that when IMRT is combined with 3D brachytherapy, the total treatment duration does not significant impact the prognosis. Further studies on this topic may provide valuable insights into the evolving landscape of cervical cancer treatment and the role of different treatment modalities.

It is essential to consider the combination of radiotherapy with other treatment modalities. For example, the use of hyperthermia in conjunction with

radiotherapy for patients with cervical cancer has been investigated. Van Leeuwen *et al.*[30] studied the effect of the interval between EBRT and hyperthermia on the rates of intracavitary recurrence, OS, and late toxicity in women with advanced cervical cancer. They found that administering hyperthermia shortly after EBRT can reduce the risk of intracavitary recurrence and improve OS, with no significant differences in late toxicity. This suggests that a combination of hyperthermia and radiotherapy may be a promising approach for the treatment of cervical cancer. Further evaluation of such combined therapies could be beneficial in optimizing treatment outcomes.

This study still has certain limitations: (1) The study is based on retrospectively obtained data. Furthermore, although the clinical data were subjected to PSM, some inherent bias in the matched data may still exist. (2) The data on adverse reactions and complications is not comprehensive, which could be attributed to the quality of data collection during the study. (3) Although the study had a relatively large sample size, the sample sizes and data of the two groups differed after applying the PSM or IPTW method. This may have introduced variability. With the gradual popularization of 3D brachytherapy, the difference in patient data may be reduced. Therefore, future research should include more prospective studies to guide clinical treatment, overcome these limitations, and provide more robust and conclusive insights into the treatment of cervical cancer.

This study's results demonstrate that when using IMRT in combination with 3D brachytherapy for the treatment of cervical cancer, the treatment duration does not need to be limited to 56 days. This flexibility can better accommodate the timing of surgeries, chemotherapy, and other adjuvant treatments for patients. Thus, it could improve patient compliance and overall treatment outcomes. However, weighing the benefits against the potential advantages of reducing the total treatment duration, such as time and cost savings, and increased utilization of imaging equipment is essential. A comprehensive assessment should consider both patient outcomes and resource utilization. It is hoped that future studies will continue to focus on providing better treatment options for patients with cervical cancer.

5. Conclusion

This study revealed significant differences in optimal radiotherapy duration for patients with cervical cancer based on various techniques. Our findings indicate that limiting treatment to 56 days can help mitigate the risks of recurrence and metastasis in patients receiving 2D brachytherapy. However, the increased incidence of complications associated with prolonged treatment in this patient group emphasizes the need for strict adherence to treatment protocols.

Conversely, 3D brachytherapy appears to provide a more favorable risk profile, allowing for extended treatment durations without significantly increasing the risk of adverse outcomes. This suggests that 3D brachytherapy is the preferred treatment approach for patients with advanced disease, as it enhances local pelvic control rates while minimizing complications.

Further studies are warranted to explore the optimal treatment protocols for different brachytherapy techniques, emphasizing the importance of close monitoring of early and late rectal and bladder reactions in all patients.

Acknowledgments

None.

Funding

This study was supported by the National Natural Science Foundation of China (Grant no.: 82373194).

Conflict of interest

Minglei Kang and Liming Xu are the Editorial Board Members of this journal but were not in any way involved in the editorial and peer-review process conducted for this paper, directly or indirectly. Separately, other authors declared that they have no known competing financial interests or personal relationships that could have influenced the work reported in this paper.

Author contributions

Conceptualization: Xiangpan Li, Liming Xu, Haonan Han,Hailing Hou
Data curation: Hailing Hou, Lin Qiu, Tingting Chen, Yanling Yang
Formal analysis: Haonan Han, Hailing Hou
Investigation: Haonan Han, Hailing Hou
Methodology: Haonan Han, Hailing Hou
Validation: Hailing Hou, Lin Qiu, Tingting Chen, Yanling Yang
Writing – original draft: Haonan Han, Hailing Hou
Writing – review & editing: Chingyun Cheng, Keying Xu, Minglei Kang, Haonan Han, Hailing Hou

Ethics approval and consent to participate

The study was approved by the Human Investigation Committee of Tianjin Medical University Cancer Hospital, Tianjin, China. The patients gave consent to participate in this study.

Consent for publication

The patients gave consent to publish their data.

Availability of data

Data is available from the corresponding author upon reasonable request.

References

1. Han K, Milosevic M, Fyles A, Pintilie M, Viswanathan AN. Trends in the utilization of brachytherapy in cervical cancer in the United States. *Int J Radiat Oncol Biol Phys*. 2013;87(1):111-119.

   doi: 10.1016/j.ijrobp.2013.05.033

2. Gill BS, Lin JF, Krivak TC, *et al.* National Cancer Data Base analysis of radiation therapy consolidation modality for cervical cancer: The impact of new technological advancements. *Int J Radiat Oncol Biol Phys*. 2014;90(5):1083-1090.

   doi: 10.1016/j.ijrobp.2014.07.017

3. Chino J, Annunziata CM, Beriwal S, *et al.* Radiation therapy for cervical cancer: Executive summary of an ASTRO clinical practice guideline. *Pract Radiat Oncol*. 020;10(4):220-234.

   doi: 10.1016/j.prro.2020.04.002

4. Tornero-López AM, Guirado D. Radiobiological considerations in combining doses from external beam radiotherapy and brachytherapy for cervical cancer. *Rep Pract Oncol Radiother*. 2018;23(6):562-573.

   doi: 10.1016/j.rpor.2018.05.007

5. Viswanathan AN, Beriwal S, De Los Santos JF, *et al.* American Brachytherapy Society consensus guidelines for locally advanced carcinoma of the cervix. Part II: High-dose-rate brachytherapy. *Brachytherapy*. 2012;11(1):47-52.

   doi: 10.1016/j.brachy.2011.07.002

6. Song S, Rudra S, Hasselle MD, *et al.* The effect of treatment time in locally advanced cervical cancer in the era of concurrent chemoradiotherapy. *Cancer*. 2013;119(2):325-331.

   doi: 10.1002/cncr.27652

7. Fyles A, Keane TJ, Barton M, Simm J. The effect of treatment duration in the local control of cervix cancer. *Radiother Oncol*. 1992;25(4):273-279.

   doi: 10.1016/0167-8140(92)90247-r

8. Perez CA, Grigsby PW, Castro-Vita H, Lockett MA. Carcinoma of the uterine cervix. I. Impact of prolongation of overall treatment time and timing of brachytherapy on outcome of radiation therapy. *Int J Radiat Oncol Biol Phys*. 1995;32(5):1275-1288.

   doi: 10.1016/0360-3016(95)00220-S

9. Petereit DG, Sarkaria JN, Chappell R, *et al.* The adverse effect of treatment prolongation in cervical carcinoma. *Int J Radiat Oncol Biol Phys*. 1995;32(5):1301-1307.

   doi: 10.1016/0360-3016(94)00635-X

10. Lanciano RM, Martz K, Coia LR, Hanks GE. Tumor and treatment factors improving outcome in stage III-B cervix cancer. *Int J Radiat Oncol Biol Phys*. 1991;20(1):95-100.

    doi: 10.1016/0360-3016(91)90143-r

11. Karlsson J, Dreifaldt AC, Mordhorst LB, Sorbe B. Differences in outcome for cervical cancer patients treated with or without brachytherapy. *Brachytherapy*. 2017;16(1):133-140.

    doi: 10.1016/j.brachy.2016.09.011

12. Campitelli M, Lazzari R, Piccolo F, *et al.* Brachytherapy or external beam radiotherapy as a boost in locally advanced cervical cancer: A Gynaecology Study Group in the Italian Association of Radiation and Clinical Oncology (AIRO) review. *Int J Gynecol Cancer*. 2021;31(9):1278-1286.

    doi: 10.1136/ijgc-2020-002310

13. Chargari C, Renard S, Espenel S, *et al.* Can stereotactic body radiotherapy replace brachytherapy for locally advanced cervical cancer? French society for radiation oncology statement. *Cancer Radiother*. 2020;24(6-7):706-713.

    doi: 10.1016/j.canrad.2020.05.003

14. Holschneider CH, Petereit DG, Chu C, *et al.* Brachytherapy: A critical component of primary radiation therapy for cervical cancer: From the Society of Gynecologic Oncology (SGO) and the American Brachytherapy Society (ABS). *Gynecol Oncol*. 2019;152(3):540-547.

    doi: 10.1016/j.ygyno.2018.10.016

15. Fields EC, Hazell S, Morcos M, Schmidt EJ, Chargari C, Viswanathan AN. Image-guided gynecologic brachytherapy for cervical cancer. *Semin Radiat Oncol*. 2020;30(1):16-28.

    doi: 10.1016/j.semradonc.2019.08.010

16. Tan LT, Tanderup K, Kirisits C, *et al.* Image-guided adaptive radiotherapy in cervical cancer. *Semin Radiat Oncol*. 2019;29(3):284-298.

    doi: 10.1016/j.semradonc.2019.02.010

17. Faye MD, Petruccelli Araujo M, Wissing MD, *et al.* Safety and efficacy of 2D brachytherapy vs. 3D image-guided adaptive brachytherapy for locally advanced cervical cancer-a single institution retrospective study. *Curr Oncol*. 2023;30(5):4966-4978.

    doi: 10.3390/curroncol30050375

18. Sturdza A, Potter R, Fokdal LU, *et al.* Image guided brachytherapy in locally advanced cervical cancer: Improved pelvic control and survival in RetroEMBRACE, a multicenter cohort study. *Radiother Oncol*. 2016;120(3):428-433.

    doi: 10.1016/j.radonc.2016.03.011

19. Lin AJ, Kidd E, Dehdashti F, *et al.* Intensity modulated radiation therapy and image-guided adapted brachytherapy

for cervix cancer. *Int J Radiat Oncol Biol Phys*. 2019;103(5):1088-1097.

doi: 10.1016/j.ijrobp.2018.11.012

20. Kim YJ, Kang HC, Kim YS. Impact of intracavitary brachytherapy technique (2D versus 3D) on outcomes of cervical cancer: A systematic review and meta-analysis. *Strahlenther Onkol*. 2020;196(11):973-982.

doi: 10.1007/s00066-020-01658-0

21. Girinsky T, Rey A, Roche B, *et al.* Overall treatment time in advanced cervical carcinomas: A critical parameter in treatment outcome. *Int J Radiat Oncol Biol Phys*. 1993;27(5):1051-1056.

doi: 10.1016/0360-3016(93)90522-w

22. Lanciano RM, Pajak TF, Martz K, Hanks GE. The influence of treatment time on outcome for squamous cell cancer of the uterine cervix treated with radiation: A patterns-of-care study. *Int J Radiat Oncol Biol Phys*. 1993;25(3):391-397.

doi: 10.1016/0360-3016(93)90058-4

23. Chatani M, Matayoshi Y, Masaki N, Inoue T. High-dose rate intracavitary irradiation for carcinoma of the uterine cervix. The adverse effect of treatment prolongation. *Strahlenther Onkol*. 1997;173(7):379-384.

doi: 10.1007/BF03038241

24. Vitzthum L, Yuan J, Jones D, Boldt A, Dusenbery K. Reducing prolonged chemoradiation treatment times for cervical cancer. *Bmj Open Quality*. 2019;8(3):e000516.

doi: 10.1136/bmjoq-2018-000516

25. Vijayakumar S, Nittala MR, Duggar WN, *et al.* The influence of patient and system factors on the radiotherapy treatment time in the treatment of non-metastatic cervical cancer patients in a rural and resource-lean state's safety-net hospital: Benefits of strategic planning. *Cureus*. 2023;15(3):e35954.

doi: 10.7759/cureus.35954

26. Dereje N, Addissie A, Worku A, *et al.* Association between waiting time for radiotherapy initiation and disease progression among women with cervical cancer in Addis Ababa, Ethiopia. *Int J Cancer*. 2021;149(6):1284-1289.

doi: 10.1002/ijc.33689

27. Nascimento MI, Silva GA. Effect of waiting time for radiotherapy on five-year overall survival in women with cervical cancer, 1995-2010. *Cad Saude Publica*. 2015;31(11):2437-2448.

doi: 10.1590/0102-311x00004015

28. Tanderup K, Nesvacil N, Kirchheiner K, *et al.* Evidence-based dose planning aims and dose prescription in image-guided brachytherapy combined with radiochemotherapy in locally advanced cervical cancer. *Semin Radiat Oncol*. 2020;30(4):311-327.

doi: 10.1016/j.semradonc.2020.05.008

29. Liu Z, Zhao Y, Li Y, *et al.* Imaging-guided brachytherapy for locally advanced cervical cancer: The main process and common techniques. *Am J Cancer Res*. 2020;10(12):4165-4177.

30. Van Leeuwen CM, Oei AL, Chin K, *et al.* A short time interval between radiotherapy and hyperthermia reduces in-field recurrence and mortality in women with advanced cervical cancer. *Radiat Oncol*. 2017;12(1):75.

doi: 10.1186/s13014-017-0813-0

ACCSCIENCE PUBLISHING

Advances in Radiotherapy & Nuclear Medicine

ORIGINAL RESEARCH ARTICLE

Efficacy and safety of stereotactic radiotherapy in oligometastases

Huan Dong[1†], Rong Li[1,2†], He-Qing Huang[1], Xing-Hua Chen[1], Zi-Yan Zhou[3], and Min Kang[1*]

[1]Department of Radiation Oncology, The First Affiliated Hospital of Guangxi Medical University, Radiation Oncology Clinical Medical Research Center of Guangxi, 6 Shuangyong Road, Nanning, Guangxi Zhuang Autonomous Region, China

[2]Department of Medical Oncology, The First Affiliated Hospital of Guangxi Medical University, Nanning, Guangxi Zhuang Autonomous Region, China

[3]Key Laboratory of Early Prevention and Treatment for Regional High-Frequency Tumor (Guangxi Medical University), Ministry of Education, Nanning, Guangxi Zhuang Autonomous Region, China

Abstract

Distant metastasis remains a leading cause of treatment failure in patients with cancer. While salvage treatments such as surgery, targeted therapy, and immunotherapy provide some benefits, they have inherent limitations. This study examines the efficacy and safety of stereotactic radiotherapy (SRT) in managing oligometastatic tumors. We retrospectively analyzed data from 96 patients with oligometastatic tumors who were treated with SRT at the Department of Radiotherapy of the First Affiliated Hospital of Guangxi Medical University between September 2019 and March 2023. Descriptive statistics were used to analyze patient characteristics, tumor response, and survival outcomes, whereas a single-sample ratio test was used to compare SRT efficacy across different tumor sites. Kaplan–Meier analysis was used to determine progression-free survival (PFS) and overall survival (OS). Three months post-treatment, the complete response, partial response, stable disease, and progressive disease rates were 26.32%, 50.00%, 21.05%, and 2.63% for liver oligometastases; 0.00%, 39.13%, 43.48%, and 17.39% for lung oligometastases; and 8.57%, 62.86%, 25.71%, and 2.86% for brain oligometastases, respectively. The objective response rate was 65.62%, and the disease control rate was 93.75%. The median PFS was 18 months, and the median OS was 27 months. The primary lesions were mainly located in the liver and lungs. Compared with previous studies where stereotactic ablative body radiotherapy achieved a median OS of 16 months for liver metastases and surgery yielded an OS of 7 – 24 months for non-small cell lung cancer with brain metastases, our SRT outcomes were significantly improved. Adverse events (≥grade 3), primarily hematological toxicity, occurred in only 5.21% of patients. SRT was both effective and well-tolerated among patients with oligometastatic tumors, offering a promising treatment option.

Keywords: Stereotactic radiotherapy; Oligometastases; Efficacy; Safety

1. Introduction

With rapid advancements in comprehensive cancer treatment, the prognosis of patients with cancer has significantly improved. However, distant metastasis remains the main

[†]These authors contributed equally to this work.

***Corresponding author:**
Min Kang
(kangmin@gxmu.edu.cn)

Citation: Dong H, Li R, Huang H, Chen X, Zhou Z, Kang M. Efficacy and safety of stereotactic radiotherapy in oligometastases. *Adv Radiother Nucl Med.* 2024;2(4):3391. doi: 10.36922/arnm.3391

Received: April 9, 2024

Accepted: June 28, 2024

Published Online: November 13, 2024

factor affecting treatment failure and the quality of life of patients. Active systemic therapy is usually used to control the increase in tumor load caused by distant metastasis. However, the survival benefits of first-line chemotherapy remain limited. For instance, in patients with advanced non-small cell lung cancer, platinum-based chemotherapy results in a median overall survival (OS) of only 9.1 months, with a 1-year OS rate of 37%.[1] In recent years, in-depth studies on targeted therapy and immunotherapy have demonstrated significant clinical benefits of their combination for advanced tumors. For instance, the median OS of patients with metastatic liver cancer receiving first-line targeted therapy is 10.7 months.[2] Similarly, in patients with metastatic colorectal cancer, combining targeted therapy or immunotherapy with chemotherapy has significantly extended OS compared with chemotherapy alone.[3] However, targeted therapy has some limitations, including restricted effectiveness to tumors with specific biomarkers, emergence of drug resistance, and new mutations resulting from target inhibition.[4] Immunotherapy also faces certain challenges, such as low response rates and the development of resistance.[5] Although surgery and local ablation have proven effective in treating oligometastatic colorectal cancer,[6] these invasive treatments carry the risk of complications. Consequently, there is a need for non-invasive, effective, and less toxic therapies for managing recurrent and oligometastatic tumors.

Stereotactic radiotherapy (SRT), including stereotactic radiosurgery and stereotactic body radiation therapy, has emerged as a promising approach. Unlike traditional radiotherapy, SRT delivers highly conformal, high-dose radiation of ≥5.0 Gy, achieving similar outcomes with equal or reduced toxicity.[7] SRT has demonstrated efficacy not only in early non-small cell lung cancer,[8] hepatocellular carcinoma,[9] pancreatic cancer,[10] and prostate cancer[11] but also in managing oligometastatic tumors.[12-15]

This study evaluates the efficacy and safety of SRT in treating oligometastatic tumors based on data collected from a single center data and compares the findings of the present study with those of previous studies to explore the efficacy and safety of SRT.

2. Methods

2.1. Data collection

This retrospective study analyzed data from 96 patients with oligometastatic solid organ tumors (defined as 1 – 5 distant metastases in a single organ) treated with SRT at the Department of Radiotherapy of the First Affiliated Hospital of Guangxi Medical University between September 2019 and March 2023.

The inclusion criteria were as follows: oligometastases confirmed by pathology and imaging, no prior systemic treatment for metastatic diseases, measurable lesions on imaging, age ≥18 years, physical status (PS) score of 0 – 2, expected survival time of >3 months, and complete clinical and imaging data. The exclusion criteria were as follows: serious complications, pregnancy or lactation, and expected survival time of <3 months.

This study was approved by the Ethics Committee of the First Affiliated Hospital of Guangxi Medical University (2023-E257-01). Patient confidentiality was strictly maintained.

2.2. Treatment process

Patients were treated in the supine position and subjected to 4D computed tomography (CT) scanning across 10 phases, with a slice thickness of 3 mm. The gross tumor target area (GTV) was defined as the tumor location identified on imaging and was delineated across 10 phases using 4D-CT scans. The internal target volume (ITV) included the GTV and any associated fusion volume. The clinical target volume (CTV) was derived by expanding the ITV by 5 mm in all directions, and the planned target volume (PTV) was determined by expanding the CTV by an additional 5 mm in all directions. Treatment plans were developed using the Monaco 5.11.03 planning system, ensuring that the PTV prescription dose exceeded 95%. The dose to organs-at-risk was managed in strict accordance with the standards outlined by Timmerman 2021.8. Expert guidelines were followed to determine appropriate treatment doses based on the tumor type. Dose ranges and fractionations were defined as follows: brain oligometastases (30 – 55 Gy/5 – 10f), lung oligometastases (24 – 60 Gy/3 – 12f), and liver oligometastases (24 – 60 Gy/3 – 12f).

Positioning accuracy was verified through KV cone-beam CT (CBCT) imaging, and treatment was administered using the Elekta Versa HD linear accelerator.

Of the 96 patients in the study, 51 (53.13%) received chemotherapy, 55 (57.29%) received targeted therapy, and 35 (36.46%) received immunotherapy.

2.3. Follow-up and response evaluation

After SRT, hematologic toxicity was assessed through monthly blood tests, including liver and kidney function tests. Imaging follow-ups, using either CT or magnetic resonance imaging, were performed every 3 months. The follow-up period concluded on September 30, 2023, or with the patient's death.

The efficacy of tumor response after SRT was evaluated based on the Response Evaluation Criteria in Solid Tumors version 1.1. Tumor response was classified as complete

response (CR), partial response (PR), stable disease (SD), or progressive disease (PD). The objective response rate (ORR) was calculated as CR + PR divided by the total number of patients. The disease control rate (DCR) was calculated as CR + PR + SD divided by the total number of patients.

Progression-free survival (PFS) was defined as the time from SRT to disease progression or death, whereas OS was defined as the duration from the initiation of SRT to death from any cause.

2.4. Endpoints and statistical analysis

The primary endpoints of the study were tumor response, OS, and PFS. The secondary endpoint was acute toxicity, which was defined as adverse events occurring from the beginning of SRT to 3 months after treatment. Acute toxicity was assessed based on the Common Terminology Criteria for Adverse Events version 5.0.

All statistical analyses were performed using IBM SPSS Statistics for Windows, version 27.0 (IBM Corp., Armonk, NY, USA). Patient characteristics and 3-month treatment outcomes were reported as frequencies and percentages. Tumor response comparisons were conducted using the Ward algorithm in a single-sample proportional test.

3. Results

3.1. Patient characteristics

This study included 96 patients with a median age of 56 (range, 18 – 83) years, comprising 70 men (72.92%) and 26 women (27.08%). The distribution of oligometastases was as follows: lung, 23 (23.96%) patients; liver, 38 (39.58%) patients; and brain, 35 (36.46%) patients. PS scores were 0, 1, and 2 in 42 (43.75%), 40 (41.67%), and 14 (14.58%) patients, respectively. In terms of the treatment methods, 38 (39.58%) patients underwent surgical resection of the primary tumor before receiving SRT. Concurrent chemotherapy was administered to 51 (53.13%) patients, whereas combined targeted therapy was administered to 55 (57.29%) patients. Immunotherapy was administered to 35 (36.46%) patients. The median radiotherapy dose was 50 Gy (range, 24 – 60 Gy), with a median of 10 (range, 4 – 12) sessions. Using an α/β value of 10, the median biological effective dose was 75 Gy (range, 39 – 100 Gy; Table 1).

Table 1. Patient characteristics

Characteristic	Total (n = 96)
Sex	
Male	70 (72.92%)
Female	26 (27.08%)
Age (years)	
≤60	61 (63.54%)
>60	35 (36.46%)
ECOG PS	
0	42 (43.75%)
1	40 (41.67%)
2	14 (14.58%)
Oligometastases (SRT for organ)	
Liver	38 (39.58%)
Lung	23 (23.96%)
Brain	35 (36.46%)
Primary tumor	
Lung	46 (47.92%)
Liver	31 (32.29%)
Alimentary tract	7 (7.29%)
Others	12 (12.50%)
Tumor histology	
Hepatocellular carcinoma	31 (32.29%)
Adenocarcinoma	44 (45.83%)
Squamous cell carcinoma	7 (7.29%)
Others	14 (14.59%)
Primary tumor surgery	
Yes	38 (39.58%)
No	58 (60.42%)
Chemotherapy	
Yes	51 (53.13%)
No	45 (46.87%)
Immunotherapy	
Yes	35 (36.46%)
No	61 (63.54%)
Targeted therapy	
Yes	55 (57.29%)
No	41 (42.71%)

Abbreviations: ECOG PS: Eastern Cooperative Oncology Group performance status; SRT: Stereotactic radiotherapy.

3.2. Efficacy outcomes

All patients survived for at least 3 months post-treatment. Among them, 13 (13.54%) achieved CR, 50 (52.08%) showed PR, 27 (28.13%) exhibited SD, and 6 (6.25%) experienced PD. The ORR was 65.62%, and the DCR was 93.75% (Figure 1).

In the subgroup with liver oligometastases (n = 38), 10 (26.32%) patients achieved CR, 19 (50.00%) patients had PR, 8 (21.05%) patients exhibited SD, and 1 (2.63%) patient showed PD. The ORR and DCR for this subgroup were 76.32% and 97.37%, respectively. Among those with

lung oligometastases (n = 23), no patient achieved CR, but 9 (39.13%) patients had PR, 10 (43.48%) patients exhibited SD, and 4 (17.39%) patients showed PD, resulting in an ORR of 39.13% and DCR of 82.61%. For patients with brain oligometastases (n = 35), 3 (8.57%) patients achieved CR, 22 (62.86%) patients had PR, 9 (25.71%) patients exhibited SD, and 1 (2.86%) patient showed PD. The ORR and DCR were 71.43% and 97.14%, respectively (Table 2).

3.3. Survival outcomes

The median follow-up time for all patients, as of September 30, 2023, was 14 (range, 3 – 47) months. The median OS was 27 (range, 3 – 47) months, and the median PFS was 18 (range, 3 – 47) months (Figure 2).

Among the 23 patients with lung oligometastases, PD occurred in 4 (17.39%) patients, and 11 (47.83%) patients died. Both the median OS and PFS for this group were 16 months. The 6-month and 1-year OS rates were 78.26% and 39.13%, respectively, whereas the corresponding PFS rates were 73.91% and 26.09%, respectively.

Among the 38 patients with liver metastases, 1 (2.63%) patient exhibited PD, and 17 (44.74%) patients died. The median OS was 33 months, whereas the median PFS could not be determined. The 6-month and 1-year OS rates were 94.74% and 76.32%, respectively, with corresponding PFS rates of 86.84% and 63.16%.

Among the 35 patients with brain metastases, 1 (2.86%) patient exhibited PD, and 16 (45.71%) patients died. The median OS was 17 months, and the median PFS was 13 months. The 6-month and 1-year OS rates were 91.43% and 60%, respectively, whereas the corresponding PFS rates were 80.00% and 48.57% (Table 3).

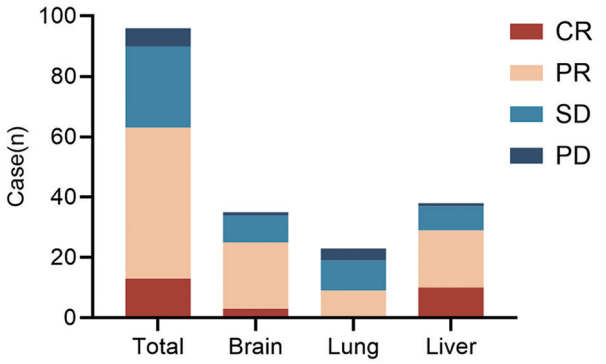

Figure 1. Tumor response following treatment
Abbreviations: CR: Complete response; PR: Partial response; PD: Progressive disease; SD: Stable disease.

3.4. Adverse events

The most common adverse events were gastrointestinal issues and myelosuppression. Anemia was the most frequent adverse event, occurring in 23 (23.96%) patients, with 21 (21.88%) cases classified as grades 1 – 2. Leukopenia was the second most common frequent adverse event, affecting 14 (14.58%) patients, with 13 (13.54%) cases classified as grades 1 – 2. Additional adverse events included thrombocytopenia, elevated bilirubin, increased aminotransferase levels, and gastrointestinal symptoms. Severe adverse events (grade 3) were rare, with 2 cases (2.08%) each of anemia and thrombocytopenia and 1 (1.04%) case of leukopenia. Importantly, no grade 4 adverse events occurred (Table 4). Symptomatic treatments effectively alleviated these adverse reactions.

4. Discussion

Malignant tumors often experience recurrence and metastasis, leading to poor outcomes, especially when systematic treatment alone is used.[16-18] Although therapeutic strategies for metastatic tumors have expanded, issues such as drug resistance and adverse effects persist despite advancements in targeted therapies and immunotherapy.[19-22] Surgical resection has shown survival benefits in patients with oligometastatic non-small cell lung cancer and brain metastases without lymph node involvement.[23,24] Approximately 50% of patients with colorectal cancer present with liver metastases at diagnosis, and surgical resection remains the gold standard

Table 2. Efficacy evaluation at 3 months after stereotactic radiotherapy

Oligometastasis	Liver (%)	Lung (%)	Brain (%)	Total (%)
CR	10 (26.32)	0 (0.00)	3 (8.57)	13 (13.54)
PR	19 (50.00)	9 (39.13)	22 (62.86)	50 (52.08)
SD	8 (21.05)	10 (43.48)	9 (25.71)	27 (28.13)
PD	1 (2.63)	4 (17.39)	1 (2.86)	6 (6.25)
ORR	76.32	39.13	71.43	65.62
DCR	97.37	82.61	97.14	93.75

Abbreviations: CR: Complete response; DCR: Disease control rate; ORR: Objective response rate; PD: Progressive disease; PR: Partial response; SD: Stable disease.

Table 3. Survival analysis

Oligometastasis	6-month PFS (%)	1-year PFS (%)	6-month OS (%)	1-year OS (%)
Liver	33 (86.84)	24 (63.16)	36 (94.74)	29 (76.32)
Lung	17 (73.91)	6 (26.09)	18 (78.26)	9 (39.13)
Brain	28 (80.00)	17 (48.57)	32 (91.43)	21 (60)
Total	78 (81.25)	47 (48.96)	86 (89.58)	59 (61.46)

Abbreviations: OS: Overall survival; PFS: Progression-free survival.

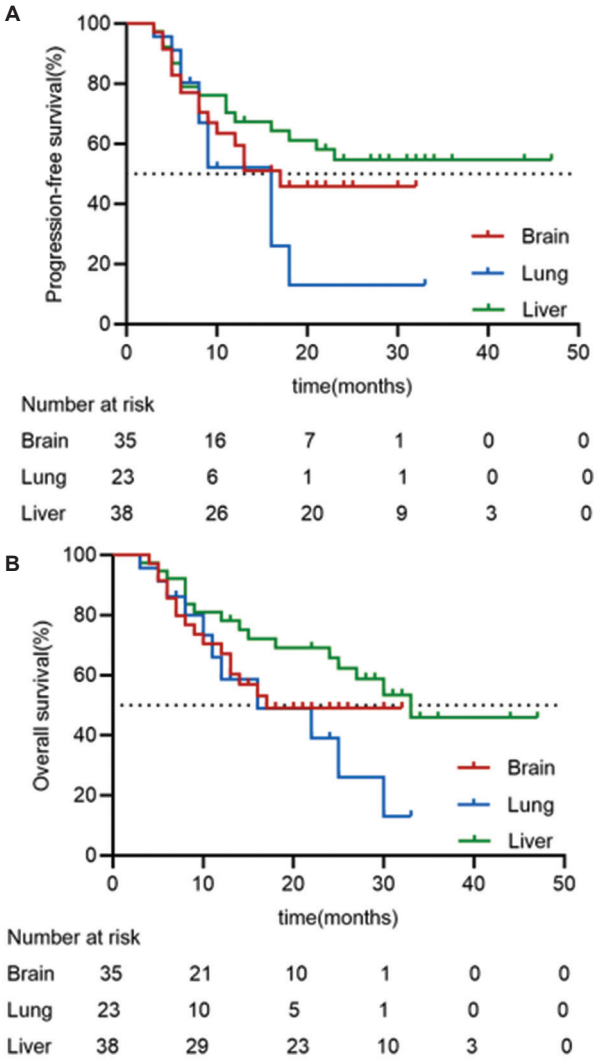

Figure 2. Kaplan–Meier survival curves for all patients. (A) Progression-free survival; (B) Overall survival

of treatment.[25,26] However, surgery may not always be feasible due to the lack of indications, patient refusal, or perioperative risks.[27] SRT has emerged as a promising alternative for treating oligometastatic tumors.

This study presents the experience of our center with SRT and compares our findings with those of previous studies. We analyzed clinical data from patients treated with SRT at our hospital, focusing on the distribution of tumor types – primarily liver and brain metastases. We also evaluated the efficacy of SRT in the treatment of metastatic lesions. In addition, we explored the median survival time and survival rate for each specific metastatic tumor after SRT administration. Finally, through statistical analysis, we concluded that adverse reactions graded as 3 or higher were infrequent during the course of SRT and primarily included anemia and leukopenia.

Our findings indicated that liver and brain oligometastases were the most commonly treated tumors with SRT, followed by lung oligometastases. Previous studies have indicated that SRT is a hyperfractionated radiotherapy predominantly used to treat large solid tumors, including those in the liver, brain, and lungs. SRT is particularly effective for managing oligometastases, which involve limited metastatic lesions.[12-15] At our hospital, liver, and brain oligometastases are the primary targets for SRT. Studies have also demonstrated that SRT can be applied to metastatic sites such as the head and neck, bones, and adrenal glands using a hyperfractionated regimen.[15,28,29] However, further exploratory research is necessary to evaluate the efficacy of SRT for these specialized sites.

We conducted a 3-month evaluation to assess the short-term efficacy of SRT in patients treated for liver and brain oligometastases. SRT showed promising results, aligning with findings from previous studies. Goodman *et al.* reported that the ORR for liver oligometastases following SRT was approximately 69%, with a progression rate of only 3%.[19] Our study revealed a similar ORR of 76.32%, with a progression rate of 2.63%, reinforcing SRT's effectiveness in treating liver oligometastases.

We examined the OS and PFS of patients treated with SRT. Across all tumor types, the median OS was 27 months, and the median PFS was 18 months, with hepatocellular carcinoma and lung cancer being the predominant primary tumors. Earlier studies on patients with non-small cell lung cancer and brain oligometastases reported a median OS ranging from 7 to 24 months following surgical intervention for lung and brain lesions.[30] In addition,

Table 4. Adverse events

Event	Grade 1 (%)	Grade 2 (%)	Grade 3 (%)	Grade 4 (%)
Nausea	6 (6.25)	2 (2.08)	0 (-)	0 (-)
Vomiting	5 (5.21)	1 (1.04)	0 (-)	0 (-)
Anorexia	8 (8.33)	2 (2.08)	0 (-)	0 (-)
Headache	11 (11.46)	4 (4.17)	0 (-)	0 (-)
Abdominal pain	8 (8.33)	3 (3.13)	0 (-)	0 (-)
Elevated liver enzymes	14 (14.58)	1 (1.04)	0 (-)	0 (-)
Elevated liver bilirubin	11 (11.46)	4 (4.17)	0 (-)	0 (-)
Elevated creatinine	3 (3.13)	0 (-)	0 (-)	0 (-)
Leukopenia	7 (7.29)	6 (6.25)	1 (1.04)	0 (-)
Thrombocytopenia	7 (7.29)	2 (2.08)	2 (2.08)	0 (-)
Anemia	10 (10.42)	11 (11.46)	2 (2.08)	0 (-)

patients with hepatocellular carcinoma oligometastases treated with stereotactic ablative body radiotherapy achieved a median OS of 16 months.[31] In comparison, our data suggest that SRT offers a more favorable survival outcome for patients with oligometastases.

Among the 23 patients with lung oligometastases treated at our hospital, the 1-year PFS rate was 26.09%, the OS rate was 39.13%, and the median OS was 16 months. These outcomes significantly surpass those of patients with advanced lung cancer treated exclusively with first-line chemotherapy, where the median OS was only 9.1 months. However, 4 (17.39%) patients experienced PD following SRT, underscoring the need for systemic maintenance therapies, such as chemotherapy, immunotherapy, and targeted therapy, to enhance treatment outcomes. Unfortunately, financial constraints prevented many patients from pursuing systemic therapies, further highlighting the importance of integrating these treatments with SRT.

In this study, the 1-year PFS and OS rates of patients with brain oligometastases were 48.57% and 60.00%, respectively, which were lower than the corresponding rates for liver oligometastases (63.16% and 76.32%, respectively). This discrepancy may stem from the distinct biological characteristics of the primary tumors. Nonetheless, SRT remains an effective treatment option for patients with brain oligometastases, significantly extending their survival compared with other therapeutic approaches.[32,33]

Our analysis of adverse events revealed a low incidence of severe side effects across all tumor types treated with SRT. The incidence of ≥grade 3 adverse events was only 5.21%, with anemia and leukopenia being the most common mild side effects. These conditions likely resulted from the impact of systemic chemotherapy on hematopoietic function and insufficient nutritional intake during treatment. Notably, SRT was associated with fewer adverse events than chemotherapy-induced myelosuppression.

In addition, the incidence of other adverse events, such as nausea and vomiting, was lower in patients treated with SRT than in those undergoing systemic chemotherapy. The side effects of SRT were also milder than those of invasive surgical procedures. Surgical treatments for liver metastases, such as traditional resection and transarterial chemoembolization, often lead to complications, including infections, edema, and liver function impairment, negatively affecting patients' quality of life. Similarly, brain surgeries, such as craniotomy or interventional therapy, carry the risk of serious complications, including brain edema, cerebral infarction, and hemorrhage. Moreover, patients with poor general health are often ineligible for surgery, making SRT a safer and more accessible treatment option.

This study had some limitations. First, the recent implementation of SRT at our hospital and the limited observation period restrict the comprehensiveness of our findings. Second, as this was a descriptive study, future controlled clinical trials are necessary to rigorously evaluate the advantages of SRT over other treatment modalities.

5. Conclusion

Our findings indicate that SRT is effective in treating liver, brain, and lung oligometastases, with fewer adverse events than other treatments. Patients demonstrated good adaptability to SRT, making it a viable alternative to surgical interventions.

Acknowledgments

None.

Funding

This work was supported by grants from the National Natural Science Foundation of China (grant numbers 82272736 and 82160467); the Research Foundation of the Science and Technology Department of Guangxi Province, China (grant number 2023GXNSFDA026009); the Research Foundation of the Health Department of Guangxi Province, China (grant number S2018087); the Autonomous Region Health Commission Self-funded Research Project (grant number Z-A20230472); and the local science and technology development projects organized under the guidance of the central government (grant number ZY18057006).

Conflict of interest

The authors declare they have no competing interests.

Author contributions

Conceptualization: Min Kang
Investigation: Huan Dong, Rong Li, He-Qing Huang, Xing-Hua Chen
Methodology: Huan Dong, He-Qing Huang, Zi-Yan Zhou
Formal analysis: Huan Dong, Rong Li
Writing – original draft: Huan Dong, Rong Li
Writing – review & editing: All authors

Ethics approval and consent to participate

The study protocol adhered to the ethical standards of the experimental committee of the responsible body and the Declaration of Helsinki. This study was approved by the Ethics Review Committee of the First Affiliated Hospital of Guangxi Medical University (No. 2023-E257-01). Due to the retrospective nature of the study, the need for patient consent for inclusion was waived.

Consent for publication

Not applicable.

Availability of data

The datasets used and/or analyzed during the current study are available from the corresponding author upon reasonable request.

References

1. Rossi A, Di Maio M. Platinum-based chemotherapy in advanced non-small-cell lung cancer: Optimal number of treatment cycles. *Expert Rev Anticancer Ther*. 2016;16(6):653-660.

   doi: 10.1586/14737140.2016.1170596

2. Llovet JM, Ricci S, Mazzaferro V, *et al*. Sorafenib in advanced hepatocellular carcinoma. *N Engl J Med*. 2008;359(4):378-390.

   doi: 10.1056/NEJMoa0708857

3. Biller LH, Schrag D. Diagnosis and treatment of metastatic colorectal cancer: A review. *JAMA*. 2021;325(7):669-685.

   doi: 10.1001/jama.2021.0106

4. Lee YT, Tan YJ, Oon CE. Molecular targeted therapy: Treating cancer with specificity. *Eur J Pharmacol*. 2018;834:188-196.

   doi: 10.1016/j.ejphar.2018.07.034

5. Li B, Chan HL, Chen P. Immune checkpoint inhibitors: Basics and challenges. *Curr Med Chem*. 2019;26(17):3009-3025.

   doi: 10.2174/0929867324666170804143706

6. Molla M, Fernandez-Plana J, Albiol S, *et al*. Limited liver or lung colorectal cancer metastases. systemic treatment, surgery, ablation or SBRT. *J Clin Med*. 2021;10(10):2131.

   doi: 10.3390/jcm10102131

7. Abel S, Lee S, Ludmir EB, Verma V. Principles and applications of stereotactic radiosurgery and stereotactic body radiation therapy. *Hematol Oncol Clin North Am*. 2019;33(6):977-987.

   doi: 10.1016/j.hoc.2019.08.007

8. Tandberg DJ, Tong BC, Ackerson BG, Kelsey CR. Surgery versus stereotactic body radiation therapy for stage I non-small cell lung cancer: A comprehensive review. *Cancer*. 2018;124(4):667-678.

   doi: 10.1002/cncr.31196

9. Kimura T, Fujiwara T, Kameoka T, Adachi Y, Kariya S. The current role of Stereotactic Body Radiation Therapy (SBRT) in Hepatocellular Carcinoma (HCC). *Cancer*s (*Basel*). 2022;14(18):4383.

   doi: 10.3390/cancers14184383

10. Myrehaug S, Sahgal A, Russo SM, *et al*. Stereotactic body radiotherapy for pancreatic cancer: Recent progress and future directions. *Expert Rev Anticancer Ther*. 2016;16(5):523-530.

    doi: 10.1586/14737140.2016.1168698

11. Haque W, Butler EB, Teh BS. Stereotactic body radiation therapy for prostate cancer-a review. *Chin Clin Oncol*. 2017;6(Suppl 2):S10.

    doi: 10.21037/cco.2017.06.05

12. Goodman BD, Mannina EM, Althouse SK, Maluccio MA, Cárdenes HR. Long-term safety and efficacy of stereotactic body radiation therapy for hepatic oligometastases. *Pract Radiat Oncol*. 2016;6(2):86-95.

    doi: 10.1016/j.prro.2015.10.011

13. Sogono P, Bressel M, David S, *et al*. Safety, efficacy, and patterns of failure after Single-Fraction Stereotactic Body Radiation Therapy (SBRT) for oligometastases. *Int J Radiat Oncol Biol Phys*. 2021;109(3):756-763.

doi: 10.1016/j.ijrobp.2020.10.011

14. Dunne EM, Fraser IM, Liu M. Stereotactic body radiation therapy for lung, spine and oligometastatic disease: Current evidence and future directions. *Ann Transl Med*. 2018;6(14):283.

doi: 10.21037/atm.2018.06.40

15. Siddiqui F, Patel M, Khan M, *et al*. Stereotactic body radiation therapy for primary, recurrent, and metastatic tumors in the head-and-neck region. *Int J Radiat Oncol Biol Phys*. 2009;74(4):1047-1053.

doi: 10.1016/j.ijrobp.2008.09.022

16. Hsieh RW, Borson S, Tsagianni A, Zandberg DP. Immunotherapy in recurrent/metastatic squamous cell carcinoma of the head and neck. *Front Oncol*. 2021;11:705614.

doi: 10.3389/fonc.2021.705614

17. Brockstein B, Haraf DJ, Rademaker AW, *et al*. Patterns of failure, prognostic factors and survival in locoregionally advanced head and neck cancer treated with concomitant chemoradiotherapy: A 9-year, 337-patient, multi-institutional experience. *Ann Oncol*. 2004;15(8):1179-1186.

doi: 10.1093/annonc/mdh308

18. Wong SJ, Machtay M, Li Y. Locally recurrent, previously irradiated head and neck cancer: Concurrent re-irradiation and chemotherapy, or chemotherapy alone. *J Clin Oncol*. 2006;24(17):2653-2658.

doi: 10.1200/JCO.2005.05.3850

19. Yokota T, Homma A, Kiyota N, *et al*. Immunotherapy for squamous cell carcinoma of the head and neck. *Jpn J Clin Oncol*. 2020;50(10):1089-1096.

doi: 10.1093/jjco/hyaa139

20. Chen L, Mo DC, Hu M, Zhao SJ, Yang QW, Huang ZL. PD-1/PD-L1 inhibitor monotherapy in recurrent or metastatic squamous cell carcinoma of the head and neck: A meta-analysis. *Am J Otolaryngol*. 2022;43(2):103324.

doi: 10.1016/j.amjoto.2021.103324

21. Lau A, Yang WF, Li KY, Su YX. Systemic therapy in recurrent or metastatic head and neck squamous cell carcinoma- a systematic review and meta-analysis. *Crit Rev Oncol Hematol*. 2020;153:102984.

doi: 10.1016/j.critrevonc.2020.102984

22. Moskovitz J, Moy J, Ferris RL. Immunotherapy for head and neck squamous cell carcinoma. *Curr Oncol Rep*. 2018;20(2):22.

doi: 10.1007/s11912-018-0654-5

23. Pfannschmidt J, Dienemann H. Surgical treatment of oligometastatic non-small cell lung cancer. *Lung Cancer*. 2010;69(3):251-258.

doi: 10.1016/j.lungcan.2010.05.003

24. Billing PS, Miller DL, Allen MS, Deschamps C, Trastek VF, Pairolero PC. Surgical treatment of primary lung cancer with synchronous brain metastases. *J Thorac Cardiovasc Surg*. 2001;122(3):548-553.

doi: 10.1067/mtc.2001.116201

25. Mohammad WM, Balaa FK. Surgical management of colorectal liver metastases. *Clin Colon Rectal Surg*. 2009;22(4):225-232.

doi: 10.1055/s-0029-1242462

26. Haddad AJ, Bani Hani M, Pawlik TM, Cunningham SC. Colorectal liver metastases. *Int J Surg Oncol*. 2011;2011:285840.

doi: 10.1155/2011/285840

27. Liu E, Stenmark MH, Schipper MJ, *et al*. Stereotactic body radiation therapy for primary and metastatic liver tumors. *Transl Oncol*. 2013;6(4):442-446.

doi: 10.1593/tlo.12448

28. Mantel F, Glatz S, Toussaint A, Flentje M, Guckenberger M. Long-term safety and efficacy of fractionated stereotactic body radiation therapy for spinal metastases. *Strahlenther Onkol*. 2014;190(12):1141-1148.

doi: 10.1007/s00066-014-0706-1

29. Zhao X, Zhu X, Fei J, *et al*. Short-term outcomes and clinical efficacy of Stereotactic Body Radiation Therapy (SBRT) in treatment of adrenal gland metastases from lung cancer. *Radiat Oncol*. 2018;13(1):205.

doi: 10.1186/s13014-018-1152-5

30. Villaruz LC, Kubicek GJ, Socinski MA. Management of non-small cell lung cancer with oligometastasis. *Curr Oncol Rep*. 2012;14(4):333-341.

doi: 10.1007/s11912-012-0240-1

31. Kim TH, Nam TK, Yoon SM, Kim TH, Choi YM, Seong J. Stereotactic ablative radiotherapy for oligometastatic hepatocellular carcinoma: A multi-institutional retrospective study (KROG 20-04). *Cancers* (*Basel*). 2022;14(23):5848.

doi: 10.3390/cancers14235848

32. Schiff D, Messersmith H, Brastianos PK, *et al*. Radiation therapy for brain metastases: ASCO guideline endorsement of ASTRO guideline. *J Clin Oncol*. 2022;40(20):2271-2276.

doi: 10.1200/JCO.22.00333

33. Niranjan A, Monaco E, Flickinger J, Lunsford LD. Guidelines for multiple brain metastases radiosurgery. *Prog Neurol Surg*. 2019;34:100-109.

doi: 10.1159/000493055

ACCSCIENCE PUBLISHING

Advances in Radiotherapy & Nuclear Medicine

ORIGINAL RESEARCH ARTICLE

Comparison of different approaches for the computation of biologically effective dose in a non-uniformly irradiated treatment target in stereotactic body radiation therapy

Vadim Y. Kuperman*, Yücel Altundal, and Rebecca Weinberg

Florida Cancer Specialists and Research Institute, Hudson, Florida, United States of America

Abstract

The biologically effective dose (BED) for a non-uniformly irradiated treatment target can be determined using two approaches: averaging BEDs for different voxels in the target and averaging the probability of tumor cell survival in the target. This study compared these approaches for the computation of BED by examining their general properties and comparing BEDs for different treatment plans. The mean BED (BED_{mean}) determined by averaging BEDs in different parts of the target and BED (BED_{nud}) determined by averaging the probability of survival were computed for 51 cases of stereotactic body radiation therapy. For each case, two treatment plans were created using dynamic conformal arcs (DCAs) and volumetric modulated arc therapy (VMAT). For the plans with DCAs, the sample mean of BED_{mean} was 18% > that of BED_{nud} (for $\alpha = 0.35$ Gy^{-1} and $\alpha/\beta = 10$ Gy). Conversely, for the VMAT plans and the same values of radiobiological parameters, the sample mean of BED_{mean} was only 5%> that of BED_{nud}. Theoretically, BED_{mean} is always $\geq BED_{nud}$. When the mean dose in the target is fixed, BED_{mean} increases with increasing variance of the target dose (σ^2). In contrast, BED_{nud} decreased with increasing σ^2. Although BED_{nud} depends on both alpha and beta parameters for the irradiated malignant cells, BED_{mean} depends only on the alpha/beta ratio. Thus, the use of BED_{mean} instead of BED_{nud} can cause incorrect ranking of treatment plans.

Keywords: Biologically effective dose; Stereotactic body radiation therapy; Dynamic conformal arc; Volumetric modulated arc therapy; Dose variance

***Corresponding author:**
Vadim Y. Kuperman
(vadimkuperman@yahoo.com)

Citation: Kuperman VY, Altundal Y, Weinberg R. Comparison of different approaches for the computation of biologically effective dose in a non-uniformly irradiated treatment target in stereotactic body radiation therapy. *Adv Radiother Nucl Med*. 2024;2(4):4826. doi: 10.36922/arnm.4826

Received: September 12, 2024

Accepted: November 7, 2024

Published Online: December 23, 2024

1. Introduction

1.1. Background

The goal of radiotherapy is to deliver a tumoricidal dose to targeted malignant cells while minimizing the risk of normal tissue complications. Conventionally, the assessment of treatment plans and their ranking in three-dimensional conformal radiotherapy or intensity-modulated radiotherapy have been performed by considering the dose distributions in the planning target volume (PTV) and critical normal structures. The employed criteria for plan evaluation are based on several established dose-volume parameters (DVPs). For example, in lung tumors treated with a standard regimen of

2 Gy/fraction, the percentage of the normal lung volume receiving doses ≥20 Gy is employed to assess the risk of radiation pneumonitis.[1]

Although DVPs and associated planning constraints for the treatment target and normal organs are still used most frequently for plan evaluation, the DVP-based criteria are indirect measures of the radiobiological effects of the treatment. A potentially better approach is based on radiobiological parameters such as tumor control probability (TCP) and normal tissue complication probability (NTCP), which can be computed using different radiobiological models of dose response in tissues.[2-4] The existing dose-response models can be divided into two groups, referred to as *mechanistic* or *phenomenological* models. The former models mathematically express dose response by considering the basic biological processes in the irradiated tissues. Conversely, the latter models aim to express the empirical relationships between the absorbed dose and the induced biological effects.

In principle, mechanistic models are more advantageous because they can be applied in various cases including different irradiated tissues and/or treatment regimens. Unfortunately, the complex phenomenon of radiation-induced tissue damage and underlying biological processes are not sufficiently understood. Consequently, mechanistic models are normally limited because they employ several assumptions and consequently are not yet fully capable of faithfully predicting treatment outcomes. Phenomenological models are utilized in clinical practice because they are simpler than the mechanistic models. Phenomenological models are typically derived using empirical data acquired for specific tissues and the conventional dose per fraction of 2 Gy.[5-10] This frequently prevents the employment of phenomenological models in clinical cases for which the parameters of these models have not been validated.

Among the radiobiological parameters used for the evaluation and comparison of treatment plans, the biologically effective dose (*BED*)[11-13] and equivalent dose in 2 Gy fractions (EQD_2)[14] are used most often. The popularity of *BED* and EQD_2 is attributed to the following: (a) both quantities are normally defined using the standard linear–quadratic (LQ) model for cell kill; (b) the computation of *BED* and EQD_2 in treatment planning systems (TPS) generally requires only the α:β ratio from the LQ model, without needing the separate values of α and β; and (c) *BED* and/or EQD_2 are frequently employed as TCP surrogates.

TCP monotonically increases with increasing *BED* and EQD_2.[15] As a result, the intercomparison of treatment plans in terms of TCP can be performed by comparing the corresponding *BED* or EQD_2. The relationship between the latter quantities and NTCP is much more tenuous. In general, NTCP depends on the organization of the organ at risk, which can be described using the concepts of volume effects, functional subunits, and serial and parallel tissues developed and employed in previous studies.[6,16-18] Because the computations of *BED*s and/or EQD_2 only involve parameters of the LQ model and are considered the treatment regimen (i.e., total dose and dose per fraction), neither *BED* nor EQD_2 should be used as NTCP surrogates.[19]

This study compares different approaches used to compute *BED* for a non-uniformly irradiated target. Because *EQD*2 is proportional to *BED* (e.g., Jones and Hoban[19]), the conclusions of this work are also applicable to the computation of *EQD*2.

In the original framework, *BED* was defined under the assumption of a uniformly irradiated organ of interest.[11] In this case, *BED* depends on the total dose, dose per fraction, and alpha/beta ratio. In practice, the absorbed dose in the treatment target is always non-uniform. Consequently, the computation of *BED* generally requires knowledge of both alpha and beta and dose distribution in the target.[19,20] The use of *BED* distribution was suggested in seminal studies by Lee *et al.*[21] and Wheldon *et al.*,[22] with the expectation that the transition from the physical dose to *BED* can facilitate plan optimization and clinical research.

The procedure for computing the *BED* distribution in[21] requires voxel-by-voxel conversion of the dose to *BED* based on the LQ model. Conversely, Niemierko[20] developed the concept of equivalent uniform dose (*EUD*), which is computed by averaging the probability of survival in the organ of interest. Jones and Hoban[19] utilized the concept of *EUD* (which is similar to BED_{nud} and EQD_2) for external beam radiotherapy to perform radiobiological comparisons of different treatment plans. O'Donoghue[23] employed *EUD* to assess the radiobiological effect of non-uniform dose distributions on tumors treated with radionuclide therapy.

1.2. Main objective

Modern TPSs include modules for computing the *BED* and EQD_2 in each voxel and the mean values of these quantities.[24-26] The mean BED (BED_{mean}) is obtained by averaging BEDs in different voxels.[25,26] This study aimed to (a) compare BED_{mean} with the corresponding BED_{nud} computed by averaging the probability of tumor cell survival in the target and (b) demonstrate that the use of BED_{mean} can lead to incorrect ranking of the compared treatment plans. To compare *BED*s, 51 cases of non-small lung cancer treated with volumetric modulated arc therapy

(VMAT) and dynamic conformal arcs (DCAs) were analyzed. The methodology employed in this study and the results are presented in Sections 2 and 3. The discussion of the results and conclusions are included in Section 4.

2. Methods

2.1. BED for a non-uniformly irradiated target

For fractionated radiotherapy delivered in N_f fractions with uniform dose per fraction d and total dose D, the probability of cell survival in the LQ model can be expressed as follows[27-29]

$$S = \exp(-\alpha D - \beta d D) = \exp(-\alpha D - \frac{\beta D^2}{N_f}) \quad (1)$$

where parameters α and β define cellular radiosensitivity. Although α and β can vary in the tissue (e.g., due to different phases of the cell cycle and spatially varying tissue oxygenation), information about their values *in vivo* is currently not available.[30] For simplicity, in the following discussion, the parameters α and β for the anatomical structure of interest will be assumed to remain spatially and temporally uniform throughout radiotherapy. In addition, Eq. (1) does not describe the repair of sublethal damage,[31-34] which may be important in the case of long fraction time (e.g., 0.3 – 0.5 h) characteristic of treatments delivered using multiple non-coplanar beams.[35]

The BED is defined as the equivalent total dose at an infinitely low-dose rate or with infinitely small well-spaced-out fractions yielding the same log cell kill as the schedule being studied.[11-13] Equation (1) yields the following expressions for *BED*[12,13]:

$$BED = D\,(1 + \frac{d}{\alpha/\beta}) \text{ or } BED = -\frac{1}{\alpha}\ln S \quad (2)$$

where S is described in Eq. (1).

In the case of non-uniform dose ("nud") in the treatment target with volume V_{tar}, one can employ a more general definition of *BED*, i.e.,

$$BED_{nud} = -\frac{1}{\alpha}\ln(S_{mean}) \quad (3)$$

where S_{mean} is the probability of survival averaged over the dose distribution in the target,[19,30] i.e.,

$$S_{mean} = \frac{1}{V_{tar}}\int exp\left(-\alpha D - \frac{\beta D^2}{N_f}\right)dV \quad (4)$$

To derive Eq. (3), one can consider the equation for cell survival in the target

$$N = \int n_0 exp\left(-\alpha D - \frac{\beta D^2}{N_f}\right)dV \quad (5)$$

where integration is performed over the target volume. In Eq. (5), N and n_0 represent the total number of surviving malignant cells and the initial (i.e., before commencement of radiotherapy) concentration of malignant cells, respectively. When n_0 is uniform, Eq. (5) yields

$$N = \frac{N_0}{V_{tar}}\int exp\left(-\alpha D - \frac{\beta D^2}{N_f}\right)dV = N_0 S_{mean} \quad (6)$$

Where $N_0 = n_0 V_{tar}$ denotes the total initial number of clonogenic cells in the target.

Let us now assume that the target is irradiated with a negligibly small, uniform dose per fraction. Using Eq. (6) and assuming that the total equivalent dose results in the same cell kill as a given, that is, non-uniform dose distribution, we obtain

$$N_0 exp\left(-\alpha BED_{nud}\right) = N_0 S_{mean} = \frac{N_0}{V_{tar}}\int exp\left(-\alpha D - \frac{\beta D^2}{N_f}\right)dV \quad (7)$$

Eq. (7) is equivalent to Eq. (3) with the average probability of survival defined in Eq. (4).

The degree of treatment success can be predicted if the corresponding TCP is known. In the framework of the LQ model and Poisson statistics for cell kill,[15,36-38] the relationship between BED_{nud} and TCP is as follows:

$$TCP = exp(-N_0 S_{mean}) = \exp[-N_0 exp(-\alpha BED_{nud})] \quad (8)$$

2.2. Relationship between *BED* and EQD_2

Instead of *BED*, one can use the equivalent dose in 2-Gy fractions, EQD_2.[14] For a given non-uniform dose distribution, EQD_2 produces the same cell kill as the given dose distribution. Straightforwardly, the relationship between *BED* and EQD_2 is as follows[19]:

$$EQD_2 = \frac{BED}{1 + \frac{2}{(\alpha/\beta)}} \quad (9)$$

For brevity, the subsequent discussion focuses on the *BED*. Because *BED* is proportional to EQD_2, the conclusions of this study are also valid for the latter quantity.

2.3. Employing the dose-volume histogram (DVH) to compute the BED

Let $V(D)$ denote the volume of the target receiving a dose equal to or greater than a given dose D. The ratio $V(D)/V_{PTV}$

defines the DVH.[39] From the definition of DVH, $DVH(D)-DVH(D+\Delta D)\approx-\left(\frac{dDVH}{dD}\right)\Delta D$ equals the relative volume of the target with the dose varying between D and $D+\Delta D$. Consequently, the average probability of survival in the target can be expressed as follows:

$$S_{mean}=-\int_{D_{tar,min}}^{D_{tar,max}} exp(-\alpha D-\frac{\beta D^2}{N_f})\frac{dDVH}{dD}dD \quad (10)$$

In practice, the DVH for an anatomical structure is given by a one-dimensional array: $DVH(i)$, $i = 1,\ldots, N_{bin}$, where the dose is divided into bins such that $D(i)$ ranges between the minimum dose $D_{min} = D(1)$ and the maximum dose $D_{max} = D(N_{bin})$ in the structure of interest. If each bin is small enough so that $dDVH \approx DVH(i+1)-DVH(i)$, we can replace the integral in Eq. (10) with a sum. The resulting equation for the average probability of survival can be written as follows:

$$S_{mean}\approx\sum_{i=1}^{N_{bin}}\exp(-\alpha D(i)-\frac{\beta D(i)^2}{N_f})\,[DVH(i)-DVH(i+1)] \quad (11)$$

2.4. Small-variance approximation

Consider a treatment target with the mean dose D_{mean}. The non-uniformity of the absorbed dose in the target can be characterized by the variance of dose σ^2, where σ^2 equals the average of $(D - D_{mean})^2$ in the target volume. To elucidate the dependence of BED on σ, it is useful to consider a special case of small non-uniformity of the target dose defined by the condition $\sigma << D_{mean}$. Under this condition, we can express the exponential function in Eq. (4) as a power series around D_{mean}. The resulting approximation for the BED_{nud} is given by[40]:

$$BED_{nud}=D_{mean}\left(1+\frac{D_{mean}}{(\alpha/\beta)N_f}\right)-\frac{\sigma^2}{2}\left[\alpha\left(1+\frac{2D_{mean}}{N_f(\alpha/\beta)}\right)^2-\frac{2}{N_f(\alpha/\beta)}\right] \quad (12)$$

For curative treatments, the probability of survival in the target volume must be small to achieve a TCP close to unity. As a result, we have

$$\alpha D_{mean}+\frac{\beta D_{mean}^{\ 2}}{N_f}>1 \quad (13)$$

Under the condition in Eq. (13), the term in the square brackets in Eq. (12) is positive. As a result, for a given D_{mean}, both BED_{nud} and TCP decrease with increasing σ. Consequently, BED and the corresponding TCP are maximized in the case of a uniform target dose. This conclusion agrees with the seminal result by Webb *et al.*[38] that a uniform dose provides the greatest TCP for a fixed integral dose in the target volume.

For a fixed alpha/beta ratio, BED_{nud} in Eq. (12) decreases linearly with increasing α. Conversely, for a fixed α, BED_{nud} approaches $D_{mean}\left(1+\frac{D_{mean}}{(\alpha/\beta)N_f}\right)$ as the alpha/beta ratio increases (Figure 1).

2.5. Computation of BED and EQD$_2$ in different TPS

To determine the BED and EQD_2 distributions in Velocity (Varian Medical Systems, Inc. Palo Alto, CA, USA) and RayStation (RaySearch Laboratories, Stockholm Sweden), these quantities are computed in each voxel of the irradiated structure. For the j^{th} voxel ($j = 1,\ldots, N_{voxel}$) receiving dose D_{voxel}, the corresponding BED_{voxel} is given by

$$BED_{voxel}(j)=D_{voxel}(j)\left(1+\frac{D_{voxel}(j)}{N_f\left(\alpha/\beta\right)}\right) \text{ and}$$

$$EQD_{2,voxel}(j)=\frac{BED_{voxel}(j)}{1+\frac{2}{\left(\alpha/\beta\right)}} \quad (14)$$

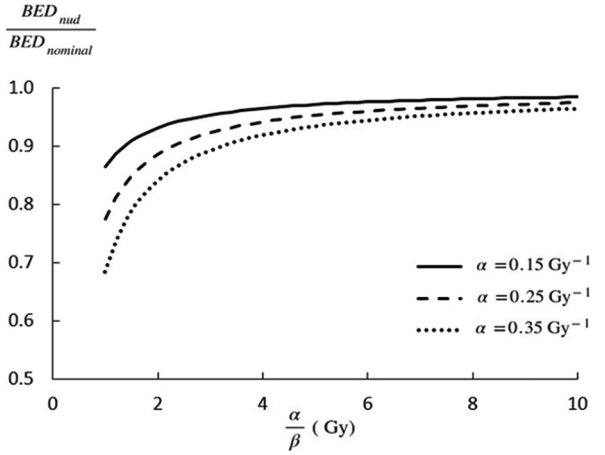

Figure 1. Ratio of BED_{nud} from Eq. (12) and $D_{mean}\left(1+\frac{D_{mean}}{\left(\alpha/\beta\right)N_f}\right)$ (denoted by $BED_{nominal}$) as a function of α/β. Other parameters are as follows: D_{mean} = 55 Gy, N_f = 5, and σ = 1.5 Gy. The results from this figure indicate the following: (a) $BED_{nud} < BED_{nominal}$ and (b) the difference between BED_{nud} and $BED_{nominal}$ decreases with the increasing α/β ratio. Abbreviation: BED: Biologically effective dose.

The mean *BED* and mean EQD_2 are defined by averaging these quantities for different voxels, that is,

$$BED_{mean} = \frac{1}{N_{voxel}} \sum_{j=1}^{N_{voxel}} \left[D_{voxel}(j) \left(1 + \frac{D_{voxel}(j)}{N_f \left(\alpha / \beta \right)} \right) \right] \text{ and}$$

$$EQD_{2,mean} = \frac{BED_{mean}}{1 + \frac{2}{\left(\alpha / \beta \right)}} \quad (15)$$

BED_{mean} can also be written in a more succinct form:

$$BED_{mean} = D_{mean} \left(1 + \frac{D_{mean}}{N_f \left(\alpha / \beta \right)} \right) + \frac{\sigma^2}{N_f \left(\alpha / \beta \right)} \quad (16)$$

where

$$D_{mean} = \frac{1}{N_{voxel}} \sum_{j=1}^{N_{voxel}} D_{voxel}(j) \text{ and}$$

$$\sigma^2 = \frac{1}{N_{voxel}} \sum_{j=1}^{N_{voxel}} \left(D_{mean} - D_{voxel}(j) \right)^2 \quad (17)$$

For a fixed mean dose to the target, BED_{mean} increases with increasing variance of the target dose (Eq. (16). In contrast, as mentioned above, BED_{nud} decreases with increasing σ^2. In addition (see Appendix), BED_{mean} always exceeds or equals BED_{nud}.

2.6. Computation of BED for clinical cases

The BED was computed for 51 cases of non-small lung cancer treated with stereotactic body radiation therapy (SBRT). The considered treatment plans were produced with 6MV flattening filter-free beams using Eclipse TPS (version 15.6, Varian Medical Systems, Inc., Palo Alto, CA). For each case, two plans were created using VMAT and DCAs.

The analytical anisotropic algorithm and a dose grid of 1.25 mm^3 were used to compute the planned dose. The same treatment regimen 10 Gy × 5 = 50 Gy was used for all cases with plan normalization such that at least 95% of the PTV received the prescribed dose.

The BED was calculated for different values of alpha and alpha/beta ratio of 10 Gy. To compute the BED_{nud} and BED_{mean}, the planned DVHs in Eclipse were exported and analyzed offline using Excel and Python scripts developed in-house.

2.7. Data analysis

The mean values and variances of D_{mean}, σ, BED_{mean}, and BED_{nud} were computed in Microsoft Excel (Microsoft Corporation, 2024: https://office.microsoft.com/excel). A two-tailed Student's t-test was used to evaluate the significance of the differences between these parameters for the DCA and VMAT plans.

3. Results

Table 1 contains the locations and volumes of the lung lesions for the studied SBRT cases. Figure 2 displays the mean value and standard deviation of the target dose for the evaluated DCA and VMAT plans. The computed BEDs are presented in Figure 3. The dashed and solid lines in Figures 2 and 3 represent the sample means of the displayed parameters for the DCA and VMAT plans, respectively. Table 2 contains the sample mean and sample standard deviation of the computed dosimetric and radiobiological parameters.

4. Discussion

4.1. General properties of BED_{mean} and BED_{nud}

BED_{mean} always exceeds or equals BED_{nud} (Appendix). In addition, BED_{nud} depends on both α and β, whereas BED_{mean} depends only on the ratio of these parameters. The third important difference between BED_{mean} and BED_{nud} is their different dependencies on the variance of the target dose σ^2. That is, if the mean dose in the target is fixed, then BED_{mean} always increases with increasing σ. Conversely, under the same condition, BED_{nud} decreases when σ increases. The differences between BED_{mean} and BED_{nud} are further discussed in the subsequent sections.

4.2. BED_{mean} vs. BED_{nud} in SBRT plans with DCA

The results confirm that the sample mean of BED_{mean} is greater than that of BED_{nud}. For example, in the considered cases, the sample mean of BED_{mean} was 9% and 18% > the sample mean of BED_{nud} for $\alpha = 0.15\ Gy^{-1}$ and $\alpha = 0.35\ Gy^{-1}$, respectively (Table 2). The latter value of the alpha is consistent with that in a recent study[41] that compared the LQ model with several other radiobiological models for nearly 3000 patients.

4.3. BED_{mean} vs. BED_{nud} in SBRT plans with VMAT

Compared with the DCA plans, the studied VMAT plans were characterized by smaller values of D_{mean} and σ (Figure 2). For the VMAT plans, we had D_{mean} = 52.9 ± 0.9 Gy and σ = 1.6 ± 0.5 Gy (Table 2). The corresponding values of D_{mean} and σ for the DCA plans were as follows: D_{mean} = 56.1 ± 1.1 Gy and σ = 3.5 ± 0.7 Gy. As in the DCA plans, the sample mean of BED_{mean} for the VMAT plans was greater than that of BED_{nud}. However, the difference between BED_{mean} and BED_{nud} was smaller for the VMAT plans than for the DCA plans. That is, for

Table 1. Tumor locations, target volumes, and corresponding equivalent sphere diameters (d_{es}) for the considered stereotactic body radiation therapy cases

Tumor location	Number of cases	$V_{PTV,min}$ (cm³)	$V_{PTV,max}$ (cm³)	$V_{PTV,aver}$ (cm³)	$d_{es,min}$ (cm)	$d_{es,max}$ (cm)	$d_{es,aver}$ (cm)
LLL	11	16.2	55.8	33.1	3.1	4.7	3.9
LUL	7	16.6	58.5	27.4	3.2	4.8	3.7
RLL	6	34.5	101.7	67.4	4.0	5.8	5.0
RML	3	10.7	21.1	14.9	2.7	3.4	3.0
RUL	24	7.0	58.4	28.6	2.4	4.8	3.7

Note that d_{es} denotes the diameter of a sphere with volume V_{PTV}.
Abbreviations: LLL: Left lower lobe; LUL: Left upper lobe; RLL: Right lower lobe; RML: Right middle lobe; RUL: Right upper lobe.

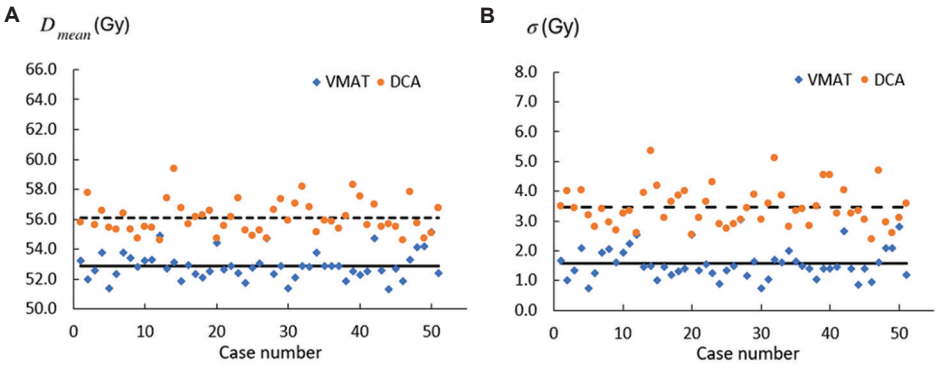

Figure 2. Computed D_{mean} and σ in (A) and (B), respectively. The presented plots indicate that the D_{mean} and σ of the studied DCA plans exceeded those of the VMAT plans.
Abbreviations: DCA: Dynamic conformal arc; VMAT: Volumetric modulated arc therapy.

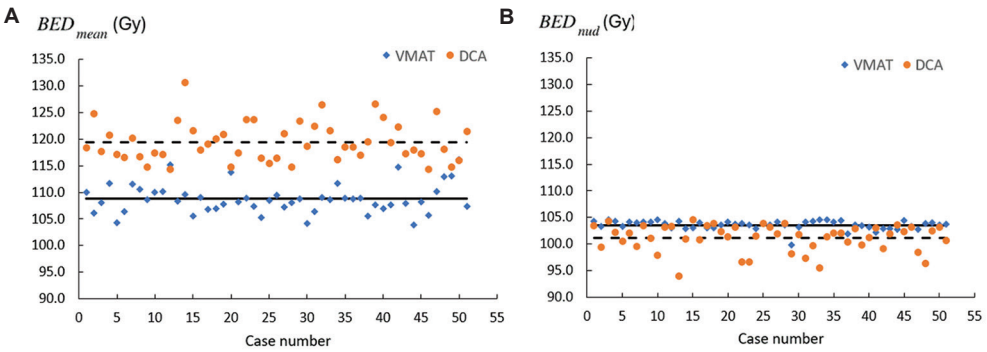

Figure 3. BED_{mean} in (A) and BED_{nud} in (B) for the considered SBRT cases. The displayed *BED*s were computed for α = 0.35 Gy^{-1} and alpha/beta ratio of 10 Gy. Although the DCA plans were characterized by greater values of BED_{mean}, the corresponding VMAT plans had a larger average BED_{nud}.
Abbreviation: *BED*: Biologically effective dose; DCA: Dynamic conformal arc; SBRT: Stereotactic body radiation therapy.

the VMAT plans, the sample mean of BED_{nud} was only 2% and 5% smaller than that of BED_{mean} for α = 0.15 Gy^{-1} and α = 0.35 Gy^{-1}, respectively (Figure 3 and Table 2). The observed smaller difference between BED_{mean} and BED_{nud} for the studied VMAT plans was due to the smaller variance of the target dose compared with that in the DCA plans.

4.4. Clinical implications of the results

The clinical ramifications of this work can be elucidated with the help of Figure 3 and Table 2.

According to the approach realized in Velocity and RaySearch, the DCA plans should be preferred in terms of their higher BED_{mean} than the VMAT plans. Conversely, if the *BED* is computed by averaging the survival probabilities in different voxels, the resulting BED_{nud} for the studied VMAT plans was on average higher than that for the corresponding DCA plans (for α = 0.35 Gy^{-1}). Fourteen DCA plans (27% of all plans) had BED_{nud} < 100 Gy. Conversely, all the studied VMAT plans were characterized by $BED_{nud} \geq 100$ Gy. The differences between

Table 2. Computed dosimetric and radiobiological parameters for the considered stereotactic body radiation therapy cases

Parameter	DCA	VMAT	*P*-value*
σ	3.5±0.7	1.6±0.5	<0.001
D_{mean}	56.1±1.1	52.9±0.9	<0.001
BED_{mean}	119.4±3.7	108.8±2.7	<0.001
BED_{nud} (α=0.15)	109.6±0.7	106.7±1.5	<0.001
BED_{nud} (α=0.35)	101.1±2.5	103.6±0.8	<0.001

Each parameter q is presented as $\bar{q}$±std, where $\bar{q}$ and std denote the sample mean and sample standard deviation of q, respectively. In this table, σ, D_{mean}, and BEDs are in Gray, whereas the parameter alpha has a unit of Gy^{-1}.
*P<0.05 was considered significant.
Abbreviations: DCA: Dynamic conformal arc; VMAT: Volumetric modulated arc therapy.

the computed dosimetric parameters (i.e., σ and D_{mean}) and the radiobiological parameters (i.e., BED_{mean} and BED_{nud}) for the studied DCA and VMAT plans were significant.

The obtained results indicate that in terms of *BED*, VMAT plans for SBRT are radiobiologically advantageous compared with the corresponding DCA plans generated with the same treatment prescription. The above-mentioned observation that, unlike the studied DCA plans, all VMAT plans had $BED_{nud} \geq 100$ Gy is important because a study[42] reported lower local recurrence and higher 3-year survival for patients treated with $BED \geq 100$ Gy than those treated with $BED < 100$ Gy.

4.5. Limitations of the considered model and future studies

As discussed previously, the results of this work were obtained in the framework of the LQ model. The validity of the LQ model in hypofractionation (i.e., when dose per fraction significantly exceeds the standard dose of 2 Gy) has been questioned in several studies that suggested alternative models for radiation-induced cell kill.[43-46] These non-LQ models predict that the survival curve, displayed as a log-linear plot, becomes linear at high doses. However, recent studies have indicated that the LQ model provides the best fit for the clinical data for SBRT.[41,47]

Besides the crucial reliance on the LQ model, this study has several other limitations. First, this study did not consider the effect of accelerated repopulation of malignant cells. Radiation-induced accelerated proliferation is assumed to begin after a delay T_k following the first fraction of radiation.[48] Because the reported values of T_k for non-small cell cancer of the lung range from 14 to 35 days.[49] the effect of accelerated repopulation on the SBRT of the lung is likely to be small.

Second, in the employed radiobiological model, the radiation-induced cell kill during each fraction is independent of cell irradiation during previous fractions. That is, damage repair, reoxygenation, and redistribution of the cell cycle occur only between successive treatment fractions. A detailed analysis of these effects, recently reviewed in,[50] is beyond the scope of this study.

In this study, BED_{mean} and BED_{nud} were computed for the PTV, which encompasses the clinical target volume (CTV). Because the PTV is always larger than the CTV, the variance of the dose in the PTV normally exceeds the corresponding dose variance in the CTV. As a result, if the CTV or gross tumor volume is used for the computation of *BED*, the effect of dose non-uniformity on *BED* will be smaller than that determined in our study.

Given the limitations of the employed LQ model, alternative models that might provide more accurate predictions of radiobiological effects in SBRT must be considered. In future studies, we intend to explore modifications of the LQ model, including the Guerrero–Li model[43] and the LQ–linear model.[45,46]

Finally, the results of this study do not imply the superiority of either the VMAT or DCA methods for lung SBRT. A comprehensive comparison of treatment plans in the clinic should include several additional factors (i.e., doses to critical normal organs, dose conformity and gradient, and plan sensitivity to motion), the evaluation of which is beyond the scope of this study.

5. Conclusion

BED_{mean}, computed by averaging *BED*s in different voxels within the treatment target, always exceeds BED_{nud} defined by the average probability of survival in the target. This result is confirmed by comparing BED_{mean} and BED_{nud} for several SBRT plans produced using DCA and VMAT. For the considered cases of SBRT, the sample mean of BED_{mean} for the DCA plans was greater than that for the VMAT plans (for $\alpha = 0.35\ Gy^{-1}$ and $\alpha/\beta = 10$ Gy). In contrast, the sample mean of BED_{nud} for the DCA plans was smaller than that for the VMAT plans. This result indicates that the use of BED_{mean} instead of BED_{nud} can lead to an incorrect ranking of the compared treatment plans.

Acknowledgments

None.

Funding

None.

Conflict of interest

The authors declare that they have no competing interests.

Author contributions

Conceptualization: Vadim Y. Kuperman
Formal analysis: All authors
Investigation: All authors
Methodology: All authors
Writing – original draft: Vadim Y. Kuperman
Writing – review & editing: All authors

Ethics approval and consent to participate

Not applicable

Consent for publication

Not applicable

Availability of data

Data are available from the corresponding author on reasonable request.

References

1. Graham MV, Purdy JA, Emami B, *et al*. Clinical dose-volume histogram analysis for pneumonitis after 3D treatment for non-small cell lung cancer (NSCLC). *Int J Radiat Oncol Biol Phys*. 1999;45(2):323-329.

   doi: 10.1016/S0360-3016(99)00183-2

2. Li XA, Alber M, Deasy JO, *et al*. The use and QA of biologically related models for treatment planning: Short report of the TG-166 of the therapy physics committee of the AAPM. *Med Phys*. 2012;39(3):1386-1409.

   doi: 10.1118/1.3685447

3. Nahum AE, Uzan J. (Radio)biological optimization of external-beam radiotherapy. *Comput Math Methods Med*. 2012;2012:329214.

   doi: 10.1155/2012/329214

4. Marks LB, Yorke ED, Jackson A, *et al*. Use of normal tissue complication probability models in the clinic. *Int J Radiat Oncol Biol Phys*. 2010;76(3 Suppl):S10-S19.

   doi: 10.1016/j.ijrobp.2009.07.1754

5. Bentzen SM, Constine LS, Deasy JO, *et al*. Quantitative analyses of normal tissue effects in the clinic (QUANTEC): An introduction to the scientific issues. *Int J Radiat Oncol Biol Phys*. 2010;76(3 Suppl):S3-S9.

   doi: 10.1016/j.ijrobp.2009.09.040

6. Lyman JT. Complication probability as assessed from dose-volume histograms. *Radiat Res*. 1985;104:S13-S19.

   doi: 10.2307/3576626

7. Kutcher GJ, Burman C. Calculation of complication probability factors for non-uniform normal tissue irradiation: The effective volume method. *Int J Radiat Oncol Biol Phys*. 1989;16(6):1623-1630.

   doi: 10.1016/0360-3016(89)90972-3

8. Emami B, Lyman J, Brown A, *et al*. Tolerance of normal tissue to therapeutic irradiation. *Int J Radiat Oncol Biol Phys*. 1991;21(1):109-122.

   doi: 10.1016/0360-3016(91)90171-Y

9. Dawson LA, Normolle D, Balter JM, McGinn CJ, Lawrence TS, Ten Haken RK. Analysis of radiation-induced liver disease using the Lyman NTCP model. *Int J Radiat Oncol Biol Phys*. 2002;53(4):810-821.

   doi: 10.1016/S0360-3016(02)02846-8

10. Seppenwoolde Y, Lebesque JV, de Jaeger K, *et al*. Comparing different NTCP models that predict the incidence of radiation pneumonitis. Normal tissue complication probability. *Int J Radiat Oncol Biol Phys*. 2003;55(3):724-735.

    doi: 10.1016/S0360-3016(02)03986-X

11. Barendsen GW. Dose fractionation, dose rate and iso-effect relationships for normal tissue responses. *Int J Radiat Oncol Biol Phys*. 1982;8(11):1981-1997.

    doi: 10.1016/0360-3016(82)90459-X

12. Jones B, Dale RG, Deehan C, Hopkins KI, Morgan DA. The Role of Biologically Effective Dose (BED) in clinical oncology. *Clin Oncol* (*R Coll Radiol*). 2001;13(2):71-81.

    doi: 10.1053/clon.2001.9221

13. Fowler JF. 21 years of biologically effective dose. *Br J Radiol*. 2010;83(991):554-568.

    doi: 10.1259/bjr/31372149

14. Barton M. Tables of equivalent dose in 2 Gy fractions: A simple application of the linear quadratic formula. *Int J Radiat Oncol Biol Phys*. 1995;31(2):371-378.

    doi: 10.1016/0360-3016(94)e0126-5

15. Nahum AE, Sanchez-Nieto B. Tumor control probability modeling: Basic principles and applications in treatment planning. *Phys Med*. 2001;17(2):13-23.

16. Schultheiss TE, Orton CG, Peck RA. Models in radiotherapy: Volume effects. *Med Phys*. 1983;10(4):410-415.

    doi: 10.1118/1.595312

17. Withers HR, Taylor JM, Maciejewski B. Treatment volume and tissue tolerance. *Int J Radiat Oncol Biol Phys*. 1988;14(4):751-759.

    doi: 10.1016/0360-3016(88)90098-3

18. Kutcher GJ, Burman C, Brewster L, Goitein M, Mohan R. Histogram reduction method for calculating complication probabilities for three-dimensional treatment planning evaluations. *Int J Radiat Oncol Biol Phys*. 1991;21(1):137-146.

    doi: 10.1016/0360-3016(91)90173-2

19. Jones LC and Hoban PW. Treatment plan comparison using

equivalent uniform biologically effective dose (EUBED) *Phys Med Biol*. 2000;45(1):159-170.

doi: 10.1088/0031-9155/45/1/311

20. Niemierko A. Reporting and analyzing dose distributions: A concept of equivalent uniform dose. *Med Phys*. 1997;24(1):103-110.

doi: 10.1118/1.598063

21. Lee SP, Leti MY, Smathers JB, McBride WH, Parker RG, Withers HR. Biologically effective dose distribution based on the linear quadratic model and its clinical relevance. *Int J Radiat Oncol Biol Phys*. 1995;33(2):375-389.

doi: 10.1016/0360-3016(95)00162-R

22. Wheldon TE, Deehan C, Wheldon EG, Barretta A. The linear-quadratic transformation of dose-volume histograms in fractionated radiotherapy. *Radiother Oncol*. 1998;46(3):285-295.

doi: 10.1016/S0167-8140(97)00162-X

23. O'Donoghue JA. Implications of nonuniform tumor doses for radioimmunotherapy. *J Nucl Med*. 1999;40(8):1337-1341.

24. Singh G, Oinam AS, Kamal R, Handa B, Kumar V, Rai B. Voxel based BED and EQD2 evaluation of the radiotherapy treatment plan. *J Med Phys*. 2018;43(3):155-161.

doi: 10.4103/jmp.JMP_29_18

25. Varian Medical Systems. *Velocity V. 4.1, Instructions for Use*. Polo Alto, CA, USA: Varian Medical Systems; 2023.

26. RaySearch Laboratories. *Biological Models Reference Information, Raystation Reference Manual*. Stockholm, Sweden: RaySearch Laboratories; 2024.

27. Dale R. The application of the linear-quadratic dose-effect equation to fractionated and protracted radiotherapy. *Br J Radiol*. 1985;58(690):515-528.

doi: 10.1259/0007-1285-58-690-515

28. Fowler JF. The linear-quadratic formula and progress in fractionated radiotherapy. *Br J. Radiol*. 1989;62(740):679-694.

doi: 10.1259/0007-1285-62-740-679

29. McMahon SJ. The linear quadratic model: Usage, interpretation and challenges. *Phys Med Biol*. 2018;64(1):01TR01.

doi: 10.1088/1361-6560/aaf26a

30. Hawkins RB. Effect of heterogeneous radio sensitivity on the survival, alpha beta ratio and biologic effective dose calculation of irradiated mammalian cell populations. *Clin Transl Radiat Oncol*. 2017;4:32-38.

doi: 10.1016/j.ctro.2017.03.001

31. Thames HD. An 'Incomplete-repair' model for survival after fractionated and continuous irradiations. *Int J Radiat Biol Relat Stud Phys Chem Med*. 1985;47(3):319-39.

doi: 10.1080/09553008514550461

32. Kuperman VY, Spradlin GS. Use of radiation protraction to escalate biologically effective dose to the treatment target. *Med Phys*. 2011;38(12):6553-6560.

doi: 10.1118/1.3656053

33. Brenner DJ, Hall EJ. Conditions for the equivalence of continuous to pulsed low dose rate brachytherapy. *Int J Radiat Oncol Biol Phys*. 1991;20(1):181-190.

doi: 10.1016/0360-3016(91)90158-Z

34. Fowler JF, Welsh JS, Howard SP. Loss of biological effect in prolonged fraction delivery. *Int J Radiat Oncol Biol Phys*. 2004;59(1):242-249.

doi: 10.1016/j.ijrobp.2004.01.004

35. Benedict SH, Yenice KM, Followill D, *et al*. Stereotactic body radiation therapy: The report of AAPM Task Group 101. *Med Phys*. 2010;37(8):4078-4101.

doi: 10.1118/1.3438081

36. Porter EH. The statistics of dose/cure relationships for irradiated tumours. Part I. *Br J Radiol*. 1980;53(627):210-227.

doi: 10.1259/0007-1285-53-627-210

37. Deasy J. Poisson formulas for tumor control probability with clonogen proliferation *Radiat Res*. 1996;145(3):382-384.

doi: 10.2307/3578994

38. Webb S, Evanst PM, Swindell W, Deasy JO. A proof that uniform dose gives the greatest TCP for fixed integral dose in the planning target volume. *Phys Med Biol*. 1994;39(11):2091-2098.

doi: 10.1088/0031-9155/39/11/018

39. Drzymala RE, Mohan R, Brewster L, Chu J, Goitein M, Harms W, Urie M. Dose-volume histograms. *Int J Radiat Oncol Biol Phys*. 1991;21(1):71-78.

doi: 10.1016/0360-3016(91)90168-4

40. Kuperman VY, Lubich LM. Impact of target dose inhomogeneity on BED and EUD in lung SBRT. *Phys Med Biol*. 2021;66(1):01NT02.

doi: 10.1088/1361-6560/abd0d1

41. Shuryak I, Carlson DJ, Brown MJ, Brenner DJ. High-dose and fractionation effects in stereotactic radiation therapy: Analysis of tumor control data from 2965 patients. *Radiother Oncol*. 2015;115(3):327-334.

doi: 10.1016/j.radonc.2015.05.013

42. Onishi H, Araki T, Shirato H, *et al*. Stereotactic hypofractionated high-dose irradiation for stage I nonsmall cell lung carcinoma: Clinical outcomes in 245 subjects in a Japanese multiinstitutional study. *Cancer*. 2004;101(7):1623-1631.

doi: 10.1002/cncr.20539

43. Guerrero M, Li XA. Extending the linear-quadratic model for large fraction doses pertinent to stereotactic radiotherapy. *Phys Med Biol*. 2004;49(20):4825-4835.

doi: 10.1088/0031-9155/49/20/012

44. Kirkpatrick JP, Meyer JJ, Marks LB. The linear-quadratic model is inappropriate to model high dose per fraction effects in radiosurgery. *Semin Radiat Oncol*. 2008;18(4):240-243.

doi: 10.1016/j.semradonc.2008.04.005

45. Astrahan M. Some implications of linear-quadratic-linear radiation dose-response with regard to hypofractionation. *Med Phys*. 2008;35(9):4161-4172.

doi: 10.1118/1.2969065

46. Park C, Papiez L, Zhang S, Story M, Timmerman RD. Universal survival curve and single fraction equivalent dose: Useful tools in understanding potency of ablative radiotherapy. *Int J Radiat Oncol Biol Phys*. 2008;70(3):847-852.

doi: 10.1016/j.ijrobp.2007.10.059

47. Ruggieri R, Stavrev P, Naccarato S, Stavreva N, Alongi F, Nahum AE. Optimal dose and fraction number in SBRT of lung tumours: A radiobiological analysis. *Phys Med*. 2017;44:188-195.

doi: 10.1016/j.ejmp.2016.12.012

48. Armpilia CI, Dale RG, Jones B. Determination of the optimum dose per fraction in fractionated radiotherapy when there is delayed onset of tumour repopulation during treatment. *Br J Radiol*. 2004;77(921):765-767.

doi: 10.1259/bjr/47388747

49. Mehta M, Scrimger R, Mackie R, Paliwal B, Chappell R, Fowler J. A new approach to dose escalation in non-small-cell lung cancer. *Int J Radiat Oncol Biol Phys*. 2001;49(1):23-33.

doi: 10.1016/S0360-3016(00)01374-2

50. Brown JM, Carlson DJ, Brenner DJ. The tumor radiobiology of SRS and SBRT: Are more than the 5 Rs involved? *Int J Radiat Oncol Biol Phys*. 2014;88(2):254-262.

doi: 10.1016/j.ijrobp.2013.07.022

Appendix

BED_{mean} vs. BED_{nud}

As mentioned previously, BED_{mean} defined in Eq. (16) always exceeds or equals the true BED (i.e., BED_{nud}) defined in Eqs. (3) and (4). To prove this statement for an arbitrary dose distribution in the target, one can express BED_{mean} as the natural logarithm of a geometric mean, that is,

$$BED_{mean} = -\alpha^{-1}\ln\left[\left(\prod_{j=1}^{N_{voxel}} S(j)\right)^{1/N_{voxels}}\right] \tag{A1}$$

where $S(i) = exp(-\alpha BED_{voxel}(i))$. Conversely, the BED_{nud} for the same dose distribution is given by the natural logarithm of the arithmetic mean, that is,

$$BED_{nud} = -\alpha^{-1}\ln\left(\frac{1}{N_{voxel}}\sum_{j=1}^{N_{voxel}} S(j)\right) \tag{A2}$$

Because the arithmetic mean is always equal to or greater than the corresponding geometric mean, we have

$$-\ln\left[\frac{1}{N_{voxel}}\sum_{j=1}^{N_{voxel}} S(j)\right] \le -\ln\left[\left(\prod_{j=1}^{N_{voxel}} S(j)\right)^{1/N_{voxel}}\right] \tag{A3}$$

which implies that $BED_{nud} \le BED_{mean}$. Note that $BED_{nud} = BED_{mean}$ if and only if the probability of survival is the same for different voxels. That is, $S(j) = const$, $j = 1, 2, \ldots, N_{voxel}$.

ACCSCIENCE PUBLISHING

Advances in Radiotherapy & Nuclear Medicine

ORIGINAL RESEARCH ARTICLE

Dosimetric differences between online adapt-to-position and offline adapt-to-shape plans for adaptive radiotherapy in cervical cancer

Kaiwen Zhou[1,2†], Jinhu Chen[3†], Junfeng Zhao[2], Xingwei An[3], Yong Yin[2*], and Zhenjiang Li[2*]

[1]Department of Graduate, Shandong First Medical University (Shandong Academy of Medical Sciences), Jinan, China

[2]Department of Radiation Oncology, Shandong Cancer Hospital and Institute, Shandong First Medical University (Shandong Academy of Medical Sciences), Jinan City, Shandong, China

[3]Academy of Medical Engineering and Translational Medicine, Tianjin University, Tianjin, China

Abstract

Radiation therapy plays a significant role in the treatment of cervical cancer. Additionally, more adaptive workflows using ATP are being implemented in the daily radiotherapy of our organization. Herein, we aimed to investigate the dosimetric differences between online ATP and offline ATS plans for magnetic resonance (MR)-guided adaptive radiotherapy in patients with cervical cancer and determine radiotherapy modalities that address clinical requirements. In total, 25 patients with cervical cancer were enrolled in this study, with 13 in the radical radiotherapy group and 12 in post-operative radiotherapy group. We aimed for the clinical target volume (CTV) to be covered by 95 – 100% of the prescribed dose (50 Gy/25 sessions/5 weeks). MR-Linac was performed daily during treatment, and the images were rigidly aligned with the local computed tomography to generate an online ATP plan. MR images acquired during the first three sessions were selected to recontour the CTV and organs at risk (OAR). Furthermore, an offline ATS plan was generated. In the radical radiotherapy group, the CTV, D98, D95 (5024.65 ± 23.34 vs. 4995.50 ± 14.99 cGy), and Dmean of the ATS were superior compared with those of the ATP. The Dmax was lower in the ATS plan than in the ATP plan. In the post-operative radiotherapy group, the CTV, Dmean, D98, and D95 (5052.61 ± 67.87 vs. 5014.41 ± 24.68 cGy) were better in the ATS plan than in the ATP plan. When evaluating the OAR in the radical radiotherapy group, the minimum doses to the bladder and rectum were greater in the ATS plan than in the ATP plan. In the post-operative radiotherapy group, the V20 of the bladder and rectum were lower in the ATS plan than in the ATP plan. Therefore, ATS is well suited for post-operative radiotherapy, whereas ATP is better suited for radical radiotherapy. Furthermore, ATP can effectively address the clinical requirements of daily workflows.

Keywords: Online adaptive radiotherapy; Adapt-to-shape; Adapt-to-position; Cervical cancer; Clinical target volume

†*These authors contributed equally to this work.*

***Corresponding authors:**
Yong Yin
(yinyongsd@126.com)
Zhenjiang Li
(lizhenjiang@email.sdfmu.edu.cn)

Citation: Zhou K, Chen J, Zhao J, An X, Yin Y, Li Z. Dosimetric differences between online adapt-to-position and offline adapt-to-shape plans for adaptive radiotherapy in cervical cancer. *Adv Radiother Nucl Med*. 2024;2(4):4919.
doi: 10.36922/arnm.4919

Received: September 23, 2024

Accepted: December 10, 2024

Published Online: December 31, 2024

1. Introduction

Cervical cancer is a highly prevalent form of malignant tumor in females.[1] Radiotherapy is becoming an increasingly important component in the treatment of cervical cancer. Advances in multimodal imaging technology have increased the accuracy of contouring clinical target volume (CTV) and organs at risk (OAR). Furthermore, image-guidance technology has considerably reduced the associated errors.[2] For cervical cancer, the power of magnetic resonance (MR) imaging (MRI)-based morphological imaging has driven advancements in response assessment and image-guided brachytherapy.[3] The Elekta Unity MR-Linac can perform daily MR imaging using a 1.5 T MRI scanner, allowing real-time monitoring of the patient's clinical target area and OAR for relevant contouring adjustments.[4] However, due to the close anatomical proximity of the cervix to the bladder and rectum in addition to the varying physiological states of the patients, daily fluctuations in the filling and positioning of these organs can cause dose distribution deviations, making online adaptive radiotherapy essential[5,6] Adaptive radiotherapy encompasses the adaptation of radiotherapy plans based on patient-specific anatomical variations that have been identified through image-guided radiation therapy (IGRT), optimization of planning, and dose delivery to ensure accurate treatment.[7]

Adaptive radiotherapy can be implemented at 3 time scales as follows: offline in adjacent fractions, online immediately before the fraction, and online during treatment.[8] Online and real-time adaptive radiotherapy protocols allow plan modification while the patient is on the couch, thereby allowing the plan to be updated on the basis of real-time anatomical changes. This enables the delineation of smaller safer borders due to the greater certainty of the tumor location. Offline adaptive radiotherapy aims to correct for systematic changes in OAR that are identified by imaging during treatment and plans are modified offline.[9,10] Online and offline adaptive radiotherapy play different roles in cancer treatment. Online adaptive radiotherapy is effective for treating pancreatic and cervical tumors,[11-16] whereas offline adaptive radiotherapy has been beneficial in patients with head and neck and lung tumors,[17-21] The Elekta Unity includes two adaptive planning strategies designed to address daily anatomical variations using the MRI: Adapt-to-position (ATP), which is also known as no-online adaptive replanning. The ATP involves optimizing the reference plan with an isocenter shift that is based on the alignment between the daily MRI and reference image. Adapt-to-shape (ATS), also known as online adaptive replanning, involves generating a new treatment plan that is based on the anatomical configuration.[22] ATP is more commonly used for brain tumors, demonstrating clinically acceptable processes and treatment times in high-grade gliomas.[23] However, ATS is more commonly used for prostate cancer, for which it has demonstrated improved dose delivery.[24] Patients treated for cervical cancer exhibit inter- or intrafraction anatomical changes. The Elekta Unity system allows for obtaining an MRI before and during treatment, facilitating daily plan adaptation. This capability enables the adjustment of treatment plans in response to daily anatomical variations, ensuring precise dose delivery to CTV with each session. Despite these advancements, some limitations exist to the wide clinical application of adaptive radiotherapy.

Herein, offline ATS planning was performed using MR images obtained during treatment. The dosimetric outcomes of the two workflows were analyzed by comparing the delivered doses to the CTV, planning target volume (PTV), bladder, rectum, small bowel, and femoral head in online ATP and offline ATS plans. This comparison allowed for an assessment of the dose distribution across the different anatomical structures in each adaptive planning approach. Herein, we aimed to investigate the dosimetric differences between online ATP and offline ATS plans in MR-guided adaptive radiotherapy for cervical cancer. Furthermore, we aimed to evaluate radiotherapy modalities for treating cervical cancer to address the clinical requirements and provide guidance on optimizing ART protocols to improve the precision of dose delivery, minimize exposure to healthy tissues, and reduce the risk of radiation-induced complications. Ultimately, we intend to support the development of adaptable patient-specific radiotherapy strategies that meet the dynamic requirements of cervical cancer treatment.

2. Methods

2.1. Inclusion criteria

Of the 30 patients with cervical cancer who underwent radiotherapy at Shandong Cancer Hospital between September 2020 and June 2023, 25 met the inclusion criteria. The following were the inclusion criteria: Age between 30 and 85 years; diagnosis of cervical cancer that had been confirmed through histopathological examination; absence of any intestinal or metabolic diseases; and adequate comprehension and communication ability of the patient. The following were the exclusion criteria: Severe cardiac, hepatic, or renal insufficiency; termination of treatment due to significant complications during or after radiotherapy such as cardiac or pulmonary issues, severe infections, and hemorrhages; and refusal to participate in the study. This study was approved by the Ethical Review

Committee of our hospital (No: SDTHEC2024007028, date: July 22nd 2024), and informed consent was obtained from all the patients and their families.

2.2. Imaging studies during the treatment

2.2.1. Computed tomography (CT) simulation

All patients were positioned supine with their hands crossed above their heads and stabilized with a customized vacuum bag. Respiratory motion was controlled by applying an abdominal compression belt, and the placement and compression intensity of the belt were documented. The patients consumed 500 mL of water before the scan. Standard axial enhancement scans were obtained using a large-aperture simulation (CT; 16-slice Brilliance Big Bore; Philips Medical Systems, Amsterdam, The Netherlands), with a 3-mm slice thickness and a 3-mm gap between slices.

2.2.2. Daily MRI during radiotherapy

All patients underwent an online MRI before treatment using the following 2D-TSE/T2WI scanning parameters: TR/TE, 1535 ms/278 ms; FOV, 400 × 400 × 300 mm^3; matrix size, 268 × 267 × 300; and voxel size, 1.5 × 1.5 × 2 mm^3. MR images from the first three treatment sessions of each patient were analyzed. Using standardized imaging parameters, we ensured that the images were comparable across patients and treatment sessions. Before each treatment session, all patients were required to follow the same bladder preparation protocol as that used during the initial CT simulation.

2.3. CTV and OAR contouring

Two radiation oncologists used the Monaco treatment planning system (TPS) (Elekta, Stockholm, Sweden) to contour the corresponding CTV and OAR on the patient's daily MR images and simulation CT. Patients were divided into the following two groups based on whether they had undergone surgery: the radical radiotherapy group and the post-operative radiotherapy group. In the radical radiotherapy group, the CTV included the primary tumor, cervix, uterus, proximal vagina (based on the area of tumor infiltration), paracervical tissues, lymph nodes (including the external iliac, internal iliac, occlusive foramen, presacral, and common iliac lymph nodes), and para-aortic and inguinal lymphatic drainage areas (based on the patient's situation). However, in the post-operative radiotherapy group, only the vaginal stump, paracervical tissue, and associated lymph nodes were contoured. The PTV was created by expanding the CTV outward by 0.5 cm to account for potential errors and organ motion during treatment. This margin ensured adequate coverage of the target area despite any slight movements or uncertainties. In both groups, the OAR contouring included the bladder, rectum, left and right femoral heads, and the small bowel because these structures are particularly sensitive and require careful monitoring to avoid excessive radiation exposure.

2.4. Treatment planning

After CT was performed for localization, the acquired images were imported into the Monaco TPS for designing the plan. Intensity-modulated radiation therapy (IMRT) was delivered using gantry angles of 180°, 130°, 80°, 30°, 330°, 280°, and 230°, with a collimator angle of 0° and a maximum dose rate of 400 MU/min. Approximately 95% of the CTV was administered 100% of the prescribed dose of 50 Gy in 25 fractions over 5 weeks. Dose constraints for the remaining OARs were established on the basis of relevant international standards.

2.5. Online ATP and offline ATS workflows

The online adaptive radiotherapy process involved obtaining a real-time MRI before each treatment session (Figure 1). Subsequently, this MRI was rigidly aligned with the planning CT using Monaco TPS. An online adaptive treatment plan was generated using the ATP workflow. During the online adaptive planning process, the CTV and OAR motions were monitored using a balanced, steady-state, and free precession sequence. For offline adaptive planning, the MR images acquired during the daily treatment were used. The corresponding CTV and OAR were contoured within Monaco TPS, and the treatment plan was designed using the ATS workflow. The plan design requirements and OAR dose constraints for the online ATP and offline ATS plans were consistent with relevant international standards. Online ATP plans were approved before the plan was implemented, while offline ATS plans were approved after they were developed offline by a physicist, clinical radiotherapist, and senior physicist.

2.6. Statistical analysis

Statistical Package for the Social Sciences (version 25.0; IBM Corporation, Armonk, New York, USA) was used to perform statistical analysis of the dosimetric parameters of CTV, PTV, and OAR, which have been expressed as means ± standard deviations. The Shapiro-Wilk test was used to assess the normality of the data distribution. The Wilcoxon signed-rank test was used, and statistical significance was set at 0.05.

3. Results

Twenty-five patients with cervical cancer were included in this study. The patient and disease characteristics are summarized in Table 1. The mean age of the patients was

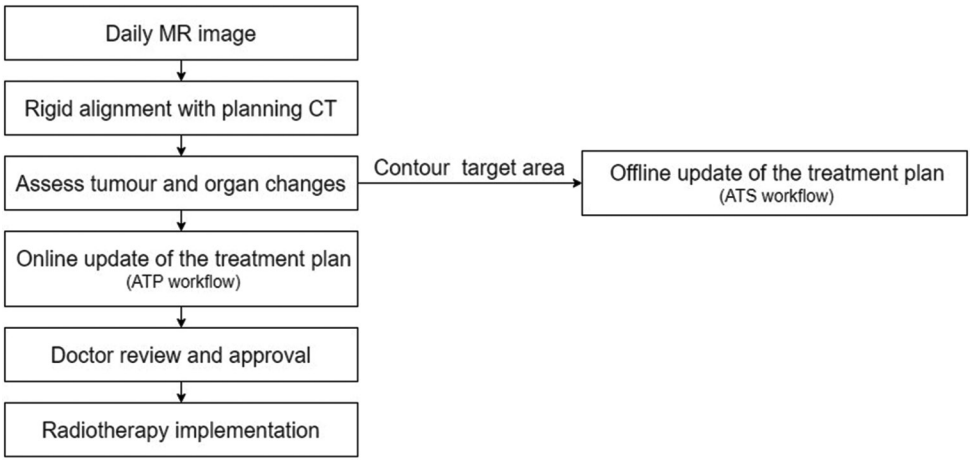

Figure 1. Flowchart of the ATP and ATS workflows
Abbreviations: ATP: Adapt-to-position; ATS: Adapt-to-shape; CT: Computed tomography.

Table 1. Characteristics of the enrolled patients and the treatment modality

Characteristics	*N*
Ages	56.4±12.2 (range, 26 – 78 years)
Body mass index (kg/m^2)	23.9±3.5
FIGO tumor stage (I: II: III: IV)	2:11:10:2
HPV (negative/positive)	21/4
Pathological diagnosis	
Squamous cell carcinoma	14
Adenocarcinoma	11
Treatment modality	
Radical radiotherapy	13
Post-operative radiotherapy	12

Abbreviations: HPV: Human papillomavirus; FIGO: International federation of gynecology and obstetrics classification.

56.4 ± 12.2 years (range, 26 – 78 years). The majority of the patients (44%) had stage II disease. In total, 13 patients were included in the radical radiotherapy group and 12 patients in the post-operative radiotherapy group. In total, 78 plans were present in the radical radiotherapy patient group (39 using ATS and 39 using ATP). In the post-operative radiotherapy patient group, 72 plans were present (36 with ATS and 36 with ATP). The ATS plan corresponded with the ATP plan in each patient.

3.1. CTV and PTV dosimetric differences

In the radical radiotherapy group, the Dmax and Dmean of the ATS and ATP plans were better than those of the original plan (Table 2). In the post-operative radiotherapy, the Dmean of the ATS and ATP plans was better than that of the reference plan (Table 3). For the target dose, in the radical radiotherapy group, the CTV, D98, D95, and Dmean of the offline ATS plan were superior compared with those of the ATP plan ($P < 0.05$; Table 4). The D95 was 5024.65 ± 23.34 cGy and 4995.50 ± 14.99 cGy in the ATS and ATP plans, respectively. The Dmax was lower in the ATS plan than in the ATP plan. A comparison of the PTVs revealed that the D95 and Dmean were better in the ATS plan than in the ATP plan ($P < 0.05$). Furthermore, the Dmax was significantly lower in the ATS plan than in the ATP plan. No statistically significant difference was observed between the homogeneity index and conformity index between the two plans. The ATS plan exhibited a good target coverage (V100% = 96% ± 1%), whereas the ATP plan exhibited significant differences in the corresponding parameters (V100% = 94% ± 1%) ($P < 0.05$).

In the post-operative radiotherapy group, the CTV, Dmean, D98, and D95 of the offline ATS plan were better than those of the ATP plan (Table 5). The D95 was 5052.61 ± 67.87 cGy and 5014.41 ± 24.68 cGy in the ATS and ATP plans, respectively. A comparison of the PTVs revealed that the Dmean of the offline ATS plan was better than that of the ATP plan. Furthermore, the ATS plan exhibited a good target coverage (V100% = 0.96% ± 0.01%), and the ATP plan exhibited similar coverage (V100% = 0.95% ± 0.009%) ($P < 0.05$).

3.2. OAR dosimetric differences

Comparison of the OAR in the radical radiotherapy group revealed that the minimum doses to the bladder and rectum were greater in the ATS plan than in the ATP plan ($P < 0.05$; Tables 6 and 7). In the post-operative radiotherapy group, the V20 values of the bladder and rectum in the ATS plan were lower than those in the ATP plan ($P < 0.05$). The rectum of Dmin in ATS was higher than that in ATP.

Table 2. Comparison of the dosimetric parameters of various PTVs and CTVs in patients undergoing radical radiotherapy

Parameter	ATP	ATS	Non-ART	*P*-value (ATS/ATP vs. non-ART)
CTV-Dmax (cGy)	5797.59±72.45	5733.71±150.40	5625.63±95.17	<0.05
CTV-Dmean (cGy)	5232.03±37.38	5251.35±61.06	5225.55±94.54	<0.05
PTV-Dmax (cGy)	5799.49±71.72	5733.72±150.41	5625.63±95.17	<0.05
PTV-Dmean (cGy)	5084.49±31.07	5088.44±127.01	5061.79±25.76	<0.05

Notes: The comparisons among the three groups were conducted using the Wilcoxon rank-sum test. Significant values were determined based on a threshold of $P<0.05$.
Abbreviations: Dmax: Maximum dose; Dmean: Mean dose; ATP: Adapt-to-position; ATS: Adapt-to-shape; PTV: Planned target volume; CTV: Clinical target volume; ART: Adaptive radiotherapy.

Table 3. Comparison of the dosimetric parameters of various PTVs and CTVs in patients undergoing post-operative radiotherapy

Parameter	ATP	ATS	Non-ART	*P*-value (ATS/ATP vs. non-ART)
CTV-Dmean (cGy)	5265.29±61.14	5305.21±125.93	5225.10±63.49	<0.05
PTV-Dmean	5092.40±40.86	5126.02±95.20	5060.55±51.03	<0.05

Notes: The comparisons among the three groups were conducted using the Wilcoxon rank-sum test. Significant values were determined based on a threshold of $P<0.05$.
Abbreviations: Dmean: Mean dose; ATP: Adapt-to-position; ATS: Adapt-to-shape; PTV: Planned target volume; CTV: Clinical target volume; ART: Adaptive radiotherapy.

Table 4. Comparison of the dosimetric parameters of various PTVs and CTVs in patients undergoing radical radiotherapy

Parameter	ATP	ATS	*P*-value
CTV-D_{98} (cGy)	4911.72±52.66	4950.25±43.89	<0.05
CTV-D_{95} (cGy)	4995.50±14.99	5024.65±23.34	<0.05
CTV-Dmax (cGy)	5797.59±72.45	5733.71±150.40	<0.05
CTV-Dmean (cGy)	5232.03±37.38	5251.35±61.06	<0.05
PTV-Dmax (cGy)	5799.49±71.72	5733.72±150.41	<0.05
PTV-Dmean (cGy)	5084.49±31.07	5088.44±127.01	<0.05
PTV-D_{95} (cGy)	4622.37±45.98	4652.12±65.32	<0.05
HI	1.09±0.11	1.08±0.02	>0.05
CI	0.71±0.03	0.70±0.04	>0.05
V100%	0.94±0.01	0.96±0.01	<0.05

Notes: The comparisons were conducted using the Wilcoxon rank-sum test. Significant values were determined based on a threshold of $P<0.05$.
Abbreviations: ATP: Adapt-to-position; ATS: Adapt-to-shape; PTV: Planned target volume; CTV: Clinical target volume; D_{98}, D_{95}: The dose received by 98%, 95% of the PTV or CTV; Dmax: Maximum dose; Dmean: Mean dose; CI: Conformity index = $(V_{t,\,ref}/V_t)\cdot(V_{t,\,ref}/V_{ref})$, where $V_{t,\,ref}$ is the target volume covered by the reference isodose line, Vt is the target volume, and Vref is the total volume covered by the reference isodose line; HI: Homogeneity index = $(D_2\text{-}D_{98})/D_{50}$; V100%: Coverage of 100% prescription dose on the PTV.

Table 5. Comparison of the dosimetric parameters of various PTVs and CTVs in patients undergoing post-operative radiotherapy

Parameter	ATP	ATS	*P*-value
CTV-Dmean (cGy)	5265.29±61.14	5305.21±125.93	<0.05
CTV-D_{98} (cGy)	4934.01±28.67	4976.18±60.90	<0.05
CTV-D_{95} (cGy)	5014.41±24.68	5052.61±67.87	<0.05
PTV-Dmean (cGy)	5092.40±40.86	5126.02±95.20	<0.05
HI	1.10±0.03	1.09±0.03	>0.05
CI	0.68±0.02	0.67±0.06	>0.05
V100%	0.95±0.009	0.96±0.01	<0.05

Notes: The comparisons were conducted using the Wilcoxon rank-sum test. Significant values were determined based on a threshold of $P<0.05$.
Abbreviations: ATP: Adapt-to-position; ATS: Adapt-to-shape; PTV: Planned target volume; CTV: Clinical target volume; Dmean, Mean dose; D_{98}, D_{95}: The dose received by 98%, 95% of the PTV or CTV; CI: Conformity index = $(V_{t,\,ref}/V_t)\cdot(V_{t,\,ref}/V_{ref})$, where $V_{t,\,ref}$ is the target volume covered by the reference isodose line, V_t is the target volume, and Vref is the total volume covered by the reference isodose line; HI: Homogeneity index = $(D_2\text{-}D_{98})/D50$; V100%: Coverage of 100% prescription dose on the PTV.

4. Discussion

Cervical cancer is a common disease for which adaptive radiotherapy is suitable and necessary. During cervical cancer radiotherapy, tumor shrinkage, movement, and volume changes in OAR between fractions negatively affect the delivery of the planned dose. For cervical cancer, online adaptive radiation therapy with IMRT and IGRT may be an effective way to meet the clinical dosimetric objectives.[2] Adaptive radiotherapy facilitates treatment plan adjustments using daily imaging, thereby ensuring accurate dose delivery to the CTV despite anatomical variations. This approach allows for dynamic modifications that maintain precise target area coverage, accommodating

Table 6. Comparison of the dosimetric parameters of various organs at risk in patients undergoing radical radiotherapy

Organ at risk	Parameter	ATP	ATS	*P*-values
Rectum	D_{40} (cGy)	3671.49±467.14	3911.85±519.92	<0.05
	D_{30} (cGy)	4008.91±455.14	4222.03±431.68	<0.05
	D_{20} (cGy)	4302.35±524.10	4532.84±324.36	<0.05
	Dmin (cGy)	579.34±523.64	1114.30±745.25	<0.05
	Dmean (cGy)	3136.20±416.57	3564.54±476.61	<0.05
Bladder	Dmin (cGy)	1028.33±391.63	1212.14±560.91	<0.05

Notes: The comparisons were conducted using the Wilcoxon rank-sum test. Significant values were determined based on a threshold of $P<0.05$.
Abbreviations: ATP: Adapt-to-position; ATS: Adapt-to-shape; D_{40}, D_{30}, D_{20}: The dose received by 40%, 30%, and 20% of the corresponding organ at risk, respectively; Dmin: Minimum dose; Dmean: Mean dose.

Table 7. Comparison of the dosimetric parameters of various organs at risk in patients undergoing post-operative radiotherapy

Organ at risk	Parameter	ATP	ATS	*P*-values
Rectum	D_{40} (cGy)	3339.24±333.24	3034.21±733.41	<0.05
	D_{30} (cGy)	3678.23±274.83	3411.82±620.59	<0.05
	D_{20} (cGy)	4051.75±222.24	3866.87±501.21	<0.05
	Dmin (cGy)	250.77±35.92	362.86±170.64	<0.05
Bladder	V_{20} (cGy)	4158.42±327.08	4017.98±381.26	<0.05

Notes: The comparisons were conducted using the Wilcoxon rank-sum test. Significant values were determined based on a threshold of $P<0.05$.
Abbreviations: ATP: Adapt-to-position; ATS: Adapt-to-shape; D_{40}, D_{30}, D_{20}: The dose received by 40%, 30%, and 20% of the corresponding organ at risk, respectively; Dmin: Minimum dose.

anatomical changes throughout the treatment course. Therefore, this approach enhances therapeutic accuracy and effectiveness. At the dosimetric level, compared with non-adaptive radiotherapy, adaptive radiotherapy can enhance the dosimetric distributions of CTV and PTV in both patient groups (Tables 2 and 5). These findings reveal that adaptive radiotherapy, which tailors treatment based on daily anatomical variations, allows for more precise tumor targeting while better sparing the surrounding healthy tissues. In both groups of patients, the implementation of adaptive planning techniques led to enhanced dose coverage and conformity to the target areas, ensuring that the prescribed dose was delivered more accurately to the CTV and PTV. Thus, adaptive radiotherapy could improve the outcomes in patients with cervical cancer patients using a more individualized approach that adapts to the evolving anatomy throughout the course of treatment.

Most previous studies on adaptive radiotherapy have been conducted using cone beam CT (CBCT). CBCT cannot provide an accurate representation of the border between the tumor and surrounding normal soft tissue. Thus, accurate delivery of doses cannot be ensured.[25] MRI enhances soft tissue contrast, facilitating superior visualization and differentiation between healthy tissues and tumors as well as aiding in detecting nuanced physiological alterations within the tissues.[26,27] Online MRgRT permits daily MRI and direct monitoring of the CTV and OAR throughout the treatment process. The MR-guided strategy provides a higher level of accuracy and an acceptable distribution of the real dose over the treatment fractions. Real-time adaptive radiotherapy is conducted using daily acquired MRIs. Gupta *et al.* evaluated MR-Linac-guided online adaptive radiotherapy in patients with nasopharyngeal carcinoma using ATS-Lite and ATP workflows.[28] The use of MR-Linac-guided radiotherapy for cervical cancer offers several advantages. Before each treatment, MR images can be used to determine the patient's daily bladder filling to ensure that the OAR meets the requirements for radiotherapy. In particular, MR-guided adaptive radiotherapy has shown promise in addressing these challenges due to its superior soft tissue contrast, which allows for clear visualization of tumor and organ changes. This imaging capability supports more precise adaptation of the treatment plan, thereby reducing potential dose discrepancies and minimizing radiation exposure to critical organs, such as the bladder, rectum, and small bowel.

ATS and ATP are two workflows of adaptive radiotherapy that exhibit distinct characteristics. ATS enables a more precise and intuitive delineation of the patient's anatomy on the day of treatment, facilitating more accurate contouring of the CTV and OAR on that day and optimizing the dose delivery. Dassen *et al.* evaluated the efficacy of ATP and ATS in contouring the corresponding target areas in adaptive radiotherapy for prostate cancer. They determined that ATS demonstrated the best performance for the prostate, including seminal vesicles (CTVproS+SV).[29] Furthermore, ATP has demonstrated clinically acceptable processes and treatment times in patients with high-grade gliomas.[23] ATP is less time-consuming than ATS, and all plans it generates meet the clinical requirements. Herein, the ATS workflow took 35.4 ± 2.4 min, and the ATP workflow took 10.3 ± 0.6 min. Although the use of ATS can increase the receptor volume in CTV and PTV, the increase is not significant and time-consuming. Therefore, we primarily use the ATP workflow in daily practice. The plans generated by the ATP workflow are sufficient to meet clinical needs. At our institution, the high volume of patients undergoing MR-Linac-guided radiotherapy limits

the practicality of extensive ATS protocols because they considerably increase the treatment time per patient and disrupt the scheduling of subsequent treatments. Extended time on the treatment couch, without timely contour adjustments, can result in positional shifts of the target area and OAR, thereby necessitating recalculations of the dose distribution. Moreover, prolonged treatment sessions may negatively impact patient compliance. Furthermore, the substantial resource demands and specialized training required for ATS protocols pose significant barriers to their widespread adoption in clinical settings.

In Peng *et al.*,[2] CBCT was used to design adaptive and non-adaptive radiotherapy plans for patients with cervical cancer and compared the dosimetry differences between workflows. They demonstrated that the CTVs of the adaptive plan were superior compared with those of the virtual non-adaptive plan in terms of the target area dose distribution. The adaptive plan, which included the rectum, bladder, and small bowel, was superior compared with the virtual non-adaptive plan. In our post-operative radiotherapy group, the ATS workflow increased the dose received by the clinical target area by approximately 0.7% for the CTV-Dmean and 0.6% for the PTV-Dmean. Furthermore, it reduced the dose to the corresponding OAR. Our finding is similar to the results of the study of Peng *et al.* However, in the radical radiotherapy group, the ATS workflow increased the dose administered to the clinical target area more effectively than the ATP plan did, with an increase of approximately 0.5% and 0.6% for the CTV D_{95} and PTV D_{95}, respectively. However, the ATS workflow also increased the dose administered to the corresponding OAR. Our finding contradicts the results of the study of Peng *et al.* which may be attributable to the fact that the target location changed as the bladder filled up. Herein, patients who were administered radical radiotherapy exhibited a significant shift in the target location as the bladder filled up when compared with patients who were administered post-operative radiotherapy (Figure 2). This indicates that patients undergoing radical radiotherapy are candidates for the ATP workflow. However, the ATS workflow is more suitable for patients undergoing post-operative radiotherapy. This is consistent with the dosimetry conclusions of our study.

However, due to the limited number of patients in our study, the smaller number of fractions analyzed, and the shorter clinical follow-up periods, and, it is not yet possible to confirm that the significant benefits to patient survival and prognosis. Furthermore, this study was conducted at a single center. Therefore, incorporating data from multiple centers in future studies are required to improve the comprehensiveness and generalizability of the results.

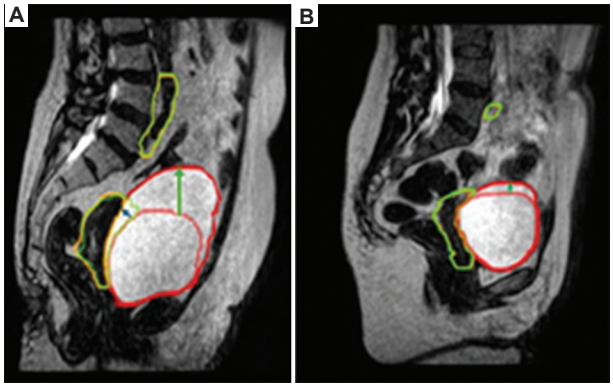

Figure 2. Bladder and CTV in patients who were administered radical radiotherapy (A) and post-operative radiotherapy (B). The green arrow indicates the change in the bladder. The blue arrow indicates the change in the CTV.
Abbreviation: CTV: Clinical target volume.

Determining the applicable range of volume changes in CTV and whether an increase in the OAR volume poses specific risks and complications is necessary. This requires further exploration and verification. Furthermore, determining whether patients require rescanning and readaptive radiotherapy due to prolonged positioning on the examination bed during each session is necessary. Consequently, future studies are required to ascertain the applicability of ATS and ATP, refine automatic dose optimization algorithms, and enhance the automatic contouring process. Parchur *et al.* used machine learning techniques that used features such as structural similarity and changes in local entropy to automatically assess whether specific routine MRI datasets require online adaptive replanning.[30] Although automated, rapid determination of the need for online adaptive replanning does not completely resolve all planning issues. However, it can contribute to reducing unnecessary manual labor and save time for patients and the treatment machine. Therefore, our future study will focus on advancing automated dose optimization algorithms and enhancing workflow efficiency.

5. Conclusion

The use of online adaptive radiotherapy determined by an ATS workflow for patients with cervical cancer considerably improves the dose distribution. When using the ATS workflow, the corresponding OAR needs to be protected during radiotherapy. In addition, the image quality, CTV contouring, and dose optimization algorithms should be further optimized to enhance the application of online adaptive radiotherapy in patients with cervical cancer. Moreover, ATS and ATP exhibit their own dosimetric advantages in cervical cancer radiotherapy, and their use should be individualized in different patients. Thus, online adaptive radiotherapy for cervical cancer is

an ideal technique to achieve individualized and precise radiotherapy in a clinical setting.

Acknowledgments

None.

Funding

This work was supported by the National Natural Science Foundation of China (Grant Nos. 82102173, 82072094, and 12275162), the Natural Science Foundation of Shandong Province (Grant No. ZR2019LZL017), the Precision Radiotherapy Submit plan 2021HZ81, the Taishan Scholars Project of Shandong Province (Grant No. ts201712098), and the Shandong Medical Association Clinical Research Fund – Qilu Special Project (YXH2022ZX02198).

Conflict of interest

The authors declare that they have no competing interests.

Author contributions

Conceptualization: Yong Yin, Zhenjiang Li
Formal analysis: Kaiwen Zhou
Investigation: Kaiwen Zhou, Jinhu Chen, Junfeng Zhao, Xingwei An
Methodology: Junfeng Zhao, Xingwei An
Writing – original draft: Kaiwen Zhou, Jinhu Chen
Writing – review & editing: Kaiwen Zhou, Jinhu Chen, Yong Yin, Zhenjiang Li

Ethics approval and consent to participate

The study was approved by the Ethical Review Committee of Shandong Cancer Hospital (ethics approval code: SDTHEC2024007028; approval date: July 22, 2024).

Consent for publication

All participants were adequately informed about the study procedures, risks, and benefits and they agreed to participate in this study voluntarily. In addition, we obtained permission from all participants regarding the publication of study results, which is reflected in the consent documentation.

Availability of data

The datasets generated and analyzed during the current study are available from the corresponding author upon reasonable request.

References

1. Bray F, Ferlay J, Soerjomataram I, Siegel RL, Torre LA, Jemal A. Global cancer statistics 2018: GLOBOCAN estimates of incidence and mortality worldwide for 36 cancers in 185 countries. *CA Cancer J Clin*. 2018;68:394-424.

   doi: 10.3322/caac.21492

2. Peng H, Zhang J, Xu N, Zhou Y, Tan H, Ren T. Fan beam CT-guided online adaptive external radiotherapy of uterine cervical cancer: A dosimetric evaluation. *BMC Cancer*. 2023;23(1):588.

   doi: 10.1186/s12885-023-11089-6

3. Tan LT, Tanderup K, Kirisits C, *et al*. Image-guided adaptive radiotherapy in cervical cancer. *Semin Radiat Oncol*. 2019;29(3):284-298.

   doi: 10.1016/j.semradonc.2019.02.010

4. Winkel D, Bol GH, Kroon PS, *et al*. Adaptive radiotherapy: The Elekta Unity MR-linac concept. *Clin Transl Radiat Oncol*. 2019;18:54-59.

   doi: 10.1016/j.ctro.2019.04.001

5. Eminowicz G, Rompokos V, Stacey C, Hall L, McCormack M. Understanding the impact of pelvic organ motion on dose delivered to target volumes during IMRT for cervical cancer. *Radiother Oncol*. 2017;122(1):116-121.

   doi: 10.1016/j.radonc.2016.10.018

6. Chen J, Liu P, Chen W, *et al*. Early changes of volume and spatial location in target and normal tissues caused by IMRT for cervical cancer. *Tumori*. 2016;102(6):610-613.

   doi: 10.5301/tj.5000413

7. Yan D, Vicini F, Wong J, Martinez A. Adaptive radiation therapy. *Phys Med Biol*. 1997;42(1):123-132.

   doi: 10.1088/0031-9155/42/1/008

8. Hunt A, Hansen VN, Oelfke U, Nill S, Hafeez S. Adaptive radiotherapy enabled by MRI guidance. *Clin Oncol* (*R Coll Radiol*). 2018;30(11):711-719.

   doi: 10.1016/j.clon.2018.08.001

9. Yan D, Wong J, Vicini F, *et al*. Adaptive modification of treatment planning to minimize the deleterious effects of treatment setup errors. *Int J Radiat Oncol Biol Phys*. 1997;38(1):197-206.

   doi: 10.1016/s0360-3016(97)00229-0

10. Yan D, Lockman D, Brabbins D, Tyburski L, Martinez A. An offline strategy for constructing a patient-specific planning target volume in adaptive treatment process for prostate cancer. *Int J Radiat Oncol Biol Phys*. 2000;48(1):289-302.

    doi: 10.1016/s0360-3016(00)00608-8

11. Han EY, Wang H, Briere TM, *et al*. Brain stereotactic radiosurgery using MR-guided online adaptive planning for daily setup variation: An end-to-end test. *J Appl Clin Med Phys*. 2022;23(3):e13518.

    doi: 10.1002/acm2.13518

12. Poon DMC, Yang B, Geng H, *et al*. Analysis of online plan adaptation for 1.5T magnetic resonance-guided stereotactic body radiotherapy (MRgSBRT) of prostate cancer. *J Cancer Res Clin Oncol*. 2022;24:1-10.

doi: 10.1007/s00432-022-03950-1

13. Ikushima H, Balter P, Komaki R, *et al*. Daily alignment results of in-room computed tomography-guided stereotactic body radiation therapy for lung cancer. *Int J Radiat Oncol Biol Phys*. 2011;79(2):473-480.

doi: 10.1016/j.ijrobp.2009.11.009

14. Gong W, Yao Y, Ni J, *et al*. Deep learning-based low-dose CT for adaptive radiotherapy of abdominal and pelvic tumors. *Front Oncol*. 2022;12:968537.

doi: 10.3389/fonc.2022.968537

15. Kensen CM, Janssen TM, Betgen A, *et al*. Effect of intrafraction adaptation on PTV margins for MRI guided online adaptive radiotherapy for rectal cancer. *Radiat Oncol*. 2022;17(1):110.

doi: 10.1186/s13014-022-02079-2

16. Nierer L, Eze C, da Silva Mendes V, *et al*. Dosimetric benefit of MR-guided online adaptive radiotherapy in different tumor entities: Liver, lung, abdominal lymph nodes, pancreas and prostate. *Radiat Oncol*. 2022;17(1):53.

doi: 10.1186/s13014-022-02021-6

17. Yan D, Liang J. Expected treatment dose construction and adaptive inverse planning optimization: Implementation for offline head and neck cancer adaptive radiotherapy. *Med Phys*. 2013;40(2):021719.

doi: 10.1118/1.4788659

18. Lee VS, SchettIno G, Nisbet A. UK adaptive radiotherapy practices for head and neck cancer patients. *BJR Open*. 2020;2(1):20200051.

doi: 10.1259/bjro.20200051

19. Zhang B, Lee SW, Chen S, *et al*. Action levels on dose and anatomic variation for adaptive Radiation Therapy using Daily Offline Plan evaluation: Preliminary results. *Pract Radiat Oncol*. 2019;9(1):49-54.

doi: 10.1016/j.prro.2018.08.006

20. Yap ML, Sun A, Higgins J, *et al*. Adaptive dose escalation using serial four-dimensional Positron Emission Tomography/ Computed tomography scans during Radiotherapy for locally Advanced Non-small Cell Lung Cancer. *Clin Oncol* (*R Coll Radiol*). 2016;28(12):e199-e205.

doi: 10.1016/j.clon.2016.08.011

21. Teo TP, Ahmed SB, Kawalec P, *et al*. Feasibility of predicting tumor motion using online data acquired during treatment and a generalized neural network optimized with offline patient tumor trajectories. *Med Phys*. 2018;45(2):830-845.

doi: 10.1002/mp.12731

22. Paulson ES, Ahunbay E, Chen X, *et al*. 4D-MRI driven MR-guided online adaptive radiotherapy for abdominal stereotactic body radiation therapy on a high field MR-Linac: Implementation and initial clinical experience. *Clin Transl Radiat Oncol*. 2020;23:72-79.

doi: 10.1016/j.ctro.2020.05.002

23. Tseng CL, Chen H, Stewart J, *et al*. High grade glioma radiation therapy on a high field 1.5 Tesla MR-Linac-workflow and initial experience with daily adapt-to-position (ATP) MR guidance: A first report. *Front Oncol*. 2022;12: 1060098.

doi: 10.3389/fonc.2022.1060098

24. Ruggieri R, Rigo M, Naccarato S, *et al*. Adaptive SBRT by 1.5 T MR-linac for prostate cancer: On the accuracy of dose delivery in view of the prolonged session time. *Phys Med*. 2020;80:34-41.

doi: 10.1016/j.ejmp.2020.09.026

25. Noel CE, Parikh PJ, Spencer CR, *et al*. Comparison of onboard low-field magnetic resonance imaging versus onboard computed tomography for anatomy visualization in radiotherapy. *Acta Oncol*. 2015;54(9):1474-1482.

doi: 10.3109/0284186X.2015.1062541

26. Yousaf T, Dervenoulas G, Politis M. Advances in MRI methodology. *Int Rev Neurobiol*. 2018;141:31-76.

doi: 10.1016/bs.irn.2018.08.008

27. Weygand J, Fuller CD, Ibbott GS, *et al*. Spatial precision in magnetic resonance imaging-guided radiation therapy: The role of geometric distortion. *Int J Radiat Oncol Biol Phys*. 2016;95:1304-1316.

doi: 10.1016/j.ijrobp.2016.02.059

28. Gupta A, Dunlop A, Mitchell A, *et al*. Online adaptive radiotherapy for head and neck cancers on the MR linear Accelerator: Introducing a novel modified Adapt-to-Shape approach. *Clin Transl Radiat Oncol*. 2021;32:48-51.

doi: 10.1016/j.ctro.2021.11.001

29. Dassen MG, Janssen T, Kusters M, *et al*. Comparing adaptation strategies in MRI-guided online adaptive radiotherapy for prostate cancer: Implications for treatment margins. *Radiother Oncol*. 2023;186:109761.

doi: 10.1016/j.radonc.2023.109761

30. Parchur AK, Lim S, Nasief HG, *et al*. Auto-detection of necessity for MRI-guided online adaptive replanning using a machine learning classifier. *Med Phys*. 2023;50(1):440-448.

doi: 10.1002/mp.16047

ACCSCIENCE PUBLISHING

Advances in Radiotherapy & Nuclear Medicine

SHORT COMMUNICATION

Simulated study relating dose-volume histogram metrics to three-dimensional gamma analysis results

Larisse Neumann Bonatto[1], Alexandre Colello Bruno[1], Oswaldo Baffa[2]*, and Juliana Fernandes Pavoni[1,2]

[1]Department of Radiotherapy, Ribeirão Preto Medical School Hospital and Clinics, University of São Paulo, Av. Bandeirantes, Monte Alegre, Ribeirão Preto, São Paulo, Brazil

[2]Department of Physics, Faculty of Philosophy, Sciences and Letters at Ribeirão Preto, University of São Paulo, Av. Bandeirantes, Monte Alegre, Ribeirão Preto, São Paulo, Brazil

Abstract

This study aims to investigate the relationship between the three-dimensional gamma index (3DGI) results and its clinical significance, proposing a correlation between changes in dose values in the dose-volume histogram (DVH) of the evaluated structures and 3DGI percentages of approval. In this study, we created 30 plans by including 1 mm displacement errors in the lateral, vertical, and longitudinal axes of each table, and compared them to a simulated, error-free treatment plan for prostate cancer. The plans were made in a commercial treatment planning system, using 6MV Varian 120-leaf multileaf collimators (MLC) linear accelerators and intensity modulated radiation therapy sliding window technique. We used a calculation algorithm-based MATLAB programming to evaluate the 3DGI analysis of fluence maps. The acceptance criteria were 3%/2 mm, 10% dose threshold, and 95% gamma passing rate. We compared 3DGI results with differences in structures DVH. DVH metrics versus 3DGI analysis showed a correlation between the percentage of point's approval and planning target volume (PTV) coverage, presenting a degree of agreement of 0.85%, 0.96%, and 0.94% in the longitudinal, lateral, and vertical axes, respectively. In summary, it was possible to establish a linear relationship between the percentage of points approved in the 3DGI analysis and the PTV dose. A similar behavior was also observed in bladder and rectum DVH, but for these structures, the relationship was not the same in the three displaced axes.

Keywords: 3D gamma index; Radiotherapy; Fluence maps; Intensity-modulated radiation therapy; Quality assurance

***Corresponding author:**
Oswaldo Baffa
(baffa@usp.br)

Citation: Bonatto LN, Bruno AC, Baffa O, Pavoni JF. Simulated study relating dose-volume histogram metrics to three-dimensional gamma analysis results. *Adv Radiother Nucl Med.* 2024;2(4):4005.
doi: 10.36922/arnm.4005

Received: June 21, 2024

Accepted: October 11, 2024

Published Online: November 13, 2024

1. Introduction

According to the 2022 global incidence of cancer, prostate cancer is projected to be the second most common cancer in men, with approximately 1,467,000 new cases being estimated, equivalent to 7.8% of the total new cases, excluding non-melanoma skin tumors.[1] Despite the high prevalence, the 5-year survival rate of patients with localized prostate cancer is 100%.[2] According to the most recent National Comprehensive Cancer Network guidelines, external beam radiation therapy should be used in the management

of localized prostate cancer.[3] Today, it is known that enhancing the local control of a disease requires a dose increase for treatment planning target volume (PTV). However, this often poses a challenge when considering the dose tolerances of adjacent normal tissues. Separately, the European Guidelines recommended the use of intensity-modulated radiation therapy (IMRT) as the standard treatment for prostate cancer.[4,5]

Planning with the IMRT technique allows the delivery of the dose to the PTV with a high degree of conformation while satisfactorily restricting the dose limit in the organs at risk. The dose increase is achieved through subfields with different sizes and intensities, which compose a single modulated field, and generally, five to nine treatment fields are employed. The IMRT technique is characterized by generating very heterogeneous dose distributions and promoting regions of high dose gradient very close to that of critical organs.

Due to this high degree of complexity, strict quality assurance is necessary to verify both the accuracy of the treatment planning system (TPS) as well as the ability to execute the radiation fields that will be configured in the linear accelerator (LINAC) during the treatment application. In addition, it is recommended by several institutions and protocols, such as the American Association of Physicists in Medicine Task Group No. 218 (AAPM TG218), that before beginning any treatment with the IMRT technique, the patient-specific quality assurance should be performed to identify possible discrepancies between the calculated dose and the dose that will be delivered to the patient.[6]

Probably, the most practiced form of patient-specific quality assurance in radiotherapy services is the comparison between the dose distributions calculated in the TPS and the measurements in the LINAC through the evaluation of the gamma index proposed by Low *et al.*,[7] which incorporates two concepts: The comparison of dose distribution (D), based on the local dose gradient, and the agreement distance between two points that present the same dose (DTA). This method independently compares the dose distributions from the displacement between the reference fluence map and the assessed creep map for each dose point. At the same time, the DTA is performed.

The gamma index is a tool for quantitative evaluation in which the limits of agreement must be found. The result of this criterion, approved versus not approved, is evaluated in terms of the unit, where values between 0 and 1 indicate that the comparison is approved in relation to the criteria of dose and distance, and for values of gamma >1, the comparison is considered failed. By computing the percentage of approved points, the treatment plan is approved for use in the patient. The acceptable gamma passing rates range from 90% to 95%.

Even so, not all the parameters for this assessment are fully established. To overcome these challenges, guidelines were developed to provide better guidance on the proper selection and use of the dosimetry tools available for IMRT QA, including algorithms, software, and devices.[8] One of the problems has been the effectiveness of using the gamma index to evaluate the clinical relevance of delivering a dose to the patient,[9-11] because the gamma passing rates in the patient-specific quality assurance phantom geometry do not reflect the position and/or the amount of dose variation in the patient's body. Consequently, the divergences in the planned and measured patient's dose-volume histogram (DVH) cannot be computed.

To contribute to the understanding of the relationship between the gamma index result and its clinical significance, we propose a simulated study to find a relationship between changes in dose values in the DVH of the evaluated structures and percentages of gamma index approval and evaluate whether such changes are acceptable according to the dose constraints of the protocol used.

2. Materials and methods

This study utilized a simulated treatment plan for prostate cancer using the solid water phantom with the target volumes of treatment, bladder, and rectum already delimited by the TG-119 protocol of AAPM.[12]

The prostate's delimited clinical volume target (CTV) is an ellipsoid, with dimensions of 4.0 × 2.6 × 6.5 cm in lateral-lateral, anteroposterior, and craniocaudal directions, respectively. Around the CTV, a symmetrical margin of 0.6 cm was generated to compose the PTV. The bladder was also delimited as an ellipsoid with dimensions of 5.0 × 4.0 × 5.0 cm in width, thickness, and length, respectively. On the other hand, the rectum is cylindrical with 1.5 cm in radius and 9.25 cm in length. The structures are represented in red, magenta, and green in Figure 1.

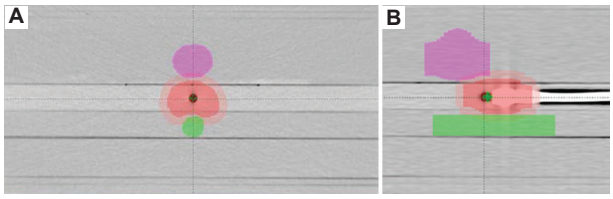

Figure 1. Images of the phantom and delineated volumes used to simulate prostate treatment: (A) Axial view and (B) sagittal view. Prostrate is represented in rede, bladder in magenta and rectum in green. The planning target volume (PTV) is represented in orange (prostate clinical volume target in dark orange and its expansion for PTV in light orange), the bladder in magenta and the rectum in green.

The dose prescription followed the usual goal of 95% of the PTV volume receiving at least 7560 cGy while 5% receiving no more than 8300 cGy. In the critical structures, the limits of 30% of the volume were adhered to, receiving a maximum of 7000 cGy and 10% received up to 7500 cGy, both for the rectum and bladder.

The plan used 6MV X-ray beams of a Varian Unique linear accelerator (Unique, Varian Medical Systems, USA equipped with an 80-leaf Millennium MLC (Millennium MLC, Varian Medical Systems, USA) using the IMRT sliding window technique. Seven fields with a 50° angle between them were used, following the guidelines of the TG-119. Such planning was carried out using Eclipse software version 15.6 (Varian Medical Systems, Palo Alto, California), using the analytical anisotropic algorithm calculation algorithm, with a dose matrix equal to 1 mm^3, without heterogeneity correction.

To compare the fluence maps and to evaluate the change in the structures' DVHs due to displacements, another 30 plans were made using the same configurations described above but including the displacements. In each new plan, known displacement errors in one direction were inserted. These displacements could be in the lateral, vertical, or longitudinal axes of the table, in increments of 1 mm, varying from −5 to +5 mm from the origin. Each new plan was created with errors in only one of the directions.

The files were exported from the TPS in the electronic medical image storage standard (DICOM) of the treatment plans (DICOM RT plan), the calculated dose matrices (DICOM RT dose) in the volumetric format with 0.1 cm^3 resolution, as well as the sets of structures (DICOM RT structure set) for each generated plan.

The dose percentages obtained from the structures' DVH were also exported in relation to the volumes of 98% (D_{98}), 95% (D_{95}), 10% (D_{10}), and 2% (D_2) in addition to the mean dose (D_{mean}) of the PTV, and for the rectum and bladder, in relation to the volumes of 30% (D_{30}), 10% (D_{10}), and 2% (D_2) and the respective average doses. To obtain the reading of the values in a practical and precise way, a script was written in the TPS itself to present the DVH data in table format.

A self-constructed Matlab programming software algorithm was used to compute the three-dimensional gamma index (3DGI). Dosimetric evaluations were performed by comparing the volumetric fluence map of the dose of each plan with an error in relation to the original plan without deviations. The evaluation criteria were at least 95% of approved points, considering the maximum difference of 3% in the dose and 2 mm DTA, using a 10% threshold (3%/2 mm/10%), as the AAPM TG-218 protocol recommends.

Quantitative analysis related to the DVH metrics was performed from plotted graphs of the percentage of dose versus structure volume values. Based on these data, it was possible to evaluate the percentage difference in the dose of the plans with an inserted error in relation to the original doses.

3. Results

Table 1 shows the percentage of points approved in the 3D gamma analysis (3%/2 mm/10%) for each simulated planning with errors inserted in relation to the original plan.

Of the 30 simulated plans, 10 were approved in the proposed analysis. Of these, the lowest percentage value of approved points was 97.12%, reaching 100% approval. Such plans refer to displacements of up to ±2 mm in both the lateral and vertical directions and ±1 mm in the longitudinal direction, which presented more significant restrictions in relation to the approval of 3DGI.

Out of the 20 failed plans, four were met with failure with a rate of up to approximately 9% in relation to the total number of points evaluated; in six plans, the differences were between 10% and 20%; in eight plans, the differences were 20 – 30%; and in two plans, the difference presented was more than 30%.

Figures 2-4 present the differences in behaviors of the evaluated structures' DVH, which were identified from the comparisons between the original clinically approved plan and the simulated plans with errors inserted.

3.1. PTV

In the comparison between the plans with errors inserted in relation to the original plan, the values of the smallest

Table 1. Percentage of points approved in three-dimensional gamma analysis

Axis	Plan with displacement (mm)									
	−5	−4	−3	−2	−1	+1	+2	+3	+4	+5
Lateral	69.18	77.22	86.92	97.15	99.99	100.00	97.12	87.03	77.59	69.39
Vertical	71.70	80.77	90.77	98.25	100.00	100.00	98.30	90.90	80.85	71.64
Longitudinal	70.85	76.36	83.23	91.15	99.82	99.82	91.19	83.27	76.41	70.79

variations of PTV coverage were along the longitudinal axis, which was 0.06% in 1 mm of caudal displacement, up to 3.45% when displaced 5 mm in the cranial direction in relation to the original plan. Along the lateral axis, the minimum variation was 0.22% when shifted 1 mm to the left, and the maximum variation was 5.93% when shifted 5 mm to the right. In the vertical axis, the minimum variation observed was 0.26% when displaced 1 mm in the posterior direction; variations were observed in the displacements of 4 mm for both directions, anterior and posterior, with a maximum variation of 10.04% of loss of coverage, in the displacement of 5 mm in anterior direction, as compared to the original plan.

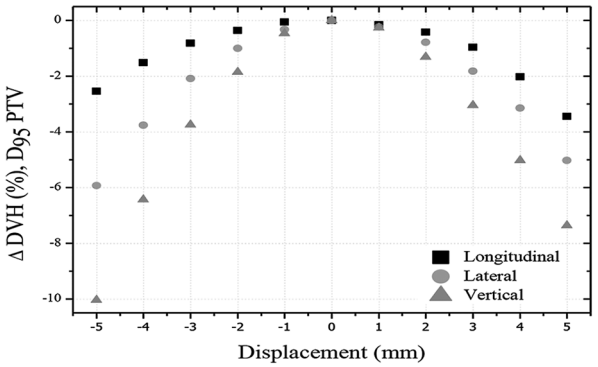

Figure 2. Dose variation of planning target volume coverage as a function of longitudinal, lateral, and vertical displacements

3.2. Bladder

Regarding variations in bladders' DVH, lateral-axis displacements demonstrated the lowest variations in overdose, recording a maximum value of 0.10% and 0.07% in D_{30} and D_{10}, respectively, related to the 2 mm left displacement. Still, in the lateral axis, the most significant variation related to sub-dosage was verified in the displacement of 5 mm to the right, reaching 1.39% for D_{30} and the same value for D_{10}. Regarding the longitudinal axis, the maximum dose increase was 9.29% and 5.64% in the volumes of 30% and 10%, respectively, when 5 mm was displaced in the cranial direction. The values of maximum sub-dosage in the longitudinal axis were found in the caudal displacement of 5 mm, recording 11.63% and 7.81% less dose in the volumes of D_{30} and D_{10}, respectively. On the vertical axis, there were maximum variations of overdosage of 16.77% and 14.70% in volumes of 30% and 10%, respectively, with a 5 mm displacement in the anterior direction, whereas a decrease of 11.59% and 16.16% in D_{30} and D_{10}, respectively, was observed when there was a 5 mm displacement in the opposite direction.

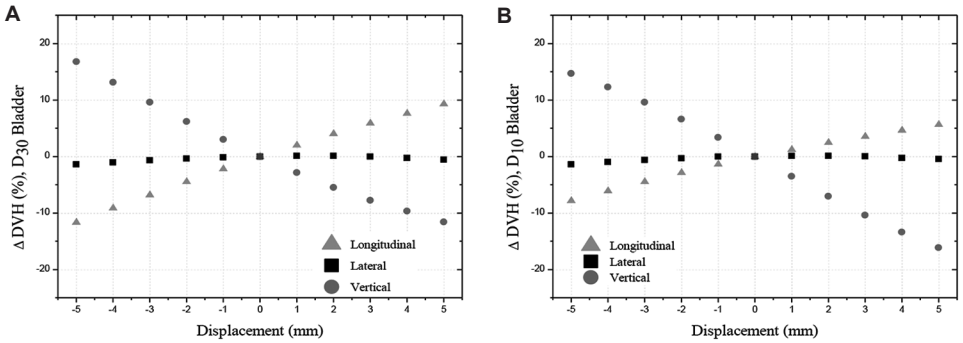

Figure 3. Variations in bladders' dose-volume histogram as a function of longitudinal, lateral, and vertical displacements for D_{30} (A) and D_{10} (B)

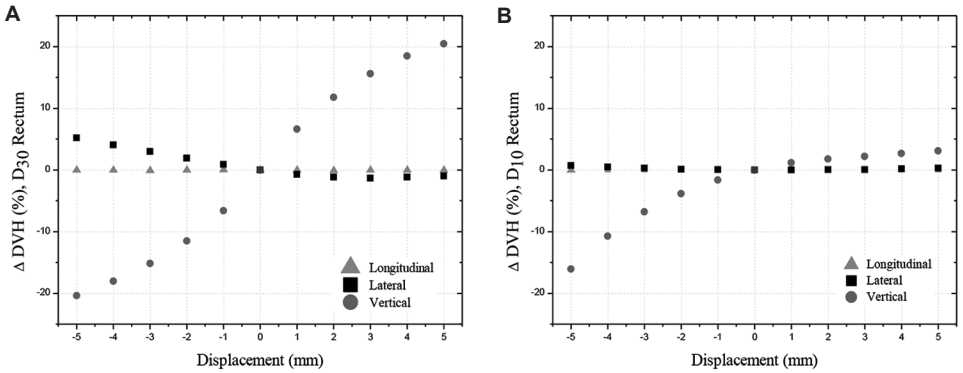

Figure 4. Variations in rectums' dose-volume histogram as a function of longitudinal, lateral, and vertical displacements for D_{30} (A) and D_{10} (B)

3.3. Rectum

The comparisons of the rectums' DVH revealed that the displacements in the longitudinal axis demonstrated the greatest stability, registering values of an overdose of only 0.01%, both for D_{30} and D_{10} when displaced 1 mm in the caudal direction, as well as maximum sub-dosage of 0.07% and 0.05% for D_{30} and D_{10}, respectively, when displaced 3 mm in the same direction. Regarding the lateral axis, however, the rectums' DVH showed an increase of up to 5.18% and 0.71% of dose tolerance for D_{30} and D_{10}, respectively, when there was a 5 mm displacement to the right. Still, on the lateral axis, the maximum sub-dosage of 1.36% for D_{30} was observed in the event of 3 mm displacement to the left, and an overdose of 0.02% for D_{10} was observed for the same displacement. More significant variations were observed in the vertical axis, reaching an overdose of up to 20.45% and 3.10% for D_{30} and D_{10}, respectively, when displaced 5 mm in the posterior direction, whereas for a 5 mm displacement in the opposite direction, a dose decrease of 20.39% and 16.09% for D_{30} and D_{10}, respectively, was noted.

4. Discussion

The present study showed that the minimum relative dose variation found for the PTV was 0.06%, reaching up to 10.04% loss of coverage. Regarding critical structures, the percentage differences of overdose found were up to 16.77% in the bladder volume and 20.45% in the rectum. For organs at risk, there were variations related to sub-dosage, reaching a minimum dose of 16.16% in the bladder and 20.39% in the rectum.

Through the comparison of the data obtained from the analysis of 3DGI, shown in Table 1, with the data related to the loss of coverage verified in the DVH along the lateral, longitudinal, and vertical axes, we were able to establish the correlation between the 3DGI tool and the DVH metric, where the behavior was presented in a linear fashion, presenting a degree of agreement of 0.96% in the lateral axis, 0.85% in the longitudinal axis, and 0.94% in the vertical axis. These values were considered acceptable and are shown in Figure 5.

In relation to critical structures, by comparing the 3DGI and the DVH metric of the bladder, it was not possible to establish such a relationship for the displacements along the lateral axis, and for the volume of the rectum, there was also no relationship along the lateral and longitudinal axes, as the variations observed, both with regard to overdosing and underdosing of volumes, did not present themselves in a linear way as observed in the correlation established with the PTV.

However, the data presented in Figures 2-4 showed that the maximum variations observed in the structures' DVHs were related to the displacements along the vertical axis. Such variations presented both overdose and significant dose decreases in critical structures. From the comparison between Table 1 and the data presented in Figures 2-4, as a function of the displacements in the vertical axis in the DVH of organs at risk, the same correlation between the 3DGI and the DVH metric was verified, and the behavior was presented in a linear way, serving as the standard established between the volume of treatment and the index of points validated through 3DGI analysis. This trend is shown in Figure 6. Similarly, such behavior was also

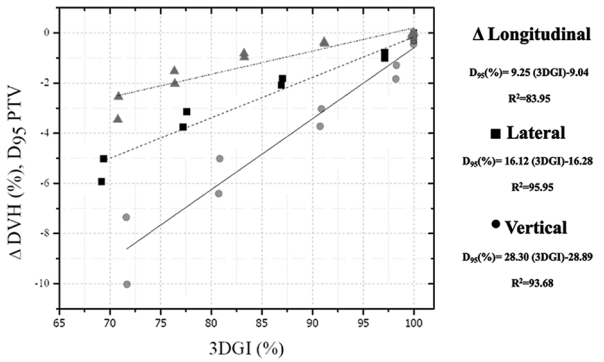

Figure 5. Relationship between the approval percentage of the three-dimensional gamma index and the planning target volume coverage variation on the longitudinal, lateral, and vertical displacements

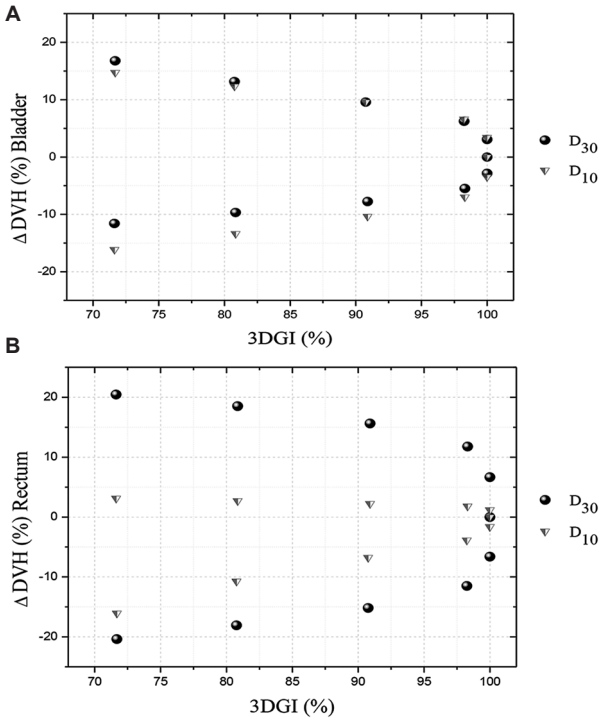

Figure 6. Relationship between the approval percentage of the 3D gamma index and the variation in the dose-volume histogram metric along the vertical displacement for bladder (A) and rectum (B)

verified in the displacements related to the longitudinal axis in relation to the bladders' DVH.

This finding of Figure 6 is justified by the dimensions of the volumes of the delimited structures and their spatial location in relation to the treatment target.

The treatment volume, as defined, presents its anteroposterior dimension considerably smaller than the others, being 35% smaller than the lateral dimension and 60% smaller than the craniocaudal dimension. Critical structures also present significant differences in their volumes, and again, the anteroposterior dimension is the smallest of all, as described above. In addition, anatomically, the prostate is situated posterior to the bladder and anterior to the rectum, precisely on the axis where all the involved structures present their smallest dimensions. Therefore, even the smallest variation in this axis will cause greater variation in irradiated volumes in relation to the other two axes in which the structures present larger dimensions than those in less critical anatomical locations.

The limitation of this study is that all the data are based on the simulated prostate cancer treatment plan using the solid water phantom created based on the TG-119 protocol of AAPM.[12] Although this study yielded some insights related to the percentage of points approved in the 3DGI analysis and DVH doses for various displacements, a larger study including human patients with anatomic variations would be necessary to validate the findings of the present study in real-world settings.

5. Conclusion

This study demonstrated that the percentage of points approved in the 3DGI analysis was linearly related to the PTV dose. Similar behavior was also observed in the DVHs for the bladder and rectum, but the relationship was not the same for these structures in lateral, vertical, and longitudinal displaced axes. Nevertheless, more robust research is warranted to assess whether such behavior will reproduce in a greater number of cases and plan with varying levels of complexity. We propose a future study to verify if 3DGI analysis can provide relevant clinical information and complementary evaluation useful for informing the approval or rejection of a treatment plan.

Acknowledgments

The authors Carlos Renato Silva and Lourenço Rocha for the technical assistance.

Funding

This work was financially supported by the Brazilian Agencies: CNPq (Grants 407471/2016-, 305827/2023-5 and 304921/2021-1); São Paulo Research Foundation (FAPESP) (Grants 2021/02254-6, and CEPID-NEUROMAT 2013/07699-0), and Sistema Único de Saúde (SUS).

Conflict of interest

The authors declare that they have no competing interests.

Author contributions

Conceptualization: All authors
Investigation: Larisse Neumann Bonatto
Methodology: All authors
Writing – original draft: Larisse Neumann Bonatto
Writing – review & editing: Alexandre Colello Bruno, Oswaldo Baffa, Juliana Fernandes Pavoni

Ethics approval and consent to participate

This work reposts a simulation study of a clinical problem; it doesn't include humans, so it is not necessary to have the local ethics committee's approval.

Consent for publication

No patients or volunteers were involved.

Availability of data

Data are available from the corresponding author upon reasonable request.

References

1. Cancer Today. Available from: https://gco.iarc.who.int/today [Last accessed on 2024 Jun 20].
2. Howlader N, Noone A, Krapcho M, *et al*. *SEER Cancer Statistics Review, 1975-2018*. National Cancer Institute; 2021. Available from: https://seer.cancer.gov/csr/1975_2018/index.html [Last accessed on 2024 Jun 20]
3. Schaeffer EM, Srinivas S, Adra N, *et al*. Prostate cancer, version 4. NCCN clinical practice guidelines in oncology. *J Natl Compr Canc Netw*. 2023;21(10):1067-1096.
   doi: 10.6004/jnccn.2023.0050
4. Tilki D, Van den Bergh RCN, Briers E, *et al*. EAU-EANM-ESTRO-ESUR-ISUP-SIOG guidelines on prostate cancer. Part II-2024 update: Treatment of relapsing and metastatic prostate cancer. *Eur Urol*. 2024;86:164-182.
   doi: 10.1016/j.eururo.2024.04.010
5. Cornford P, Van den Bergh RC, Briers E, *et al*. EAU-EANM-ESTRO-ESUR-ISUP-SIOG guidelines on prostate cancer-2024 Update. Part I: Screening, diagnosis, and local treatment with curative Intentt. *Eur Urol*. 2024;86(2):148-163.
   doi: 10.1016/j.eururo.2024.03.027
6. Miften M, Olch A, Mihailidis D, *et al*. Tolerance limits and

methodologies for IMRT measurement-based verification QA: Recommendations of AAPM Task Group No. 218. *Med Phys*. 2018;45(4):e53-e83.

doi: 10.1002/mp.12810

7. Low DA, Harms WB, Mutic S, Purdy JA. A technique for the quantitative evaluation of dose distributions. *Med Phys*. 1998;25(5):656-661.

doi: 10.1118/1.598248

8. Low DA, Moran JM, Dempsey JF, Dong L, Oldham M. Dosimetry tools and techniques for IMRT. *Med Phys*. 2011;38(3):1313-1338.

doi: 10.1118/1.3514120

9. Tamborra P, Martinucci E, Massafra R, *et al*. The 3D isodose structure-based method for clinical dose distributions comparison in pretreatment patient-QA. *Med Phys*. 2019;46(2):426-436.

doi: 10.1002/mp.13297

10. Nelms BE, Zhen H, Tomé WA. Per-beam, planar IMRT QA passing rates do not predict clinically relevant patient dose errors. *Med Phys*. 2011;38(2):1037-1044.

doi: 10.1118/1.3544657

11. Stasi M, Bresciani S, Miranti A, Maggio A, Sapino V, Gabriele P. Pretreatment patient-specific IMRT quality assurance: A correlation study between gamma index and patient clinical dose volume histogram. *Med Phys*. 2012;39(12):7626-7634.

doi: 10.1118/1.4767763

12. Ezzell GA, Burmeister JW, Dogan N, *et al*. IMRT commissioning: Multiple institution planning and dosimetry comparisons, a report from AAPM Task Group 119. *Med Phys*. 2009;36(11):5359-5373.

doi: 10.1118/1.3238104

ACCSCIENCE PUBLISHING

Advances in Radiotherapy & Nuclear Medicine

SHORT COMMUNICATION

Dose prescription and reporting in stereotactic radiosurgery: A single institutional study

Egor Borzov*, Raquel Bar-Deroma, Salem Billan, and Tomer Charas

Department of Radiotherapy, Division of Oncology, Rambam Health Care Campus, Haifa, Israel

Abstract

Stereotactic body radiotherapy and stereotactic radiosurgery are advanced radiotherapy techniques used to treat a variety of malignancies with high precision. However, there is significant variability in dose prescription and delivery, which may impact treatment consistency and efficacy. This work presents an analysis of retrospective dosimetric data collected from 300 stereotactic body radiotherapy/stereotactic radiosurgery (SBRT/SRS) clinical treatment plans. The study evaluated the dosimetric variability across different disease sites, including lung, brain, prostate, pelvis, liver, and bone, as well as among individual treatment planning strategies. Parameters analyzed included $D_{0.1cc}$, D_{50}, D_{95}, D_{99}, homogeneity index, and conformity index. The results showed that, despite variations in tumor types and planning approaches, a standardized protocol at our institution helped minimize dosimetric variability. These data may facilitate interinstitutional comparisons and help to enrich the SBRT/SRS data pool for treatment standardization.

Keywords: Stereotactic body radiotherapy; Stereotactic radiosurgery; Dose prescription; Dose reporting

***Corresponding author:**
Egor Borzov
(e_borzov@rambam.health.gov.il)

Citation: Borzov E, Bar-Deroma R, Billan S, Charas T. Dose prescription and reporting in stereotactic radiosurgery: A single institutional study. *Adv Radiother Nucl Med*. 2024;2(4):5450. doi: 10.36922/arnm.5450

Received: October 23, 2024

Accepted: November 26, 2024

Published Online: December 10, 2024

1. Introduction

Stereotactic body radiotherapy (SBRT) and stereotactic radiosurgery (SRS) are advanced hypofractionated radiotherapy techniques that typically involve 1 – 6 treatment fractions. These methodologies are employed across various clinical contexts, notably in treating malignancies in the lung, prostate, brain, liver, and other sites. With technological advancements continuing to emerge, the precision of SBRT/SRS has significantly improved, achieving submillimeter accuracy in both positioning and delivery. This level of precision is achieved through the integration of patient immobilization devices, pre- and intra-treatment imaging guidance, and high-definition collimators that shape radiation beams to conform tightly to tumor volumes.

Despite these advancements, one of the most critical parameters influencing treatment outcomes – radiation dose – remains insufficiently standardized. Variability in the prescription, reporting, and delivery of doses across institutions, raises significant concerns regarding treatment consistency and efficacy.[1]

Issues related to dose prescription in SBRT/SRS treatments have been widely discussed previously in the literature.[2] Prior studies have highlighted inconsistencies in dose delivery and reporting, raising concerns about the uniformity of treatment

protocols. For instance, while some literature addresses SBRT treatments in general,[3] others focus on specific anatomical sites, such as lung SBRT,[4] or prostate SBRT,[5] illustrating the challenges associated with different tumor locations and types.

Moreover, the introduction of volumetric modulated arc therapy (VMAT) has further complicated the problem of dose prescription. VMAT enables the delivery of non-uniform doses conformally to irregularly shaped treatment volumes. While this technique enhances tumor targeting and spares the surrounding healthy tissues, it also magnifies the variability in dose interpretation and distribution. These variations may not significantly impact clinical outcomes, such as disease-free or overall survival. However, they may compromise the uniformity of clinical trials and could introduce unwanted discrepancies in treatment delivery, both within the same institution and across national and international health-care settings.

In light of these challenges, the International Commission on Radiation Units and Measurements (ICRU) has issued guidelines in its ICRU-91 publication, aiming to provide a framework for more consistent SBRT/SRS practices.[6] In addition, the European Society for Therapeutic Radiation Oncology (ESTRO) has developed specific guidelines for lung SBRT,[7] whereas various national study groups across Europe have released their own benchmarks and recommendations.[8] These efforts are crucial in the promotion of a more standardized approach to radiation therapy, which can improve patient outcomes and facilitate better inter-institutional comparisons.

This study was designed to evaluate the dosimetric variability inherent in SBRT/SRS treatments, focusing on different disease sites and individual planning strategies. By analyzing this variability, this study aimed to provide a critical view of our department's specific radiation guidelines. Furthermore, these data could serve as a valuable resource for inter-institutional comparisons, contributing to ongoing efforts toward standardization in radiation therapy. Ultimately, enhancing our understanding of dosimetric variability may lead to improved protocols, better patient care, and more reliable outcomes.

2. Materials and methods

2.1. Study design

A single-institution retrospective analysis was conducted to evaluate the dosimetric variability in SBRT/SRS treatments. Clinical treatment plans utilized for patient radiotherapy were collected for this study, reflecting actual practice within our institution.

2.2. Patient and treatment plan selection

Inclusion criteria for treatment plans required adherence to established SBRT/SRS protocols. Treatment plans were excluded from analysis in the case of:

1. The dose distribution of the planning target volume (PTV) was significantly compromised (e.g., re-irradiation plan, extremal proximity of PTV to organs at risk [OARs], etc.)
2. Cases involved single-isocenter multiple metastases, varied prescription doses, or SRS where the PTV was < 1 cc, as these may not provide adequate dosimetric data.

This selection process ensured that the collected data accurately reflected the clinical practices currently in use.

2.3. Treatment planning

All treatment plans were developed using the Monaco treatment planning system (TPS, Elekta AB, Sweden), employing a 2 mm spatial grid for precise dose calculations. The Monte Carlo dose calculation algorithm was utilized to ensure high accuracy in determining dose distributions.

The treatments were delivered using an Elekta Versa HD (Elekta AB, Sweden) linear accelerator equipped with a 6 FFF photon beam. Each treatment plan included several key dosimetric parameters:

- $D_{0.1cc}$: The near-maximum dose received by the most irradiated 0.1 cc of the PTV
- D_{50}: The mean dose delivered to the target volume
- D_{95}: The dose received by 95% of the PTV, indicating the volume coverage
- D_{99}: The near-minimum dose received by 99% of the PTV.

In addition, the homogeneity index (HI) and conformity index (CI) were calculated for each treatment plan. The HI was calculated as the difference between D_{99} and $D_{0.1cc}$, divided by D_{50}, whereas the CI was calculated exactly following the ICRU-91 recommendation. In all calculations, the 100% isodose level was defined as the prescription dose per fraction, as documented in the Record and Verify System (MOSAIQ). This standardization allowed for consistency in comparing dosimetric outcomes across different plans.

2.4. Quality assurance and data analysis

Each case was reviewed by a radiation medical physicist (RMP) and an attending radiation oncologist (RO) to ensure adherence to treatment protocols and quality assurance standards. This collaborative oversight was critical in validating the treatment plans and ensuring that all dosimetric calculations were accurate and reflective of

clinical intent. Statistical analysis of the collected dosimetric data was performed to identify variability and correlations among treatment outcomes. Descriptive statistics were utilized to summarize the findings, with appropriate tests employed to evaluate differences and similarities.

3. Results

A total of 300 VMAT SBRT/SRS plans were analyzed following the application of exclusion criteria. The study included radiotherapy patients treated by nine radiation oncologists, with treatment plans developed by four RMPs. The distribution of disease sites among the patient cohort was as follows: lung (34.0%), brain (20.7%), prostate (19.6%), bones (13.0%), pelvic soft tissue (7.7%), and liver (5.0%). The treatments were delivered in 3, 5, or 6 fractions, with the dose per fraction varying between 5 and 13 Gy.

The variability in PTV volumes by disease site is illustrated in Figure 1. The smallest median PTV volume was observed in brain cases (9.4 cc), whereas the largest median volume was noted in prostate cases (107.2 cc). This significant difference highlights the variations in treatment planning and delivery across different tumor types.

Figure 2 illustrates the relationship between the delivered monitor units (MU), normalized to the prescription dose per fraction (MU/cGy), and the PTV volume for each treatment site. Notably, for larger-volume prostate cases, the corresponding SBRT plans required 37% more MU compared to the average for other cases, indicating a greater complexity in delivering the prescribed dose effectively.

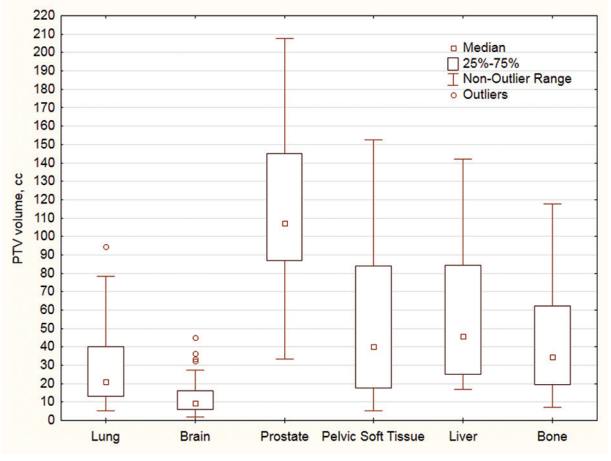

Figure 1. Variation in PTV by disease site. This figure illustrates the differences in median PTV volumes across various disease sites. Brain tumors exhibit the smallest median volume (9.4 cc), whereas prostate tumors have the largest median volume (107.2 cc), highlighting the variability in treatment planning for different tumor locations.
Abbreviation: PTV: Planning target volume.

The distribution of various dose-volume characteristics is shown in Figure 3. Hotspot values, which are defined as the maximum dose received by a specified volume, were significantly lower ($P < 0.05$) in treatment plans for the brain and prostate compared to other disease sites.

According to ICRU-83 recommendations,[9] it is advised to maintain the HI as low as possible for 3DCRT and IMRT plans. However, for SBRT plans, higher HI values may be acceptable due to the steep dose gradients.[10] In our study, the mean HI was 0.20 (standard deviation: 0.05), indicating a reasonable level of homogeneity in the treatment plans.

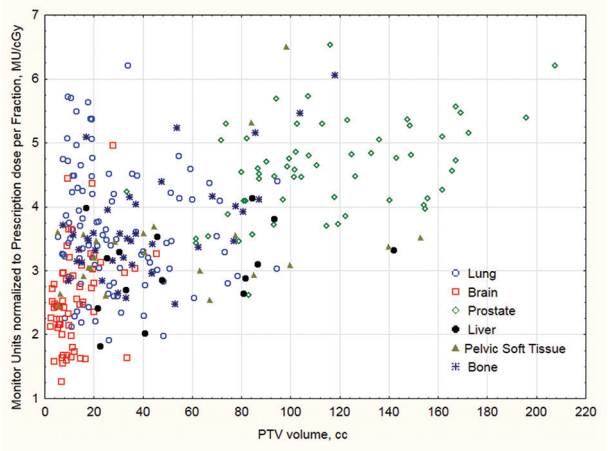

Figure 2. Relationship between delivered monitor units (MU) and PTV volume by disease site. This graph shows the correlation between the delivered MU normalized to the prescription dose per fraction (MU/cGy) and PTV volume across treatment sites. Prostate cases require 37% more MU compared to the average for other sites, reflecting the higher complexity in planning for larger target volumes.

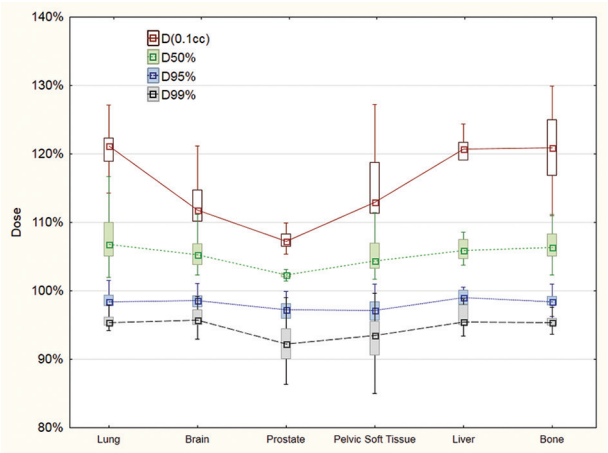

Figure 3. Distribution of dose-volume characteristics across disease sites. This figure presents the distribution of dose-volumetric parameters. Hotspot values for brain and prostate plans are significantly lower compared to other disease sites. Other dose-volume characteristics show overall uniformity in planning strategies.

For the conformity index (CI), a general guideline suggests maintaining values below 1.20 for SBRT/SRS plans.[11] Our findings revealed a mean CI of 1.17 (standard deviation: 0.07), which aligns with this recommendation.

Further analysis examined the dependence of HI and CI on the treatment planning approach used by each physicist, as illustrated in Figure 4. Statistical analysis (Kruskal–Wallis test, $P < 0.05$) demonstrated that plans developed by RMPs significantly differed in combined values of CI and HI, suggesting variability in planning strategies among the physicists.

4. Discussion

In this single-institution retrospective study, we reported various treatment planning and reporting parameters used for SBRT/SRS clinical plans. Treatment sites included the lung, brain, prostate, pelvis, liver, and bony regions. The median PTV volumes were in the range of 20 – 45 cc for all cases, while 9.2 cc for brain targets and 105.6 cc for prostate targets. The mean amount of MUs for all cases was about 3600, and its dependency on PTV volumes was analyzed. It is well-known that the target volume impacts the amount of MUs needed for a proper VMAT treatment plan: smaller target volumes correlate to a higher amount of MUs. However, as demonstrated in Figure 3, prostate cases formed a specific pattern, requiring a large amount of MU (mean value of 4600) for clinical plan optimization. This can be due to at least two possible reasons: (1) prostate targets are deeply seated in the body, requiring penetration through the femur heads, and (2) high complexity of the treatment plan due to high dose modulation close to OARs, such as the urethra, trigone, bladder, and rectum.

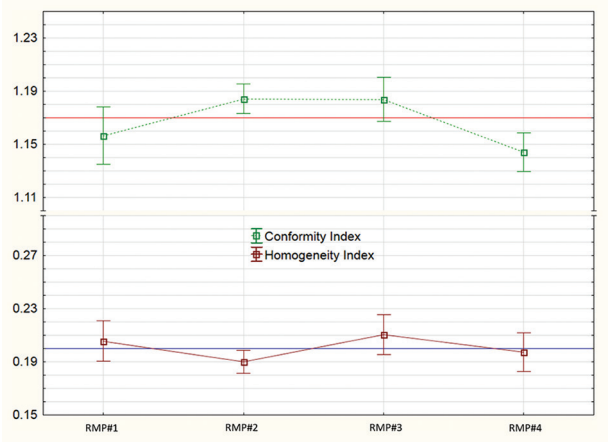

Figure 4. Impact of radiation medical physicist's (RMP) approach on homogeneity index (HI) and conformity index (CI). This figure illustrates the variability in HI and CI values based on the planning approach employed by different RMPs.

The analysis and comparison of dose-volumetric parameters strongly depend on the definition of the prescription dose. Some institutions use D_{100}, D_{95}, D_{80}, or D_{50} as the dose prescription for SBRT/SRS plans. However, these doses may be addressed to PTV or gross tumor volume, and may also depend on the treatment site or the dose calculation algorithm.[12] These discrepancies make comparisons between different studies and trials nearly impossible when using various dosimetric metrics. ICRU-91 made noticeable progress in defining dose prescriptions and reporting for SBRT/SRS treatments. However, a worldwide consensus on SBRT/SRS planning, delivery, and measurable metrics has yet to be achieved. Nevertheless, particularly at our institution, we have standardized the approach for all treatments and sites, such that the prescription dose in the Record and Verify and Treatment Planning systems is set at the 100% isodose level required for PTV coverage. Other standardized requirements include the limitation of the hotspot dose to 130%, D99 > 95% as a mandatory criterion, and D95 > 95% as an acceptable deviation. As shown in Figure 3, this standardization was clearly reflected in the consistency of dose-volumetric parameters across different treatment sites and regimes. Notably, brain cases had a slightly lower mean hotspot, likely due to the planner's preference to avoid escalating the dose to brain tissue, especially in cases of tumor bed irradiation, whereas prostate cases were limited by a 110% hotspot, as outlined in our specific prostate SBRT protocols. Like any standardization, our approach has a certain level of clinically acceptable variations. This work illustrates that such variations were sufficient to create treatment plans that reflect an individual planner's impact in terms of HI and CI.

One notable limitation of this study is the exclusion of cases where the dose distribution of the PTV was significantly compromised, particularly in situations where PTV coverage was affected by the proximity of OARs. In such cases, the dose distribution becomes more challenging to describe and standardize. In addition, while reirradiation cases present unique challenges in treatment planning, such as accounting for prior radiation doses to critical structures and the increased risk of normal tissue toxicity, these cases were not included in our analysis, and are usually discussed separately in the literature.[13,14] Since reirradiation often requires more advanced dosimetric planning and specialized dose distribution strategies, excluding these cases limits the applicability of our findings to patients undergoing retreatment.

5. Conclusion

In this study, we collected and analyzed dosimetric data from 300 SBRT/SRS treatment plans. These data represent different treatment plan characteristics: $D_{0.1cc}$, D_{50}, D_{95},

D_{99}, conformity, homogeneity indexes, and dose-metrics dependencies on the treatment site and RMP approach. Due to the unification applied in our hospital during the last years, the data demonstrated relatively low variability despite having some site- and planner-specific features. Our standardization advanced through the continuous implementation of auto-contouring programs, treatment planning systems, and QA automation software, which allow the creation of templates for each step of the radiation treatment workflow. For example, organ nomenclature and dose-volume metrics can be easily pre-defined for planning and reporting.

Further multi-institutional comparisons and the adoption of standardized SBRT practices across countries and institutions could significantly accelerate the availability of coherent clinical data, thereby enhancing both the quality and efficiency of radiation therapy globally.

Acknowledgments

None.

Funding

None.

Conflict of interest

The authors declare they have no competing interests.

Author contributions

Conceptualization: Salem Billan, Egor Borzov
Formal analysis: Egor Borzov
Investigation: Egor Borzov
Methodology: Egor Borzov
Writing–original draft: Egor Borzov
Writing–review & editing: Tomer Charas, Raquel Bar-Deroma

Ethics approval and consent to participate

This research was approved by IRB as a retrospective data analysis trial. The trial number is 0222-23-RMB-D.

Consent for publication

Not applicable.

Availability of data

Data are available from the corresponding author upon reasonable request.

Further disclosure

Part of this study was presented as a Digital Poster in the FARO-ESTRO Congress @ ESTRO meets Asia 2024, Kuala Lumpur, Malaysia, August 23 – 25, 2024.

References

1. Das IJ, Yadav P, Andersen AD, *et al.* Dose prescription and reporting in stereotactic body radiotherapy: A multi-institutional study. *Radiother Oncol*. 2023;182:109571.

   doi: 10.1016/j.radonc.2023.109571

2. Schiff PB. Dose dissonance in radiation oncology: Consensus needed when prescribing dose in radiation therapy. *Pract Radiat Oncol*. 2017;7(6):e579-e580.

   doi: 10.1016/j.prro.2017.04.018

3. Moustakis C, Blanck O, Ebrahimi F, *et al.* Time for standardization of SBRT planning through large scale clinical data and guideline-based approaches. Zeit für eine Standardisierung der SBRT-Planung mithilfe großer klinischer Datenmengen und leitlinienbasierter Ansätze. *Strahlenther Onkol*. 2017;193(12):1068-1069.

   doi: 10.1007/s00066-017-1216-8

4. Moustakis C, Blanck O, Ebrahimi Tazehmahalleh F, *et al.* Planning benchmark study for SBRT of early stage NSCLC: Results of the DEGRO Working Group Stereotactic Radiotherapy. Planvergleichsstudie bei der SBRT des NSCLC im Frühstadium: Ergebnisse der DEGRO AG Stereotaxie. *Strahlenther Onkol*. 2017;193(10):780-790.

   doi: 10.1007/s00066-017-1151-8

5. Eaton DJ, Naismith OF, Henry AM. Need for consensus when prescribing stereotactic body radiation therapy for prostate cancer. *Int J Radiat Oncol Biol Phys*. 2015;91(1) :239-241.

   doi: 10.1016/j.ijrobp.2014.09.025

6. *ICRU Report 91: Prescribing, Recording, and reporting of Stereotactic Treatments with Small Photon Beams*; 2017.

7. Guckenberger M, Andratschke N, Dieckmann K, *et al.* ESTRO ACROP consensus guideline on implementation and practice of stereotactic body radiotherapy for peripherally located early stage non-small cell lung cancer. *Radiother Oncol*. 2017;124(1):11-17.

   doi: 10.1016/j.radonc.2017.05.012

8. Moustakis C, Blanck O, Chan MKH, *et al.* Planning benchmark study for stereotactic body radiation therapy of liver metastases: Results of the DEGRO/DGMP working group on stereotactic radiation therapy and radiosurgery. *Int J Radiat Oncol Biol Phys*. 2022;113(1):214-227.

   doi: 10.1016/j.ijrobp.2022.01.008

9. *ICRU Report 83: Prescribing, Recording, and Reporting Photon-Beam Intensity-Modulated Radiation Therapy (IMRT)*; 2010.

10. Patel G, Mandal A, Choudhary S, Mishra R, Shende R. Plan evaluation indices: A journey of evolution. *Rep Pract Oncol Radiother*. 2020;25(3):336-344.

    doi: 10.1016/j.rpor.2020.03.002

11. Akbari F, Taghizadeh S, Pearson D. A retrospective study to establish recommendations for plan quality metrics in Lung SBRT. *Med Dosim*. 2022;47(2):111-116.

doi: 10.1016/j.meddos.2021.10.001

12. Lacornerie T, Lisbona A, Mirabel X, Lartigau E, Reynaert N. GTV-based prescription in SBRT for lung lesions using advanced dose calculation algorithms. *Radiat Oncol*. 2014;9:223.

doi: 10.1186/s13014-014-0223-5

13. Spatola C, Milazzotto RM, Tocco A, *et al*. Metachronous NSCLC in previously irradiated patients: Is re-irradiation with SBRT a good option as definitive treatment? *J Radiother Pract*. 2020;19(3):215-218.

doi: 10.1017/S1460396919000773

14. Pontoriero A, Critelli P, Bosurgi A, *et al.* Recurrent gynecological tumors in previously irradiated patients. Does re-irradiation with stereotactic body radiotherapy have a role? A systematic review. *Clin Exp Obstet Gynecol.* 2023;50(6):134.

doi: 10.31083/j.ceog5006134

ACCSCIENCE PUBLISHING

Advances in Radiotherapy & Nuclear Medicine

CASE REPORT

Chemotherapy for a malignant peripheral nerve sheath tumor: A case report

Phuong Cam Pham[1,2,3], Hien Quang Le[1,3], Duong Binh Nguyen[3], Hoang The Tran[3], Khoa Trong Mai[1,2], and Thai Van Pham[1,3]*

[1]The Nuclear Medicine and Oncology Center, Bach Mai Hospital, Hanoi, Vietnam

[2]Department of Oncology and Nuclear Medicine, University of Medicine and Pharmacy, Vietnam National University, Hanoi, Vietnam

[3]Department of Nuclear Medicine, Hanoi Medical University, Hanoi, Vietnam

Abstract

Malignant peripheral nerve sheath tumors (MPNSTs) are uncommon and aggressive soft-tissue sarcomas. They are difficult to manage due to their aggressiveness and limitations in early diagnosis and management. Complete surgical resection with or without adjuvant radiotherapy is the most effective treatment for patients with primary disease, whereas in those with metastatic disease, cytotoxic chemotherapy is beneficial. We herein present the case of a woman who complained of severe lower back pain. Computed tomography and magnetic resonance imaging revealed multiple bone and lung lesions. The patient underwent a bone lesion biopsy and was diagnosed with an advanced MPNST, which was appropriately treated with systemic chemotherapy.

Keywords: Malignant peripheral nerve sheath tumor; Treatment; Chemotherapy; Metastasis; Anthracycline; Enhancement; Rare cancer; Rare disease

***Corresponding author:**
Thai Pham Van
(phamvanthai@hmu.edu.vn)

Citation: Pham PC, Le HQ, Nguyen DB, Tran HT, Mai KT, Pham TV. Chemotherapy for a malignant peripheral nerve sheath tumor: A case report. *Adv Radiother Nucl Med.* 2024;2(4):3462. doi: 10.36922/arnm.3462

Received: April 21, 2024

Accepted: October 28, 2024

Published Online: December 10, 2024

1. Introduction

Malignant peripheral nerve sheath tumors (MPNSTs) are rare, aggressive tumors that account for 5 – 10% of all soft-tissue sarcomas,[1] and 50 – 60% of MPNST cases are associated with neurofibromatosis Type 1, whereas others are radiation-induced or sporadic types.[1] High-resolution positron emission tomography scans are used for diagnosing MPNSTs, and surgical excision is their definitive treatment. Distant metastases, usually to the lung, liver, or bones, are found in 40 – 70% of patients.[2] Localized disease is treated with radical surgery accompanied by adjuvant chemotherapy or radiotherapy. Post-operative radiation therapy influences disease-free survival rates. Chemotherapy is administered to patients with systemic disease. In general, MPNST has a poor prognosis and high mortality rates. The median survival depends largely on the subtypes of tumor and variations in the molecular biology profiles. In Vietnam, currently, no official data on the morbidity and mortality due to this malignant disease have been reported. Here, we report a clinical case of metastasis MPNST treated by chemotherapy.

2. Case presentation

A 43-year-old woman was admitted to our hospital because of severe lower back pain that lasted for 3 weeks and severe lower limb numbness and weakness. She had no

defecation or urination disorders. No special signs were noted on clinical examination, except for paralysis in both lower extremities, with muscle strength of 4/5.

Her blood cell counts and blood biochemistry test results were within the normal range. Magnetic resonance imaging (MRI) of the lumbar and sacral spine revealed multiple hyperintense lesions in T2-weighted imaging (T2WI) and fluid-attenuated inversion recovery, rim enhancement in the vertebral body, and vertebral pedicle on both sides of L4. The lesions, including a large 22 × 12-mm focus, exhibited substantial spinal membrane and soft-tissue infiltration, causing nerve compression at the L4 level. The area of damage to the left L2 pedicle was comparable, measuring 14 × 17 mm. The D11–D12 vertebral body had foci of hyperintense lesions on T2WI and strong gadolinium enhancement. The invasive D12 lesion damaged the bone cortex and grew into the spinal canal (Figure 1).

Thoracic computed tomography revealed several solid nodules with well-circuited rounded lesions of varying sizes and heterogeneous gadolinium enhancements scattered on both sides of the lungs (Figure 2). The bone lesions in right rib V, rib arches IV and VI, and bilateral sternoclavicular joint caused bone destruction and adjacent soft-tissue invasion (Figure 3A-C). Abdominal computed tomography revealed two nodules with poor contrast enhancement in the right and left liver lobes. No malignant cells were found in the biopsy of the right lobe nodule (Figure 3D).

Extensive bone lesions with similar destructive and invasive features were observed in L4 and L5 vertebrae, pelvic bone, left pubis, and left femur, with the largest lesion measuring 57 × 64 mm (Figure 4). The biopsy of the pubis lesion exposed uniform spin hyalinization stroma. The tumor stained positive for S100 in immunohistochemistry (Figure 5). These features indicated a malignant epithelioid peripheral nerve sheath tumor.

The patient also underwent esophagogastroduodenoscopy and colorectal endoscopy, which revealed no abnormal lesions suggestive of malignancy.

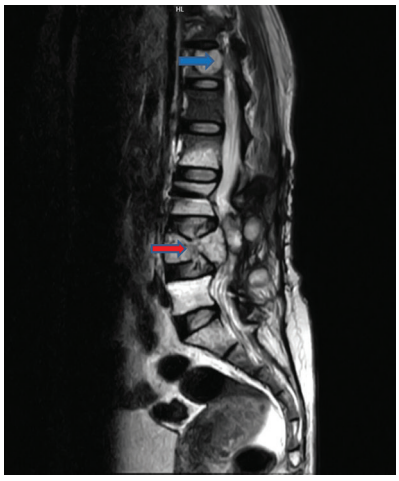

Figure 1. Magnetic resonance imaging of the lumbar and sacral spine revealed multiple lesions with peripheral gadolinium enhancement in D11, D12 (blue arrow), and L4 vertebral bodies (red arrow) and invasion of adjacent soft-tissue structures

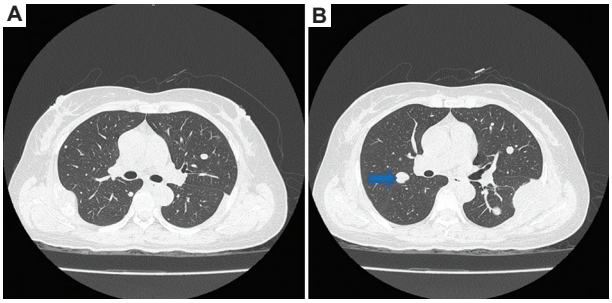

Figure 2. Chest computed tomography scan showing solid nodules scattered in the lung fields on both sides. (A) Solid nodule (red arrow) in left upper lobe lung. (B) Solid nodule in the right lower lobe lung (blue arrow) and some nodules with the same characteristic in the left lung.

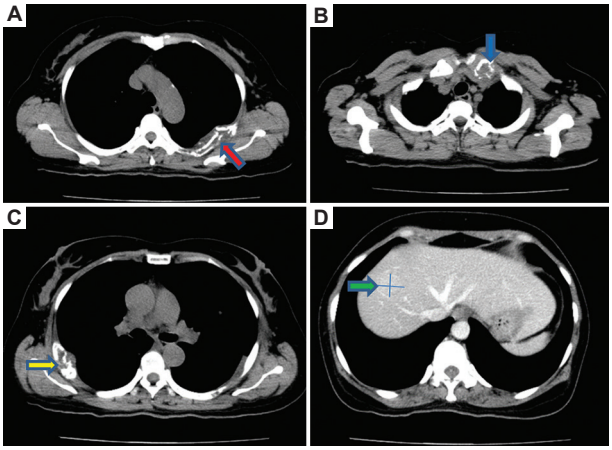

Figure 3. Chest and abdominal computed tomography scans. (A–C) Secondary multifocal bone lesions. Secondary multifocal bone lesion in left IV rib arches (A - Red arrow), left sternoclavicular joint (B - Blue arrow), right rib V (C - Yellow arrow). (D) Mass in the right lobe of the liver; biopsy showed no malignant cells (green arrow).

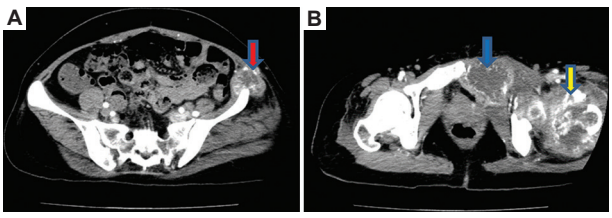

Figure 4. Abdominal computed tomography scans showing secondary pelvic and femoral bone lesions. (A) The lesion in the left pelvic bone (red arrow). (B) The lesion in the left pubis (blue arrow) and left femur bone (yellow arrow).

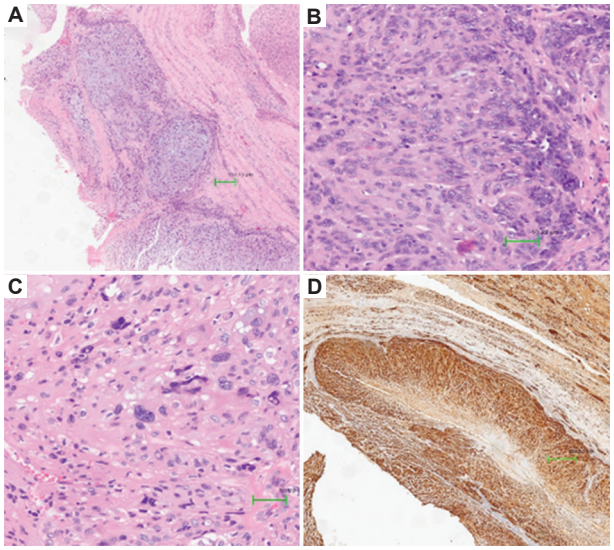

Figure 5. Histopathological features on microscope. (A). Low-power view of a malignant peripheral nerve sheath tumor (MPNST) demonstrating variable hypocellular and hypercellular areas. (B and C). Moderate-power view showing elongated, spindle-like shaped cells with a hyperchromatic nucleus, with cell necrosis and mitosis are common features in the histopathology in MPNSTs. (D). The tumor was positive for S100 in immunohistochemistry.

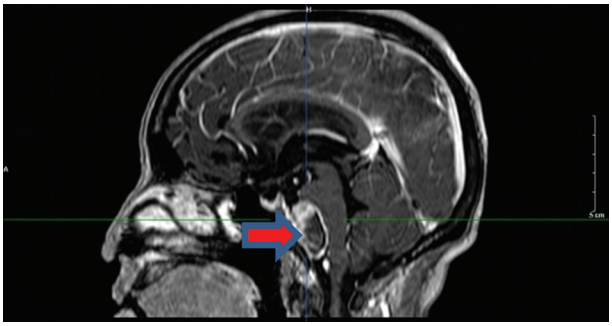

Figure 6. Lesions anterior to the pons are metastatic nerve sheath tumors (red arrow)

The patient was diagnosed with MPNST cT4N0M1, multifocal bone and bilateral lung metastases, and bilateral lower limb paralysis.

The patient received chemotherapy with the doxorubicin–ifosfamide–mesna regimen:

- Doxorubicin 30 mg/m^2; intravenous infusion on days 1 and 2.
- Ifosfamide 3.75 g/m^2; intravenous infusion over 4 h, days 1 and 2.
- Mesna 750 g/m^2; intravenous infusion before each ifosfamide session and at 4 and 8 h after ifosfamide infusion.

Each cycle lasted for 21 days.

During treatment, the patient developed mild anemia that did not require a blood transfusion and did not exhibit any other adverse effects, such as infection, thrombocytopenia, nausea, vomiting, or hair loss.

However, after three chemotherapy cycles, the patient experienced bilateral lower limb weakness, left-side dominance, left cranial nerve VI paralysis, and blurred vision in the left eye. The patient underwent contrast-enhanced cranial MRI, which revealed an 18 × 31-mm lesion ventral to the pons, with mixed signals and strong and heterogeneous enhancements after contrast injection, and thickening of the adjacent meninges (Figure 6).

The physician explained that the disease was progressing despite chemotherapy; however, the patient and her family refused to continue treatment and chose palliative care and symptomatic management in medical facilities.

3. Discussion

MPNSTs account for 5 – 10% of all soft-tissue sarcomas[1] and occur in approximately 1/100.000 individuals in both sexes.[3] This disease has a poor prognosis and exhibits rapid progression, often metastasizing primarily to the lungs in the early stages. To achieve a negative resection margin, surgical treatment is the only radical treatment for localized disease. In cases of distant metastasis, chemotherapy is an essential treatment modality. The disease generally has a poor prognosis, with an overall 5-year survival rate of 15 – 66%,[1] 5-year event-free survival rate of 24 – 53%,[1] and local recurrence rate of 20 – 85.7%.[1] Patients with metastatic disease have poor survival, with a median progression-free survival of approximately 4 months and overall survival of 13 months.[2]

Patients usually present with a rapidly enlarging mass that may be painful or cause local neurological symptoms such as weakness or paresthesias. In most cases, the mass is >5 cm at presentation.[4] In the present case, the patient was diagnosed with a late-stage MPNST, with multiple metastatic lesions in the bones and lungs leading to severe pain and debilitation. Pubic bone lesion biopsy results and immunohistochemical staining revealed spindle cells positive for S100, a protein characteristic of MPNSTs. The only viable treatment option for the patient was systemic chemotherapy. Chemotherapy with single agents (dacarbazine, doxorubicin, epirubicin, or ifosfamide) or anthracycline-based combination regimens (doxorubicin or epirubicin with ifosfamide and/or dacarbazine) has been widely used for patients with advanced, unresectable, or metastatic disease.[5] Anthracycline-based therapy is the standard first-line treatment for MPNST.[6] Kroep *et al.* demonstrated that the doxorubicin–ifosfamide (AI) combination was associated with a lower risk of relapse and better response rate than other regimens.[7] Some chemotherapy regimens appropriate for MPNSTs, mainly anthracycline-based regimens, are listed in

Table 1. Some chemotherapy regimens suitable for malignant peripheral nerve sheath tumors (Abstract from NCCN Guidelines Version 3.2024)

Treatment modalities	Chemotherapy regimens
Neoadjuvant/adjuvant therapy	• AI (doxorubicin, ifosfamide, and mesna) • Ifosfamide, epirubicin, and mesna
First-line therapy for advanced/metastatic disease	• Anthracycline-based regimens: • Doxorubicin • Epirubicin • Liposomal doxorubicin • AD (doxorubicin and dacarbazine) • AI • Ifosfamide, epirubicin, and mesna
Subsequent lines of therapy for advanced/metastatic disease	• Eribulin • Trabectedin • Gemcitabine and docetaxel

Table 2. Adverse effects of the doxorubicin–ifosfamide (AI) regimen

Drugs	Common adverse effects
Doxorubicin	• Cardiotoxicity: Doxorubicin causes heart damage and arrhythmias due to the generation of free radicals, leading to oxidative stress that damages the membrane of cardiomyocytes. • Gastrointestinal toxicity: nausea, vomiting, mucositis, and diarrhea. • Hematologic toxicity: Doxorubicin causes myelosuppression, leading to neutropenia, anemia, and an increasing risk of secondary cancers such as leukemia. • Endocrinology and metabolism toxicity: high uric acid levels.
Ifosfamide	• Urotoxicity: hemorrhagic cystitis, usually managed with intravenous infusion of mesna. • Hematologic toxicity: similar to doxorubicin. • Neurotoxicity: cognitive dysfunction, ifosfamide encephalopathy, and peripheral neuropathy. • Falconi syndrome (rare). • Nausea and vomiting. • Alopecia. • High liver enzyme levels.

Table 1. The adverse effects of the AI regimen are presented in Table 2. Before treatment, the patient's blood cell count, liver enzyme levels, and glomerular filtration rate were within normal limits. During treatment, the patient tolerated the drug well and experienced no adverse effects, such as anemia, nausea, hair loss, diarrhea, heart failure, or hypersensitivity reactions. The patient received chemotherapy until the disease progressed, and metastasis led to the emergence of new brain lesions. Unfortunately, the patient and her family chose to discontinue treatment immediately afterward. The disease progressed after only three cycles and accurately reflects the malignant and frequently recurring nature of this tumor.

4. Conclusion

MPNSTs are rare soft-tissue sarcomas with non-specific clinical and imaging characteristics. To decide the most appropriate treatment, integrating radiological findings and histological results is essential. In localized disease, a combination of radical surgery and adjuvant radiotherapy or chemotherapy is recommended. Anthracycline-based cytotoxic chemotherapy is the standard treatment for advanced and metastatic disease; however, it is often less effective.

Acknowledgments

The authors would like to thank the participating patients, as well as the colleagues and nurses who made this work possible.

Funding

None.

Conflict of interest

Phuong Cam Pham is an Editorial Board Member of this journal but was not in any way involved in the editorial and peer-review process conducted for this paper, directly or indirectly. Separately, other authors declared that they have no known competing financial interests or personal relationships that could have influenced the work reported in this paper.

Author contributions

Conceptualization: Khoa Trong Mai, Phuong Cam Pham, Thai Van Pham, Hien Quang Le
Investigation: All authors
Methodology: Phuong Cam Pham, Hien Quang Le
Writing – original draft: Duong Binh Nguyen, Hoang The Tran
Writing – review & editing: Phuong Cam Pham, Khoa Trong Mai, Thai Van Pham

Ethics approval and consent to participate

This study was approved by the Ethics Committee of Bach Mai Hospital (approval no: 4460/BM-HĐĐĐ). Written informed consent was obtained from the patient before her participation.

Consent for publication

Informed consent was obtained from the patient to publish her data.

Availability of data

The original data of the study are included in the article. Further inquiries can be directed to the author.

References

1. Cai Z, Tang X, Liang H, Yang R, Yan T, Guo W. Prognosis and risk factors for malignant peripheral nerve sheath tumor: A systematic review and meta-analysis. *World J Surg Oncol*. 2020;18:257.

   doi: 10.1186/s12957-020-02036-x

2. Sobczuk P, Teterycz P, Czarnecka AM, *et al*. Systemic treatment for advanced and metastatic malignant peripheral nerve sheath tumors-a sarcoma reference center experience. *J Clin Med*. 2020;9(10):3157.

   doi: 10.3390/jcm9103157

3. Knight SWE, Knight TE, Santiago T, Murphy AJ, Abdelhafeez AH. Malignant peripheral nerve sheath tumors-a comprehensive review of pathophysiology, diagnosis, and multidisciplinary management. *Children* (*Basel*). 2022;9(1):38.

   doi: 10.3390/children9010038

4. Farid M, Demicco EG, Garcia R, *et al*. Malignant peripheral nerve sheath tumors. *Oncologist*. 2014;19(2):193-201.

   doi: 10.1634/theoncologist.2013-0328

5. Mehren M von, Kane JM, Agulnik M, *et al*. Soft tissue sarcoma, version 2.2022, NCCN clinical practice guidelines in oncology. *J Natl Compr Canc Netw*. 2022;20(7):815-833.

   doi: 10.6004/jnccn.2022.0035

6. Gronchi A, Miah AB, Dei Tos AP, *et al*. Soft tissue and visceral sarcomas: ESMO-EURACAN-GENTURIS clinical practice guidelines for diagnosis, treatment and follow-up☆. *Ann Oncol*. 2021;32(11):1348-1365.

   doi: 10.1016/j.annonc.2021.07.006

7. Kroep JR, Ouali M, Gelderblom H, *et al*. First-line chemotherapy for Malignant Peripheral Nerve Sheath Tumor (MPNST) versus other histological soft tissue sarcoma subtypes and as a prognostic factor for MPNST: An EORTC Soft Tissue and Bone Sarcoma Group study. *Ann Oncol*. 2011;22(1):207-214.

   doi: 10.1093/annonc/mdq338

Our Journals

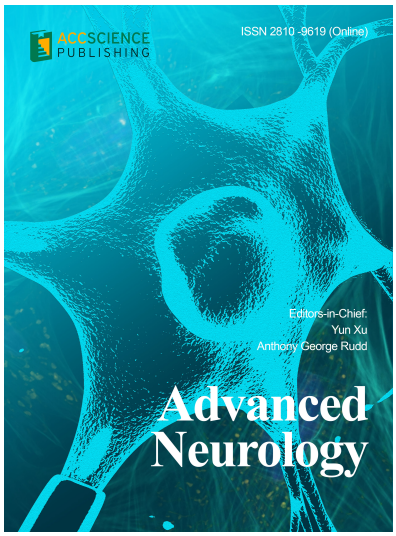

Advanced Neurology is a peer-reviewed and open-access journal that aims to publish and disseminate novel research in the breadth of neurology and neuroscience. The journal aims to advance our understanding in the nervous system and provide a platform to neuroscientists and physicians to showcase their findings in original fundamental and clinical research as well as to present new ideas that highlight the changes in the neurological clinical practice.

Advanced Neurology covers subject areas, including but not limited to the following:

- Neurological disorders
- Neurodegenerative disease
- Cerebrovascular disease
- Epilepsy and movement disorders
- Neuroimmune disease
- Neurological infections
- Muscle disease
- Molecular and cellular neuroscience
- Systems neuroscience
- Cognitive neuroscience
- Computational modeling of nervous system

Global Translational Medicine is a quarterly journal that focuses on medicine, biological sciences, and biomaterials engineering. The goal of *Global Translational Medicine* is to provide a platform to researchers for showcasing their latest research works in translational medicine so as to advance the field towards the betterment of human health. Despite the advancement of omics and new technologies, the process of transforming these technologies and scientific research results into effective therapies and putting them into clinical use still has a long way to go. *Global Translational Medicine* provides a platform to fill the gaps in preclinical and inter-disciplinary research, to promote clinical translation of scientific research results, and to contribute to the conception of new and improved preventive measures as well as diagnostic and therapeutic techniques of diseases.

Global Translational Medicine covers the following themes: cardiovascular disease, metabolism/diabetes/obesity, neuroscience/neurology, cancer, biomaterials and their applications in medicine, proteomics/metabolomics, pharmacogenomics, biomarkers, bioinformatics and data mining, animal and clinical research, and medical methods arising from interdisciplinary crossover.

Start a new journal

Write to us via email if you are interested to start a new journal with AccScience Publishing. Please attach your CV, professional profile page and a brief pitch proposal in your email. We shall inform you of our decision whether we are interested to collaborate in starting a new journal.

Contact: info@accscience.com

https://accscience.com/journal/ARNM

Contact
www.accscience.com
8 Burn Road, #15-03 Trivex, Singapore 369977
Email: editorial@accscience.com
Phone: +65 8182 1586